"Simulations of phase behavior in non-equilibrium systems"

Dissertation

(kumulativ)

Zur Erlangung des Grades

„Doktor der Naturwissenschaften"

am Fachbereich Physik, Mathematik und Informatik

der Johannes Gutenberg-Universität in Mainz

vorgelegt von

Florian Dittrich

geboren am 17.12.1988 in Neuwied

Mainz, 31. August 2023

Florian Dittrich
Simulations of phase behavior in non-equilibrium systems
August 31, 2023

Oral examination: 14.12.2023

Supervisor: apl. Prof. Dr. Peter Virnau
Reviewers: apl. Prof. Dr. Peter Virnau, Prof. Dr. Peter G. J. van Dongen

Dedication

My work is dedicated to

the ones who shaped me and would be proud of me

my mother

Gerti (†1994)

my mother since the age of six

Jutta (†2022)

my grandmother

Gertrud (†1997)

and to the ones who still shape me and are proud of me

my father

Jürgen

my grandfather

Alfred

Table of contents

List of Publications

The publications A1-A3 are part of this cumulative thesis. Publication B1 is based on previous work, but fundamental for the methods applied in A1 and A2. Publications B1 and B2 are based on the concepts introduced in A3, but are not relevant for the scope of this thesis.

[A1] [1]
„Critical behavior in active lattice models of motility-induced phase separation" (Eur. Phys. J. E 2021, 44, 53)
F. Dittrich, T. Speck, P. Virnau

[A2] [2]
„Growth and aging in a few phase-separating active matter systems" (Phys. Rev. E 2023, 108, 024609)
F. Dittrich, J. Midya, P. Virnau, S. K. Das

[A3] [3]
„Skyrmion Lattice Phases in Thin Film Multilayer" (Adv. Funct. Mater. 2020, 30, 2004037)
J. Zázvorka, F. Dittrich, Y. Ge, N. Kerber, K. Raab, T. Winkler, K. Litzius, M. Veis, P. Virnau, M. Kläui

[B1] [4]
„Critical behavior of active Brownian particles" (Phys. Rev. E 2018, 98, 030601)
J.T. Siebert, F. Dittrich, F. Schmid, K. Binder, T. Speck, P. Virnau

[B2] [5]
„Magnetic Direct-Write Skyrmion Nanolithography" (ACS Nano 2020, 14, 14960-14970)
A. V. Ognev, A. G. Kolesnikov, Y. J. Kim, I. H. Cha, A. V. Sadovnikov, S. A. Nikitov, I. V. Soldatov, A. Talapatra, J. Mohanty, M. Mruczkiewicz, Y. Ge, N. Kerber, F. Dittrich, P. Virnau, M. Kläui, Y. K. Kim, A. S. Samardak

[B3] [6]
„Commensurability between Element Symmetry and the Number of Skyrmions Governing Skyrmion Diffusion in Confined Geometries" (Adv. Funct. Mater. 2021, 31, 2010739)
C. Song, N. Kerber, J. Rothörl, Y. Ge, K. Raab, B. Seng, M. A. Brems, F. Dittrich, R. M. Reeve, J. Wang, Q. Liu, P. Virnau, M. Kläui

Summary

Non-equilibrium systems cover a tremendously wide range of different systems, in experiments and in simulations as well as in the real world. The fact that these systems are not in thermodynamic equilibrium is in many cases responsible for unique effects and behavior. A fundamental understanding of non-equilibrium systems is crucial to gain insights into such behavior and exploit it in a manifold of use cases. A recent growth in attention to non-equilibrium systems is a consequence. Especially deep insights into the nature of certain non-equilibrium systems can be gained through the study of phase behavior in these very systems. To do so, this thesis utilizes computer simulations of different systems: Discrete and continuous active matter systems on the one hand and skyrmion lattices on the other hand.

The active matter systems being discussed in this work consist of active particles. These particles are not only subject to Brownian motion but they are in addition "actively" performing directed motion, which drives the systems out of equilibrium. Active lattice gas models are studied as a discrete realization of such particles with comparably low computational effort. At sufficiently high activity they undergo a motility induced phase separation (MIPS) that closely resembles the gas-liquid transition known from equilibrium. However, a determination of critical points and exponents for different model realizations performed in this work showed some model dependent deviations from 2D Ising universality class. This raises the question, whether the concept of universality holds for active matter and non-equilibrium systems at all.

The critical behavior of active Brownian particles (ABPs) around MIPS has already been studied before and showed even stronger deviations. In this work additional focus is put on quenches of ABPs from homogeneous phase right into the phase separated regime and to the critical point. Following the quench, the systems far-from-steady-state dynamics, structure growth and aging can be studied. Results obtained in this work appear to be similar to those observed during phase separation in the 2D Ising model. However, for the active lattice models, there are deviations in the case of quenches inside the coexistence regions.

Skyrmion lattices consist of densely packed skyrmions. These topologically stabilized whirls of magnetization can be described as quasiparticles. By modelling them as soft disks similar to ABPs, the underlying interaction potential of experimental skyrmions was determined with the help of computer simulations in this work. Furthermore, different experimental skyrmion lattices were characterized according to their phase state and degree of hexagonal order with the help of a newly developed parameter. Thereby the onset of a hexatic phase was found.

Introduction and overview

In order to outline the common theme throughout this thesis, I will start with a brief overview about the non-equilibrium nature of the systems examined. This will be followed by a closer look on the properties and phenomena related to their phase behavior. By subsequently addressing each system and publication individually, I will provide more details about the commonalities and findings. My main contribution in all publications is focused on writing and performing simulations in addition to analyzing the data generated by them.

This work is primarily based on the broad field of non-equilibrium systems and especially the phase behavior in these systems. Prominent examples of non-equilibrium systems are our atmosphere and the weather in it as well as all living creatures, including human bodies. Unlike equilibrium systems, non-equilibrium systems are not in thermodynamic equilibrium. This is true for most of the real-world systems, since there are many drivers, that can bring a system out of equilibrium. Nevertheless, many of these real-world systems are still close enough to equilibrium to apply equilibrium concepts to describe them. But as soon as the systems are "far enough" out of equilibrium, new effects and significant deviations from equilibrium systems can be found. Therefore, it is important to keep in mind, that concepts derived from equilibrium assumptions do not necessarily hold in non-equilibrium systems. Precise analysis and carefully drawn conclusions are essential to find the real underlying nature of the examined system.

Even though the common classical theory of equilibrium systems (shaped by Clausius, Gibbs, Boltzmann, and others) exists in essential parts since more than hundred years (not considering quantum statistics), there is still no comparable theory of non-equilibrium systems. A development of such a theory is for sure a "Grand Challenge" of statistical physics to which the work performed within the framework of this thesis aims to add small contributions by looking into various non-equilibrium systems.

The variety of possible systems and drivers to bring them out of equilibrium is immense. To account for that, three different approaches are presented in the publications [A1]-[A3]. In [A1] and [A2] active matter systems are the primary subject, where [A1] models active matter in the framework of lattice gas models and [A2] additionally examines continuous systems that consist of active particles. The particles in these continuous systems (and equivalently in the lattice gas systems) are not only subject to Brownian Motion as in the equilibrium case but are additionally actively propelled along a certain direction. This additional directed velocity component solely drives the systems out of equilibrium. In [A2] the systems are on top of that brought out of steady state with sudden quenches. These immediate changes of parameters for example quench the system from a mixed state to a phase

separated state, inducing a nucleation process which can be studied subsequently. Finally, [A3] covers systems of skyrmions – topologically stabilized whirls of magnetization that can be described as quasiparticles. One can easily argue that these magnetic whirls are intrinsic non-equilibrium systems as they are only stabilized due to their topological structure. They can be propelled by electric currents or quenched into different phases. In [A3], systems of skyrmions in a liquid phase are rapidly driven into a densely packed hexagonal structure (so called skyrmion lattices) by increasing their diameter and thus increasing the system's density. The emerging structures and the underlying interaction potential are examined with the help of computer simulations.
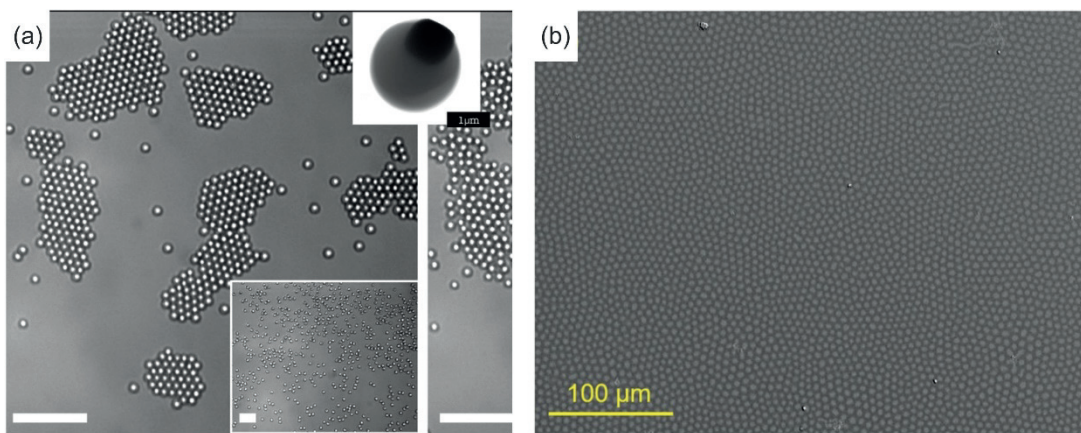

Figure 1 Examples of experimental systems under consideration in this work: (a) Suspension of synthetic photoactivated colloidal particles, that show active behavior when illuminated by blue light. The big picture shows living crystals assembled from a homogeneous distribution (inset) under illumination by blue light [7]. (From Jeremie Palacci et al., Living Crystals of Light-Activated Colloidal Surfers. Science 339, 936-940 (2013). DOI: 10.1126/science.1230020. Reprinted with permission from AAAS.). (b) Kerr microscope image of a skyrmion lattice with μm sized skyrmions – a hexagonal order is visible [A3]. Except for the difference in overall density, the two examples (a) and (b) look very similar even though they are completely different systems.

In this work, the active matter systems are solely studied through simulations and the skyrmion lattices are studied through experiments as well as corresponding simulations. While the active matter systems show clear non-equilibrium dynamics, this is less so for the skyrmion systems. In fact, it is shown that the examined skyrmion lattices can be described in a coarse-grained way with the help of classical equilibrium physics. Besides these differences, all of the systems undergo phase transitions and are studied for the case of two spatial dimensions only. But there is more that makes the skyrmion lattices in [A3] methodically even more similar to the ABPs in [A2]: In skyrmion lattices the individual skyrmions can be modelled coarse-grained as soft disks. They follow two dimensional Brownian dynamics with an additional term (the Magnus force for skyrmions, similar to the active force

for ABPs) and exhibit a purely repulsive potential. Figure 1 shows experimental realizations of these two classes of systems with (a) showing an active matter system similar to active Brownian particles and (b) showing a skyrmion lattice that is also simulated in [A3]. Even though the underlying nature of these two systems is fundamentally different, the dominating soft disk character makes them visually and structurally similar.

The goal of the research performed in the framework of this thesis is to better understand basic fundamentals in non-equilibrium systems. To do so, a strong focus is put on phase transitions and critical behavior of the examined systems. Determination of phases, phase transitions and in particular critical points, turns out to be very challenging in non-equilibrium systems for various reasons. A big part of the work performed therefore includes development and evaluation of new methods to tackle the many challenges occurring in the measurement of quantities in the considered non-equilibrium systems.

Knowledge about phase transitions and critical behavior in a given system does not only significantly broaden the understanding of the system. It is also crucial for many applications and some of the most important properties of the system. Besides the obvious applications, there are also lesser-known ones: Systems in the state of critical behavior, like supercritical fluids, are a very versatile tool for processing materials [8]. An everyday example is the extraction of caffeine with supercritical carbon dioxide to produce decaffeinated beverages and pharmaceuticals [9].

Active matter and skyrmions both promise unique behavior and new applications. It is well worth the effort to better understand them. Active particles for example are interesting for effective drug delivery [10] or self-assembly of materials and technical systems [11]. Even contraceptive use cases come to mind as sperm cells are actually self-propelled active particles [12], [13]. Skyrmions are potentially useful for computer memory and logic devices [14]. Even though it is easy to move them with external electric currents or fields [15], their movement does not move any matter or induce any direct currents, as skyrmions are only quasiparticles. This is an advantage compared to classical computational devices that rely on moving electrons and thus inducing currents and heat – the reason why CPUs need to be cooled.

Phase transitions and critical phenomena

Phases are well known from everyday life, as everyone is familiar with the solid, liquid and gas phase of water and the transitions between them (melting / freezing, boiling / condensation and sublimation / deposition). The critical point as well as the triple point of water are also quite prominent

examples, that can of course not only be found in water. At the critical point, the differences between liquid and gas phase vanish and water becomes a supercritical fluid. At the triple point in contrast, all three phases coexist.

Not only water, but a countless number of systems do feature different phases, phase transitions and critical points as well as triple points. Which current phase they are in depends on thermodynamic variables, such as for example temperature, pressure and density. By changing the relevant variables, a system can be brought from one phase to another undergoing a phase transition. These phase transitions can typically be categorized in phase transitions of first order and phase transitions of second order. While [A1] and [A2] deal with second order phase transitions, [A3] deals mainly with first order phase transitions.

According to Ehrenfest's classification, phase transitions of first order are called discontinuous because they are marked by certain discontinuities in the first partial derivative of thermodynamic potentials. Examples are the solid / liquid or the liquid / gas transition of water, the volume leap between liquid and gas phase is a corresponding discontinuity. Phase transitions of second order are in contrast called continuous as there is no discontinuity in the first derivative, but in the second. In a more modern classification first order transitions are simply called discontinuous and related to the latent heat involved in the phase transition while second order transitions are called continuous with no latent heat involved [16], [17].

Second order phase transitions can be characterized by an order parameter which becomes zero at the phase transition. They show a highly interesting set of critical phenomena like a divergence in correlation length at the phase transition, finite size effects in (small) simulation geometries, universality and critical slowing down. The critical point is such a second order phase transition. It can not only be found in water but in all systems that have liquid and gas phases as well as similar systems like the Ising model and the active matter models discussed in this work.

Observable	Critical exponent	Scaling	2D Ising value
Heat capacity C	α	$C \propto |\tau|^{-\alpha}$	0
Order parameter m	β	$m \propto |\tau|^{\beta}$	0.125
Susceptibility χ	γ	$\chi \propto |\tau|^{-\gamma}$	1.75
Correlation length ξ	ν	$\xi \propto |\tau|^{-\nu}$	1
Order parameter correlation	η	$\langle m(0)m(r)\rangle$ $\propto r^{-d+2-\eta}$	0.25

Table 1 Overview of some critical exponents, their scaling relation and 2D Ising value [16]–[21]. The distance to the critical point is given by τ (reduced temperature). For the order parameter correlation, r indicates the spatial distance and d the dimensionality of the system.

Because the correlation length is diverging at the critical point, it becomes much larger than the effective particle interaction range. The whole system becomes rather dominated by critical fluctuations than by the specific particle interaction. This remarkable process leads to universality: A wide range of systems with rather different forms of particle interactions behave the same way at their respective critical point [16], [17]. They can be categorized according to their universality class, which allows a deeper understanding of them. To determine which universality class a given system belongs to, one has to determine its critical exponents. Typical critical exponents are given in table 1. The scaling is valid in the vicinity of the critical point. Furthermore, the critical exponents are not independent, but obey scaling relations. A particularly important one is the hyperscaling relation [22]–[24]:

$$\gamma + 2\beta = 2\nu$$

For the 2D Ising system, the exact values of the critical exponents have been derived analytically while for many other systems one has to resort to approximations and / or simulations (e.g., 3d Ising) [16]–[20]. A well-established procedure to measure the critical exponents in simulations and thereby determine the universality class is described and applied in [A1] and similarly in [B1].

In contrast, a somewhat different approach is presented in [A2]. By instantaneously quenching active matter systems to the critical point on the one hand and deep inside the phase separated region on the other hand, more insight towards dynamical behavior is gained and conclusions about universal behavior and the comparison to 2D Ising can be drawn.

Another particularly interesting phase behavior can be found in two-dimensional continuous particle systems. Depending on the density, there is a disordered liquid phase and a densely packed solid phase. But in addition, there can be a hexatic phase in between the two phases. The solid phase is characterized by long-range orientational and quasi long-range positional order, while both are short ranged in the liquid phase. The intermediate hexatic phase is characterized by short-range positional and quasi long-range orientational order. Systems of soft disks with a repulsive power-law potential show a first-order liquid-hexatic and a continuous hexatic-solid transition. Depending on the exponent of the power-law potential, the liquid-hexatic transition becomes continuous and of the Kosterlitz-Thouless-Halperin-Nelson-Young (KTHNY) type [25]–[28]. There has been a long-standing controversy on the nature of these transitions in two dimensional systems with alternative theories suggesting a conventional first-order liquid-solid transition in the absence of a hexatic phase [29], [30]. The controversy has been resolved only recently by establishing that the fundamental hard-disk model has indeed a first-order liquid-hexatic transition and in contrast a

continuous hexatic-solid transition [28]. This remarkable phase behavior is studied closer for systems of two-dimensional skyrmion lattices in [A3], that can be modelled as soft disks. For obvious reasons the experimental realization of ideal two-dimensional systems is of great interest here, but also challenging. Skyrmions are a promising approach battling this challenge as they can be stabilized with thicknesses down to sub-nm and diameters in the range of micrometers, bringing them very close to a perfect two-dimensional system [A3].

Active matter and motility-induced phase separation (MIPS)

Active matter consists of self-propelled particles, which means that each particle is actively propelled along a certain direction. This direction is a specific property of each particle and therefore also called orientation. The orientation of each particle is furthermore subject to rotational diffusion. Dependent on the strength of the rotational diffusion, the particle's orientation changes over time: The stronger the rotational diffusion, the faster the changes in the orientation and vice versa. The velocity component with which each particle is propelled along its orientation is called active velocity. The higher the active velocity, the faster the particle's movement along its direction and vice versa. One can easily imagine, that with regard to the persistence of the particle's directed motion, active velocity and rotational diffusion are both relevant drivers. The combination of the two of them determines the actual magnitude of activity present in the active matter system. Low rotational diffusion and high active velocity account for highly directed motion and thus high activity. With more rotational diffusion or lower active velocity, the particle's path gets less directed. Infinite rotational diffusion or zero active velocity brings the system back to plain Brownian motion with no activity.

Besides simulations that are the subject of this thesis, there is a manifold of real-world active matter systems [21]: On the one hand, there are many biological systems that show active behavior, like bacteria [31], [32], biopolymer networks [33]–[35], sperm cells [12], [13], or even flocks of birds and sholes of fish [36], [37]. On the other hand, there are many experimental realizations of active particles [38]: By only partially coating particles with a coating material that interacts with the surrounding environment, a symmetry breaking propulsion can be achieved. This can be, for example [21], due to catalytic reactions [39]–[41], self-thermophoresis [42], certain flows [43]–[45], artificial flagella [46], or the local demixing in a supercritical fluid [47]–[49]. So-called Janus particles can be a concrete realization of the last-mentioned. They are particularly close to the ABPs discussed in [A2]. Janus particles consist of two different hemispheres, e.g., a silica particle that is coated by

gold or carbon on one hemisphere. When placing them in a water-lutidine mixture at a temperature just slightly below the mixture's critical temperature of 307K, they are solely subject to Brownian motion. But if they are illuminated by a laser, the coated hemisphere will pick up more heat than the other, causing the surrounding solvent to demix around the coated hemisphere and thus causing a directed propulsion [49]. The system then becomes active.

The activity itself is not a direct particle-particle interaction but rather a property of each of the particles in the system. It's beneficial to use very minimal forms of particle-particle interactions in order to best examine the effects of activity. The active matter systems studied in [A1] and [A2] are only subject to a simple repulsive particle interaction, there is no attraction between the particles. A phase transition to a solid or hexatic state can of course be achieved in purely repulsive particle systems by simply increasing density to very high packing fractions. This is done in [A3]. However, purely repulsive active matter systems exhibit phase transitions at much lower densities and that is what makes them so special [48].
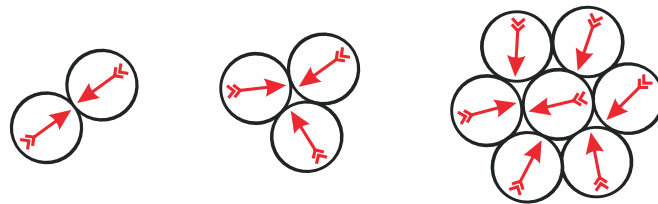

Figure 2 Schematic sketch of active particles blocking each other. From left to right: Two particles with opposite direction of active motion block each other. While the particles are reorienting, a third particle arrives and blocks the other two and vice versa. More particles join the emerging cluster and thus the inner particle is blocked, no matter how it is oriented.

If the rotational diffusion of the particles' orientations is low enough in relation to the active velocity, particles can block each other. Particles that initially block each other form a nucleation cluster. This happens by chance if particles collide with opposed orientations and hence opposed directed motions. Due to the rotational diffusion, the particles at the edge of such a cluster might turn away from it and the cluster would dissolve. For a low enough rotational diffusion this takes so much time, that in the meantime other particles collide with the cluster and join it. The newly joined particles subsequently block the inner particles from leaving the cluster (see figure 2). The cluster grows and phase separation occurs. The active velocity on the one hand moves the particles together, forming and stabilizing clusters. On the other hand, it is also the driver for a more directed motion of particles in the dilute phase, allowing them to reach emerging clusters faster than with

plain Brownian motion only. This kind of phase separation in active matter is called motility-induced phase separation (MIPS).

The phase behavior of MIPS is surprisingly similar to the gas liquid phase behavior in equilibrium systems. Not only is MIPS in contrast a non-equilibrium phenomenon, but the underlying mechanism causing the phase separation is also very different. Nevertheless, MIPS shows a similar binodal curve of coexisting densities terminated by a critical point. Therefore, it is of fundamental interest whether or not the phase behavior around such a non-equilibrium critical point is universal, and whether it can be attributed to one of the standard universality classes. These questions have also stirred up an ongoing controversy [4], [50]–[52]. While we found critical exponents for two-dimensional ABPs [B1] that are incompatible with any of the known universality classes, other numerical studies of related but different models have come to other conclusions, supporting Ising universality in two dimensions for off-lattice active Ornstein-Uhlenbeck particles [50] and a lattice variant of ABPs [52] (as well as for ABPs in three dimensions [53], [54]). These discrepancies and deviations from ideal Ising behavior could potentially be explained by recent new renormalization group studies of active models [51], [55]. They find additional fixed points to the Wilson-Fisher fixed point, which is connected to the Ising universality. The range in which the Wilson-Fisher fixed point determines the phase behavior can be limited by these additional points.

Therefore, the question arises, whether active matter's MIPS falls into a given universality class at all, or whether there are some model-dependent deviations from universality. The work in [A1] and [A2] shines more light one this question and highlights some of the model-dependent deviations from two dimensional Ising universality class.

A common approach to determine the critical point in equilibrium systems is to run simulations in a grand canonical ensemble (variable particle number / density) and measure density fluctuations throughout the simulation. In order to account for finite system size and diverging correlation length at the critical point, Binder's cumulant ratio is utilized [56], [57]:

$$Q_l(\tau) = \frac{\langle m_l^2 \rangle^2}{\langle m_l^4 \rangle}$$

Where m is the order parameter and τ the distance to the critical point. At the critical point Q_l becomes independent of the system size l, therefore the critical point can be determined as the cumulant's crossing for differently sized systems.

Nevertheless, in active matter systems it is unfortunately very challenging to accurately determine the critical point and the corresponding critical

exponents, that characterize a universality class. This is mainly due to two reasons:

First of all, there is up to now no suitable definition of chemical potential in any of these systems. Simulations can't be run in a grand canonical ensemble like equilibrium systems, they have to be run with fixed particle number and density. As a consequence, there are at any time coexisting phases of different densities within one simulation setup that is run within the phase separated regime. Still the order parameter of these systems is density, so there is a need to measure the differences in densities for the two phases around the critical point. An established method to do so is the so called subbox method, that divides the simulation box into smaller subboxes [58]–[60]. Since the particles can move freely within the simulation box, the particle numbers of the individual subboxes are not fixed and local density differences can be sampled. This method turned out to not work very well for active matter and doesn't work at all for lattice systems in two dimensions. This is due to interfaces between the different phase regions within the simulation box that obstruct a proper density distribution sampling.
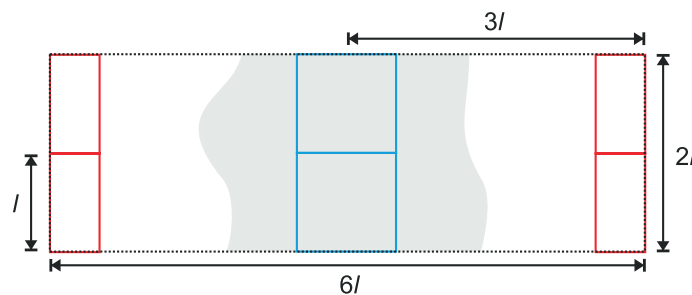

Figure 3 Schematic illustration of improved subbox method in a 1:3 geometry with two subboxes above each other in each of the two phase regimes.

Fortunately, I was able to develop an improved subbox method in the course of my diploma thesis: By using elongated simulation boxes, the two phases separate rather clearly because of the application of periodic boundary conditions along the short side of the box in a slab-like geometry. This allows us to determine the areas occupied by dense and dilute phases via the center of mass, so that the subboxes can be placed to avoid obstructing interfaces (see figure 3). More computational effort is the downside of that improvement. Still this method yielded good results in [A1] and [B1] as well as in other publications where it was adapted by other groups [50], [52], [61], [62].

The second reason is closely related to that downside: Only a small part of the simulation box can actually be used for measurements and thus generation of statistics. This alone means a three times higher computational

17

effort compared to a grand canonical simulation. But on top of that, the stability of the slab geometry and the interfaces is rather low for active matter. This does not come as a surprise as there are no attractive particle interactions. The slab might break and re-emerge in the course of the simulation which leads to severe deterioration in the quality of the statistical data. Consequently, an even higher amount of data has to be generated, resulting in way more computational effort. Last but not least, the instabilities grow with the size of the simulation box and limit the possible accuracy of measurements that way further.

MIPS and all the fundamentals of active matter described in this chapter do of course not only apply for simulations but also for experimental setups. There are various experimental realizations of active matter systems that all show the outlined genuine behavior. One of the benefits of simulations is however, that high densities and activities can be reached and studied easily. This is still difficult and limited in experimental setups. Especially the highly interesting region around the critical point can be accessed by simulations but less so by experiments as of today.

Active lattice systems

Discrete lattice systems are fairly simple systems that are lightweight in implementation and simulation. Nevertheless, they contain most, if not all the relevant properties found in equivalent continuous systems. Within the framework of this work simulations of MIPS around the critical point in continuous systems remained highly demanding. An immense amount of simulation data is required to gain reliable statistics and precise results. Therefore, active lattice systems turned out to be the more practicable approach to accessing static critical order parameters of MIPS.

While the simulations of continuous systems in [A2] and [A3] are run as Brownian dynamics (BD) simulations, the discrete lattice simulations in [A1] are run as Monte Carlo (MC) simulations. One of the most basic and common models to realize active matter in continuous simulations is that of active Brownian particles. They are the subject of the next chapter and [A2].

For the implementation of active matter in discrete lattice geometries, there is no such agreed upon model. Two possible implementations have been proposed recently and I will according to [A1] and [A2] refer to them as Model I [52] and Model II [63]. They differ a bit in the implementation of the rotational diffusion and in the lattice geometry (see figure 4). Model I was proposed on a hexagonal lattice (hex.) and Model II on a square lattice (sq.). To check for the effect of the underlying lattice geometry, I additionally implemented Model I on a square lattice. In total I programmed simulations for three different lattice models and used these in [A1] and [A2]. Beyond

this, I also varied the parameters and the actual implementation of these models in different aspects to examine the influence on the phase behavior. There seems to be an effect even on the critical behavior, but much more data is needed to make clear statements. This is why I had to focus on the three different models presented in [A1] in the end. For efficiency all lattice simulations were written in C.
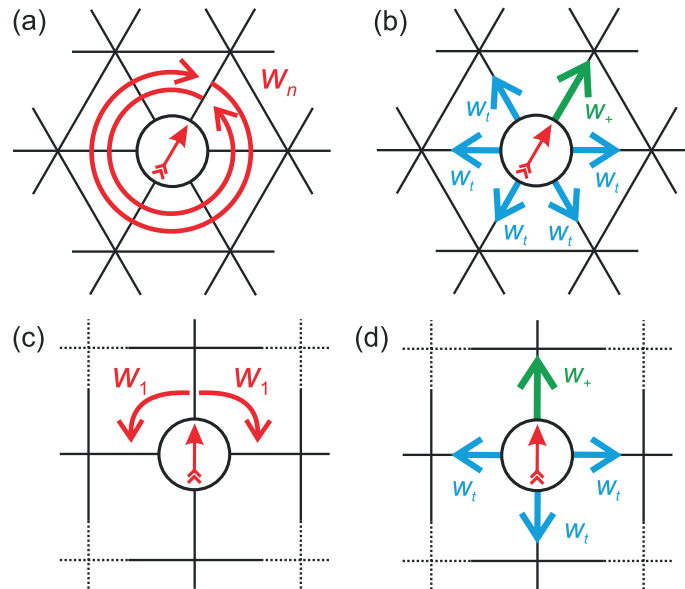

Figure 4 Schematic illustration of rotational diffusion in Model I (a) and Model II (c) as well as translational movement in Model I (b) and Model II (d). More details about the models and their implementation can be found in [A1].

In the two models, each lattice space can be occupied only by one particle at a time. This implements a hard disk like repulsion. Apart from that, there is no other interaction. Each particle has a discrete direction, which points to one of the possible four or six neighboring lattice spaces. This direction gets changed at random with a certain probability. The probability for direction changes thus determines the amount of rotational diffusion. A particle can only move to one of the neighboring lattice spaces at a time (in one MC step). An attempted move is always accepted if the destination lattice site is empty and rejected otherwise. The direction in which a move is attempted is set at random by a certain probability scheme: Movements in the particle's direction have a higher probability than a movement ("diffusion") in any other direction. The probability for moves in the particle's direction hence sets the amount of active propulsion in the system. Rotation and translation are serial in Model I and concurrent in Model II. More details about the models and their implementation can be found in [A1] and also in [A2].

Determining the critical points and the corresponding critical exponents β, γ and υ for all three models is the core analysis performed in [A1]. For this I ran

several simulations in elongated simulation boxes of different sizes around multiple activities around the critical point of each model. Each data point is backed by a cumulated CPU runtime of about half a year. I analyzed the data from the elongated simulation boxes with the improved subbox method discussed above. This enabled me to determine the critical points via the crossing of the Binder cumulant for different system sizes. Subsequently, I extracted the critical exponent v from the slope of the Binder cumulant around the critical point, β from the density differences of dense and dilute phase in the vicinity of the critical point and finally γ from the susceptibility (fluctuations of the order parameter) around the critical point. The analysis is analogous to that performed in [B1]. More details are provided in [A1].

Model	β	γ/v	$1/v$	$\gamma/v + 2\beta/v$
2D Ising	0.125	1.75	1	2
2D Ising (sim.)	0.113(1)	1.751(2)	0.97(3)	1.97
ABPs [B1]	0.45	1.47	0.67	2.07
Model I (hex.)	0.1567(3)	1.678(2)	1.03(2)	2.00
Model I (sq.)	0.1528(1)	1.695(3)	1.023(8)	2.00
Model II (sq.)	0.2208(1)	1.649(1)	1.021(7)	2.10

Table 2 Summary of obtained critical exponents for various simulated systems.

The results obtained are summarized above in table 2. The first three columns show the numerical results for the critical exponents for the different models and for comparison the 2D Ising model (exact results from theory and simulation results applying the same methodology as for active systems). The active lattice models show a systematic deviation from 2D Ising universality class that becomes even clearer in comparison to the results from 2D Ising simulations, as the applied methods appear to systematically underestimate β. Even more interestingly, the magnitude of these deviations varies between the different models. One might argue, that the deviations are due to limitations of the methods utilized for analysis. However, the combined result of all acquired order parameters (approximately) fulfill hyperscaling [22]–[24] for each model, as shown in the last column ($\gamma/v + 2\beta/v = 2$). This rather indicates, that there is some systematic deviation inherent to the models. This deviation is even stronger for ABPs, as argued in [B1]. A closer discussion about possible causes will be given in the conclusion chapter.

Active Brownian particles (ABPs)

Active Brownian particles (ABPs) are widely used in continuous simulations of active matter [64]–[71]. As their name suggest, they are an "extension" of

Brownian particles towards non-equilibrium active matter. The equations of motion are given by an overdamped Langevin equation [B1], [A2]:

$$\dot{\mathbf{r}}_k = -\frac{D_t}{k_B T} \nabla_k U + v_0 \begin{pmatrix} \cos \varphi_k \\ \sin \varphi_k \end{pmatrix} + \sqrt{2D_t} \mathbf{R}_k$$

The first term describes the particle-particle interaction, with the potential U arising from a purely repulsive Weeks-Chandler-Andersen (WCA) potential between the ABPs. This potential is in essence a short-ranged, purely repulsive and therefore shifted Lennard-Jones potential with a cut-off distance of $r = 2^{1/6}$. Analogously the potential's steepness is given by the parameter ε and the diameter of the ABPs is set to $\sigma = 1$. The translational diffusion constant is also set to $D_t = 1$, the Boltzmann constant is denoted as k_B and the temperature as T. In the second term, the active velocity v_0 propels each particle with constant speed along its orientation which is described by the angle φ_k. Thus, this term adds the activity to the equations of motion. Finally, the last term models Brownian motion as Gaussian noise with $\mathbf{R}_k$ being normal distributed Gaussian noise.

Furthermore, the particles' orientations described by φ_k are not constant but undergo free rotational diffusion with diffusion coefficient D_r as given by:

$$\dot{\varphi}_k = \sqrt{2D_r} R_r$$

More details about the precise implementation of ABPs utilized in this work can be found in [B1] and [A2]. While in [B1] inhouse code is used, [A2] uses the particle simulation toolkit HOOMD-blue [72] for simulating ABPs.

An analysis to determine the critical exponents analogous to the one performed on the active lattice systems in [A1] has previously already been done for ABPs in [B1]. Despite a tremendous amount of CPU time utilized for [B1], the statistical accuracy is limited and way behind the accuracy reached for the active lattice systems in [A1]. Determining the critical exponents for ABPs with higher accuracy would greatly help shining more light on the somewhat model dependent results for the critical exponents found in [A1] as this would allow to test and compare variations of the ABPs' implementation parameters. Throughout the course of this thesis, I therefore tried to improve accuracy for ABPs in numerous time-intensive attempts. Even though, none of them yielded significant enhancement, I want to shortly summarize these attempts and the rationale behind them:

First, we tried to improve statistics. Shifting from inhouse code (MPI accelerated) to HOOMD-blue (GPU accelerated) improved simulation speed and accordingly statistics. This benefit turned out to be limited by a comparably smaller number of available GPUs and the fact, that only very big simulation boxes of more than 100.000 particles can be run efficiently on GPUs. Simply simulating more particles in one system (bigger simulation

boxes) is no straight forward solution since this leads to less stable slabs, as discussed before. Hence, subsequent efforts followed which focused on improving slab stability and measuring methods.

Tests with other simulation geometries than 1:3, such as more elongated ones (like 1:4) or less elongated ones (like 1:2), did not provide a big improvement potential as opposed effects come to play: For more elongated geometries (with constant density) the relative interface area of a single slab becomes smaller and the interfaces are shifted away from the subboxes within the slab as the slab becomes broader. But on the other hand, the broader single slab then tends to break into several smaller slabs that distribute all over the simulation box, making any subbox measurement useless. For less elongated geometries the single slab is less prone to break apart, but then the interfaces are shifted closer to the subboxes within the slab as the slab becomes narrower. Since the interfaces are not straight but fluctuate a lot, the narrower slab increases the probability of interfaces crossing the subboxes and hence deteriorating the quality of the measured data. All in all, the 1:3 geometry already seems to be a good compromise between these effects.

Improving the data quality by shifting the interfaces away from the subboxes can also be achieved by using smaller but more subboxes within the given simulation box. In particular, I tested geometries with three and six instead of two subboxes above each other. However, the smaller subboxes are more affected by finite size effects that limit accuracy. To reach decent subbox sizes, the overall simulation box needs to be larger in this case. But then the vicious circle begins, considering that larger simulation boxes lead to less stable slabs. Obviously, there is an inherent limitation with this method that compromised all my attempts to improve accuracy.

Nevertheless, I also tried improving the placement of the subboxes to account for slab instabilities occurring for bigger system sizes. Usually only one overall center of mass for the whole simulation box is calculated and all the subboxes probing the dense phase are placed in that center of mass. This works fine, if the slab is perfectly parallel to the short side of the simulation box. But with increasing system size the slab is more likely to be crooked or show other deformations. I accounted for that by placing each subbox individually according to the center of mass of the respective horizontal slice it is placed in. For this the simulation box is sliced along the elongated side into as many equal stripes as there are subboxes to be placed above each other. Then each subbox gets placed according to the respective center of mass of the individual stripe and not according to the center of mass of the whole system (i.e. all the stripes combined). While this modification appeared promising at first, the overall data quality did not improve significantly. In conclusion, significant improvement likely requires

more fundamental changes to the methodology. I will discuss some basic ideas later on in the conclusions.

A similar direction I looked into, is if and how changes in the simulation parameters of ABPs can improve the data quality by making interfaces more stable throughout the simulation. The activity can for instance be controlled via the rotational diffusion or the active velocity. While one parameter is tuned, the other one stays constant. The value at which the constant parameter is fixed, can of course be chosen freely. In [B1] and [A2] for example, the rotational diffusion is fixed at $D_r = 3/d_{\mathrm{BH}}^2 \approx 2{,}4486$ with an effective hard disk Barker Henderson diameter $d_{\mathrm{BH}} = 1{,}10688$ [73] for a WCA potential with $\varepsilon = 100$. I tested higher and lower values for fixing the rotational diffusion. Furthermore, I tested fixing the active velocity at several values and tuning the rotational diffusion instead. And I also tested other values for the WCA parameter ε, hence changing the repulsive potential's steepness. This makes the ABPs exhibit a more soft-disk (lower ε) or hard-disk-like character (higher ε). All these variations should "in theory" be equivalent to each other. The concept of the so called Péclet number [70], [71] suggests, that all variations can be mapped to the same results (i.e., phase diagram). However, it turns out that this is not fully true for non-equilibrium systems, as the following interesting (but not published) observations show:

The shape and width of the phase diagram of ABPs depend on the applied active force or equivalently the applied active velocity. The higher the active velocity, the "broader" the phase diagram and vice versa. This means, that the binodal line for the dense phase is shifted towards higher densities with increased active velocity. When tuning the activity via rotational diffusion, the shift is determined by the set fixed value for the active velocity. When tuning the activity via active velocity, the shift increases with the activity along the binodal line. Mapping the different phase diagrams via the concepts of Péclet number and effective hard disk diameter reduces the discrepancies to some degree but not fully. This effect also depends on the parameter ε of the WCA potential. A softer potential gives a stronger effect, while a harder potential weakens the effect. As a consequence, there seems to be no simple way to an implementation independent phase diagram for ABPs.

These observations can easily be understood, if one imagines figuratively that the active force pushes the particles in the dense phase closer together. A closer packing is equivalent to a higher density. Hence the shift of the binodal line for the dense phase towards higher densities. At the same time the binodal line for the dilute phase is not affected (there is obviously no aggregation) which in sum results in a broader phase diagram. The active lattice systems do of course not show such an effect, because they are implemented as real "hard disks" – one lattice space can only be occupied

by one particle and there is no space between the lattice spaces. In equilibrium, the effective hard disk diameter, also called Barker–Henderson diameter, should map soft disks to effective hard disks. It accounts for the random force due to Brownian motion but not for the additional active force propelling the particles in non-equilibrium systems. The described observations have been shown more closely by Yannik Muche in his bachelor thesis [74], which I co-supervised.

While varying simulation parameters yielded interesting findings, none of the variations did contribute to the improvement of the measuring accuracy. Therefore, I was unfortunately not able to further examine whether the variation of rotational diffusion, active velocity or WCA potential do have an influence on the critical exponents or their measurement. Since the (measurement of the) critical exponent β depends on the coexistence densities, the shape of the phase diagram might hint to such an influence.

Exploring the discussed possible accuracy improvements went hand in hand with very time-consuming simulations of different activities and simulation box sizes around the critical point. Each of these simulations requires a fairly long runtime (minimum one week, depending on the system size) to achieve a descent level of equilibration and statistics. Only then a first assessment whether the quality of the Binder cumulant crossing is improved or not can be made. A more defined crossing is the pre-condition for a more exact determination of the critical exponents. One of the above-mentioned enhancements or a wise combination of them might lead to slightly better results in an even longer run. However, I was looking for a "game changer" but did not find it in any of the options discussed.

It's important to note, that the dominant problem of instable slabs in ABPs is less of a problem in lattice systems. I will come back to this in the conclusions.

Even though my work did not succeed in yielding a better determination of critical exponents for ABPs, I was able to further investigate critical behavior in these systems. To do so, the study in [A2] focusses on dynamical properties in active systems.

Dynamics in active systems

The dynamical properties of active systems can be studied by quenches of homogeneous configurations to state points inside the miscibility gaps and to the critical point. Following the quench, the system's far-from-steady-state dynamics can be investigated by calculating quantities associated with structure and characteristic length scales. An understanding of non-equilibrium dynamics following these quenches is of fundamental as well as

practical relevance and recent focus has been especially on active matter systems [75]–[83].

The work performed in [A2] studies the dynamical properties of ABPs as well as of the active lattice systems already introduced in [A1]. Before the quench takes place, all the systems are equilibrated in the homogeneous phase, i.e., at an activity well below MIPS. After sufficient equilibration the systems are quenched by suddenly changing the activity to a much higher value. Subsequently the active systems start to form clusters as MIPS takes place. The emerging structures and their growth provide insights to the dynamical behavior. In [A2] two different types of quenches are studied: Quenches to state points inside the miscibility gaps (i.e., deep inside the phase separated regime) on the one hand and quenches right to the critical point on the other hand. For the quenches to the critical point, the information about critical activity and density obtained in [B1] and [A1] is crucial.

The growth following a quench inside the coexistence region is dominated by power-law behavior, i.e., $l \propto t^\alpha$ with l being the length scale, t the time and α the growth exponent (not to be mistaken with the critical exponent α). The growth is furthermore self-similar in nature, meaning that the emerging patterns at different times only differ from each other in terms of the length scale. The two-point equal time correlation function therefore scales with l, too [83].

The aging phenomena is another important property that can be studied following the quench. It is captured in the relaxation behavior of the two-time order-parameter auto-correlation function and attributes an age to the system. This means, that the development state of the system can be distinguished at different points in time. In contrast to equilibrium states, the time translation invariance in growing systems is not obeyed and the two-time order-parameter auto-correlation function scales like

$$C_{ag} \propto \left(\frac{t}{t_w}\right)^{-\alpha\lambda}$$

with t_w being the age and λ the aging exponent [84].

In case of quenches to the critical point, the correlation in the system is expected to grow over time as $\xi(t) \propto t^{1/z}$ with z being the dynamic critical exponent [79], [85], [86]. In addition, the two-point equal time correlation function can be rewritten with respect to the fractal nature of the structure (see [A2]) in the form of

$$C(r,t) \propto r^{-d+2-\eta}C(r/\xi(t))$$

with the critical exponent η being accessible via two-point equal time correlation function and correlation length $\xi(t)$ [85], [87].

The values of α, λ and z and their determination are of fundamental importance in the field of dynamics of phase transitions. The results for structure growth and aging of ABPs in [A2] appear to be quite similar to those observed during phase separation in the 2D Ising model. However, for the active lattice models, there are deviations in the case of quenches inside the coexistence regions, but none in the case of quenches to the critical point. These deviations still need further assessment in the future and were not included and discussed in [A2].

Skyrmions

Skyrmions are certain mathematical objects which are realized in many areas of physics [88]. The concept was first suggested by nuclear physicist Tony Skyrme while studying pion fields around 1960 [89]–[91]. Later on, the concept of skyrmions was generalized: A skyrmion can be defined as "a topologically stable, smooth field configuration describing a non-trivial surjective mapping from coordinate space to an order parameter space with a non-trivial topology" [88].

The subject in this work are magnetic skyrmions. They are topologically stable solitons that were predicted theoretically [92]–[94] and demonstrated in experiments [15], [95], [96]. These magnetic whirls are quasiparticles that can be created in a variety of materials ranging from bulks of ferromagnets to thin films [14]. Depending on the material, there are two main types of skyrmions: Bloch-type [97] and Neel-type [98] skyrmions. In bulks of ferromagnets Bloch-type chiral skyrmion can be stabilized due to bulk Dzyaloshinskii-Moriya interaction (DMI) [14], [99]. In thin films Neel-type hedgehog skyrmions can be stabilized due to interfacial DMI [14], [100]. The different spin structures of the two types are shown in figure 5. In bulk systems skyrmions are not necessarily 2D like, as the "skyrmion tube" length can easily exceed the skyrmion diameter. This is different in magnetic thin film systems where skyrmions with diameters three orders of magnitudes larger than their thickness can be stabilized as done in [A3], making them almost perfectly two-dimensional. Furthermore, skyrmions interact in a coarse-grained manner with a repulsive interaction potential which opens up the possibility to model them as soft disks. While ABPs are genuinely regarded soft matter, skyrmions are regarded hard matter, as they reside in solid magnetic materials. Such a differentiation is misleading here: As shown in [A3] the coarse-graining allows to treat the ensemble behavior of skyrmions with the very same set of instruments as used for soft matter.
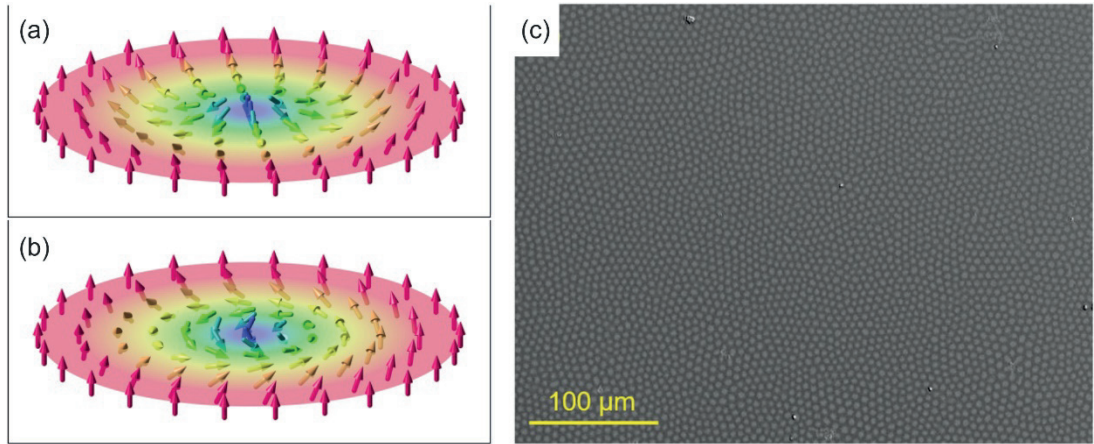
Figure 5 Left hand side: The vector field of magnetic skyrmions with (a) being a hedgehog skyrmion (Neel-type) and (b) a spiral skyrmion (Bloch-type). Picture by Karin Everschor-Sitte and Matthias Sitte licensed under CC BY 3.0 (https://commons.wikimedia.org/wiki/File:2skyrmions.PNG)
Right hand side (c): Kerr microscope image of a skyrmion lattice with μm sized skyrmions, showing the disk like character of skyrmions in magnetic thin film systems. [A3].

Skyrmions can externally be moved or manipulated using spin-transfer torques [101], [102] and spin-orbit torques [103] with the latter being very power efficient for possible use cases in electronics. In addition, skyrmions can be subject to magnetic pinning [104] and the skyrmion-Hall effect [105]. For the coarse-grained approach presented in this work, these effects are of secondary importance and will therefore not be covered further.

Although the behavior of single or few skyrmions can be simulated on a micromagnetic level, this is not feasible for larger numbers of skyrmions. A common coarse graining approach on particle-level is based on the Thiele equation yielding a set of Langevin equations [106]–[109]:

$$\eta \boldsymbol{v}_i = \boldsymbol{F}_i^M + \boldsymbol{F}_i^S + \boldsymbol{f} \quad \text{with} \quad \boldsymbol{F}_i^M = \beta \hat{z} \times \boldsymbol{v}_i$$

Where $\boldsymbol{v}_i(t)$ is the skyrmion drift velocity, η the damping coefficient, $\boldsymbol{F}_i^S$ a repulsive skyrmion-skyrmion interaction, $\boldsymbol{f}$ thermal white noise and $\boldsymbol{F}_i^M$ the Magnus force acting on the direction perpendicular to the skyrmion's velocity. The strength of the Magnus force is set by the parameter β.

The Thiele equation is a simplification of the Landau-Lifshitz-Gilbert (LLG) equation derived by projecting the LLG equation onto the relevant translational modes [110], [111]. The resulting Magnus force term of the Thiele equation is related to the physics of a so-called Berry phase [88], [110]–[112]. Once a skyrmion is moving in an electric current, the Magnus force arises from the interplay (spin-torque coupling) of dissipationless spin currents circulating around each skyrmion and the spin currents induced by the electric current [112], [113]. It pushes the moving skyrmion perpendicularly to its direction of motion. The rotating spin currents of the skyrmion act in the electric current similar to a rotating ball in the

surrounding air flow in the case of the classical Magnus effect, hence the name [88].

The Langevin equation for skyrmions shown above is very similar to the one describing ABPs: Both equations feature repulsive interaction, a velocity dependent additional force and thermal noise. However, the Magnus force is non-dissipative, since it is acting perpendicular to the skyrmion's velocity [108], [114]–[118].

Closely packed systems of skyrmions are called skyrmion lattices and are the prime subject of [A3]. Please note, that these "lattices" are not comparable to what is commonly associated with lattice systems or lattice order in solid bodies. Skyrmions in a skyrmion lattice can still move around and change places, however the movement is very limited due to the high density. Hence, the individual skyrmion velocity is very low and therefore the associated Magnus force becomes more or less negligible. This opens up the possibility of further coarse graining: Modelling skyrmions in a skyrmion lattice as soft disks without a magnus force turns out to be sufficient to capture their statical and to some degree dynamical behavior. In this regard, the modelling becomes identical to the one for ABPs with zero activity.

The first question of interest then is, how the skyrmion-skyrmion interaction potential looks like and especially how steep it is. Unfortunately, the forces between the skyrmions can't be measured directly in the experimental setup. A common approach to access the interaction potential indirectly is to run an iterative Boltzmann inversion on the one-dimensional pair-correlation function. This approach turned out to be meticulous for the systems examined in the course of this thesis. Therefore, the more robust technique of combining simulations and experiments as shown in [A3] was developed and used. It also laid the foundation for further work where iterative Boltzmann inversion was successfully adapted to similar systems in an advanced procedure [119]. As shown in [A3], the skyrmion-skyrmion interaction potential can also be reconstructed solely with the help of simulations:

In a simulated system of density equal to the experimental system, the potential is adjusted until the one-dimensional pair-correlation function of the simulated system matches the experimentally measured one. Within certain inaccuracies and limitations, the simulated potential and the real-world potential of the experimental skyrmion lattice are identical in this case [120], [121]. This method is also a nice example, how simulations and experiments can complement each other.

In order to make the matching work, first of all, the experimental skyrmion lattice is visualized and recorded via Kerr-microscope imaging. The resulting black and white movies show the skyrmions floating around as disks on a

plane. Their position and density have to be determined from these movies. A standard tracking package can handle this job sufficiently accurate if all parameters are chosen correctly. The pair-correlation function is then calculated straightforwardly from the skyrmion positions. The Skyrmion density is simply the number of skyrmions detected in the area of the image frame.

As already mentioned, one of the interesting things about two dimensional systems of soft disks is, that with increasing density they undergo a phase transition from liquid to solid phase with an intermediate hexatic phase. Since the experimentally created skyrmions in [A3] can be regarded as almost ideal two-dimensional systems and are acting like soft disks, this immediately raises the question, whether skyrmion lattices show a similar phase behavior.

Determining the phase state of the skyrmion lattice is again a very challenging task. It turns out that the equilibration of a two-dimensional system of soft disks in the hexatic (as well as in the solid phase) takes a profound amount of time. While the local structure and therefore the pair-correlation function form out rather quickly, the quasi-long range orientational order takes a multiple of that time to emerge. This is a manageable problem for simulations, but it was not possible to stabilize the experimental skyrmion lattice in [A3] for a sufficient amount of time. The common approach of determining the phase via the long range orientational order is not well suited in this case. In [A3] another approach is therefore presented:

The local orientational order parameter is a standard measure to quantify, as the name suggests, the local orientational order of a system [26], [122]. In case of a hexagonal order, it is also called hexagonal order parameter and given by:

$$\psi_6(k) = \frac{1}{n_k} \sum_{l=1}^{6} e^{i6\theta_{kl}}$$

Where θ_{kl} describes the angle of the connecting line between a (central) skyrmion k and the lth of its n_k nearest neighbours with respect to a defined fixed axis [26]. The absolute value of this parameter yields $|\psi_6| = 1$ for a perfect hexagonal order, and a value between 0 and 1 otherwise.

One can utilize the spatial correlation of the hexagonal order parameter in order to quantify the long range orientational order in a system, which results in very poor signals for the experimental skyrmion lattices, as explained before. Instead, I found in [A3], that for soft disks with power law potential, the mean value of the hexatic order parameter appears to yield a fixed absolute value at the liquid-hexatic phase transition. This value was found to

be roughly $\langle|\psi_6|\rangle \approx 0.69$, independent of the exponent of the underlying power law potential.

With the help of this heuristic finding, the experimental skyrmion lattices in [A3] could be characterized and the degree of hexagonal structure in them could be mapped over the external experimental parameters. So, we were able to determine, which set of parameters drives the skyrmion lattice towards the hexatic / solid phase and which setup already shows the onset of these highly interesting phase states. Figure 2 in [A3] nicely summarizes these results and shows, how the structure of the skyrmion lattice depends on the magnetic out-of-plane field and the temperature. A setup at 338K temperature and 20μT out-of-plane field was found to be in an emerging hexatic or even solid phase exhibiting clusters of around 100 skyrmions with the same orientation of hexagonal order (see figure 6). This shows, that skyrmion lattices can be used as 2D model systems with advantages in terms of tunability and speed compared to conventionally used 2D model systems such as colloids [A3].
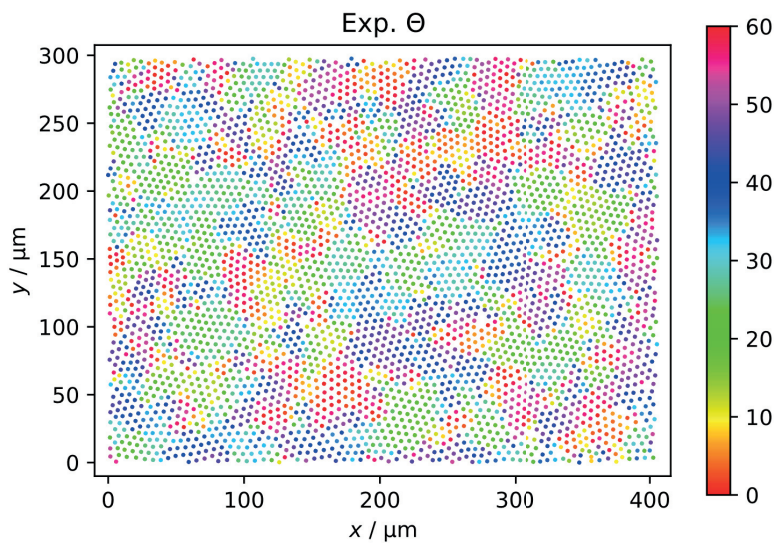
Figure 6 Spatial distribution of the local orientational order parameter ψ_6 of individual skyrmions for the experimental setup at 338K temperature and 20μT out-of-plane field (as shown in figure 3 in [A3]). The color-coding visualizes the orientation of ψ_6, that is, the orientation angle θ. Similar coloring indicates clusters of skyrmions with the same orientation of hexagonal order.

Publication [A1] [1]

„Critical behavior in active lattice models of motility-induced phase separation" (Eur. Phys. J. E 2021, 44, 53)

F. Dittrich, T. Speck, P. Virnau

Author Contributions

"PV and TS designed the research. FD wrote and performed the simulations and analyzed the data. All authors contributed to writing the manuscript."

Personal impact

Gathering and analyzing the data on which this work is based is my main contribution. For this I coded the different models in C. In pre-production runs I roughly determined the critical point, in order to choose the final simulation parameters and range. I ran the final simulations on the Mogon cluster of the University of Mainz. After that I analyzed the data gathered from the simulations with self-written Python scripts, generated the plots and extracted the critical exponents from them. I further contributed all the figures and sketches, as well as a substantial amount of writing of the manuscript. The paragraph on the hyperscaling relation in Appendix A was developed and written by T. Speck.

THE EUROPEAN
PHYSICAL JOURNAL E

Regular Article - Flowing Matter

Critical behavior in active lattice models of motility-induced phase separation

Florian Dittrich, Thomas Speck[a], and Peter Virnau[b]

Institute of Physics, Johannes Gutenberg-Universität, Mainz, Germany

Abstract Lattice models allow for a computationally efficient investigation of motility-induced phase separation (MIPS) compared to off-lattice systems. Simulations are less demanding, and thus, bigger systems can be accessed with higher accuracy and better statistics. In equilibrium, lattice and off-lattice models with comparable interactions belong to the same universality class. Whether concepts of universality also hold for active particles is still a controversial and open question. Here, we examine two recently proposed active lattice systems that undergo MIPS and investigate numerically their critical behavior. In particular, we examine the claim that these systems and MIPS in general belong to the Ising universality class. We also take a more detailed look on the influence and role of rotational diffusion and active velocity in these systems.

1 Introduction

Non-equilibrium active systems composed of self-propelled particles offer a wide range of interesting behavior and applications [1–3]. A fundamental phenomenon is the so-called motility-induced phase separation (MIPS) [4]: At large propulsion speeds and low rotational diffusion, self-propelled particles block each other due to excluded volume and form initial clusters. If the timescale for the rotational diffusion of the particle orientations at the border of such a cluster is larger than the time it takes to enrich the cluster with additional particles, a dynamical instability leading to non-equilibrium phase separation is induced. Although the phase-separated state resembles passive liquid–gas separation with dense domains surrounded by an active gas, no explicit attractive interactions are required. Still, the phase behavior is very similar, with the binodal curve of coexisting densities terminated by a critical point below which the system remains homogeneous for all densities. The question whether or not the behavior close to such a non-equilibrium critical point is universal, and whether it can be attributed to one of the standard universality classes, is not only of fundamental interest but has also stirred up an ongoing controversy [5–8].

Numerical studies of active Brownian particles (ABPs) [9–16] are a common approach to investigate MIPS in a simple continuous system. These particles are modeled as disks interacting with each other via a purely repul-

sive Weeks–Chandler–Anderson potential in the framework of an overdamped Langevin equation. In addition, they are propelled with constant speed along their orientation, which is subject to rotational diffusion. For this system, we have determined the location of the critical point in two dimensions and reported critical exponents, which are incompatible with any of the known universality classes [5]. To gain access to the critical point and the critical exponents, we have proposed a novel method to sample subboxes that minimizes the influence of interfaces on density fluctuations.

In contrast, subsequent numerical investigations of related but different models have come to a different conclusion, supporting Ising universality in two dimensions for off-lattice active Ornstein–Uhlenbeck particles [8] and a lattice variant of ABPs [7] (and for ABPs in three dimensions [17,18]). Following generic arguments of renormalization [19], however, all these models (in two dimensions) should fall into the same universality class and thus exhibit the same critical exponents. Indeed, in a first renormalization study of an active field theory ("active model B+" [20,21]) it was found that the critical behavior is controlled by the Wilson–Fisher fixed point [6]. What, then, is the reason for the reported differences? Regarding geometry and subboxes, all three numerical works have employed the same method (for details, see Sec. 2.2). One reason could be insufficient statistics, or insufficient range of system sizes leading to a biased estimate of critical exponents. Or, more intriguingly, are there additional features that characterize universality classes in active matter? We stress that MIPS of repulsive particles is a genuine non-equilibrium phenomenon. The effect of self-propulsion on the critical behavior in models that

---

[a] e-mail: thomas.speck@uni-mainz.de (corresponding author)

[b] e-mail: virnau@uni-mainz.de

∯ Springer

exhibit phase separation already under equilibrium conditions has been studied for Lennard-Jones interactions [22] and a three-dimensional Asakura–Oosawa model [23] driven by a Vicsek-type force [24–26] and found to be compatible with the 3d Ising universality class [27].

In this manuscript, we take another step toward a comprehensive understanding of critical behavior in active matter. To this end, we numerically investigate different variants of two-dimensional active lattice gases with excluded volume and dynamics that break detailed balance. While a range of active lattice gas models has been investigated [28–33], we focus on two variants that mimic active Brownian particles. In particular, we study two lattice geometries (the square and hexagonal lattice) and two implementations of the dynamics, either treating rotation and translation serial [7] or concurrently [34]. Our numerical results indicate that details of the dynamics have an influence on the critical behavior and question the proposition that MIPS falls into Ising universality.

2 Methods

2.1 Critical behavior

Before embarking on the computational study, let us recall some of the properties close to a critical point. We consider systems that undergo phase separation with two coexisting phases having different densities ρ. The two phases are identified with gas (ρ_{gas}) and liquid (ρ_{liq}). The (average) order parameter is the difference, $m = \rho_{\text{liq}} - \rho_{\text{gas}}$. As we approach the critical point, the gap in m closes and follows a path through the critical point. Hence, we observe

$$m \sim \tau^{\beta}, \tag{1}$$

whereby τ measures the distance to the critical point (typically the reduced temperature) and β is the corresponding critical exponent. The transition is continuous, with $m > 0$ for $\tau > 0$ and $m = 0$ in the homogeneous phase for $\tau < 0$. In addition, both the susceptibility χ and the correlation length ξ diverge at the critical point,

$$\chi \sim \tau^{-\gamma}, \qquad \xi \sim \tau^{-\nu}, \tag{2}$$

defining two more exponents. Of particular importance is Ising universality in equilibrium systems with short-range interactions and scalar order parameter, for which in two dimensions the exponents can be obtained analytically [35–37]

$$\beta = \tfrac{1}{8}, \qquad \gamma = \tfrac{7}{4}, \qquad \nu = 1. \tag{3}$$

Note that these three critical exponents are not independent but obey the *hyperscaling relation*
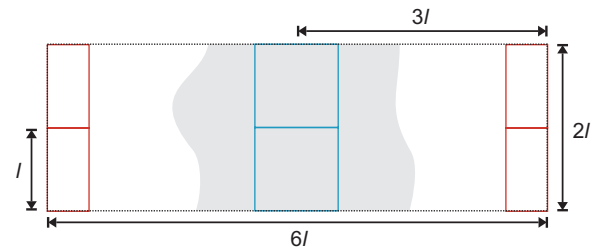
$$\gamma + 2\beta = 2\nu. \tag{4}$$

Fig. 1 Sketch to illustrate the simulation box setup. The evaluated subboxes of size $l \times l$ are placed in the dense (cyan) and dilute (red) phase. The overall simulation box is set to size $2l \times 6l$

Arguments why this relation might still be valid for driven active systems are sketched in "Appendix" A.

The diverging correlation length ξ implies that the critical behavior is modified in finite systems, where the correlation length is bounded by the system size l. One of the most remarkable successes of computational statistical physics is that the critical behavior can still be extracted from simulations of finite systems [38,39]. To locate the critical point, we turn to Binder's cumulant ratio

$$Q_l(\tau) = \frac{\langle m_l^2 \rangle^2}{\langle m_l^4 \rangle}, \tag{5}$$

which becomes independent of l exactly at the critical point. Note that $m_l = (N_l - \langle N_l \rangle)/l^2$ in the lattice gas formulation with N_l being the number of particles. Plotting the ratio Q_l as a function of some parameter for different l thus allows—notwithstanding systematic effects as discussed below—to locate the critical point from the intersection of curves. Moreover, the derivative $dQ_l/d\tau|_{\tau=0} = 1/\nu$ yields the inverse of the critical exponent ν. Once we have located the critical point, we can extract β from plotting $\langle m_l \rangle$ as a function of τ. Finally, we exploit the scaling form $\chi_l = l^{\gamma/\nu}\tilde{\chi}(l/\xi)$ for the susceptibility with scaling function $\tilde{\chi}$ that depends on system size through the ratio l/ξ. Plotting the susceptibility (obtained from the fluctuations of the order parameter) as a function of l allows to extract the ratio γ/ν. We thus have access to the three critical exponents ν, γ and β.

2.2 Simulations

While the ensemble of choice for simulations of critical behavior in equilibrium is the grand canonical ensemble, for driven active systems breaking detailed balance this route is not available due to the absence of a comprehensive framework in which a chemical potential is defined (although attempts have been made [40,41]).

Therefore, we closely follow the method and analysis proposed in Ref. [5]. All simulations were performed in a periodic box with 1:3 geometry. In such elongated boxes, the dense phase nucleates to a slablike struc-
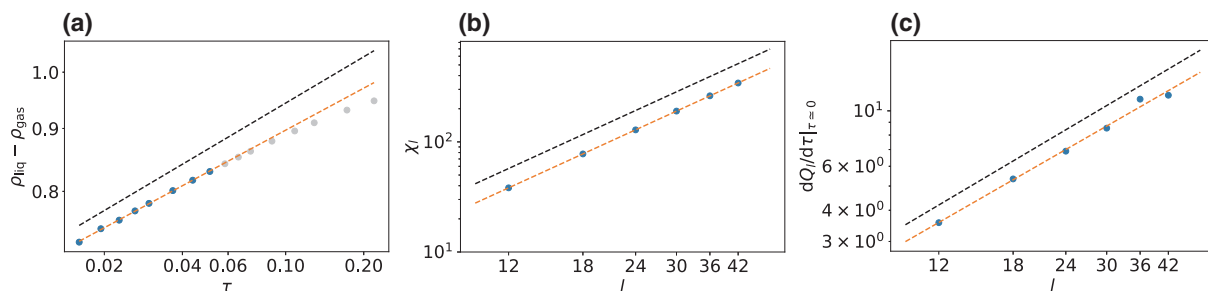
Fig. 2 Estimation of the critical exponents for the 2d Ising model. The black dashed lines show the slopes with the analytical values [Eq. (3)]. Gray dots in (a) were excluded from the analysis since they are too far from the critical point and have moved away from the power-law scaling

ture, cf. Fig. 1. The slab arises along the short side of the box and connects to itself via periodic boundary conditions. Its position inside the simulation box can be easily determined as the center of mass of all particles.

In order to measure dense and dilute phase, as well as to avoid interface regions between the two phases, we place two quadratic subboxes of size l above each other right in the center of mass to sample the dense phase (see Fig. 1). Another set of two subboxes is placed shifted away by one half of the simulation box's width from the center of mass to sample the dilute phase. In total, we sample the number of particles N_l within the four subboxes of size l in a simulation box of total size $2l \times 6l$. Note that N_l is counted for each of the four subboxes separately, resulting in four measurements for each snapshot. By adjusting the size of the simulation box through the subbox size, we couple the maximum correlation length to l and achieve a clear crossing point of Q_l for different l. The susceptibility is evaluated as $\chi_l = \langle (N_l - \langle N_l \rangle)^2 \rangle / \langle N_l \rangle$. Coexistence densities of dense and dilute phase (ρ_{liq} and ρ_{gas}) are obtained as plateau values of density profiles generated from a simulation box of size 252×84 (corresponding to $l = 42$) at activities slightly above the tentative critical point.

We use the same system sizes of $l = 12, 18, 24, 30, 36, 42$ for all simulations, resulting in simulation boxes of size 24×72, 36×108, 48×144, 60×180, 72×216, 84×252. The number density is always 0.5, which gives the corresponding particle numbers 864, 1944, 3456, 5400, 7776, 10584. Furthermore, we chose all activities to be at comparable relative distance to the critical point.

As reference, in Fig. 2 we show our analysis applied to the 2d Ising model. Since the 2d Ising model is subject to critical slowing down, we get somewhat poorer statistics (see "Appendix" B). Nevertheless, the analysis yields the following critical exponents

$$\beta \simeq 0.113(1), \quad \gamma/\nu \simeq 1.751(2), \quad 1/\nu \simeq 0.97(3) \quad (6)$$

in good agreement with the analytical values. Errors in this and later sections refer to statistical errors

obtained by splitting respective data sets into three parts and calculating the standard error of the mean. While γ/ν agrees exactly, there is a slight underestimation for $1/\nu$ and a noticeable underestimation for β. While the error of $1/\nu$ might be within statistical uncertainties, the deviation observed for β is more systematic: The power-law scaling is clearly only valid very close to the critical point. However, measuring points closer to the critical point than shown in Fig. 2 is challenging. Below we show that the active lattice models follow a power-law behavior over a wider range.

3 Model I: serial rotation/translation

3.1 Model description

We first turn to the model studied in Ref. [7] employing a hexagonal lattice, which we will refer to as model I. On a hexagonal lattice each particle has six neighboring sites and six discrete directions it can be orientated toward (Fig. 3). Specifically, each Monte Carlo (MC) step works as follows:

1. A particle is picked at random.
2. A Gaussian distributed random number (with standard deviation σ and zero mean) is drawn and rounded to the nearest integer n. The current orientation of the particle is adjusted by that integer ($n = 1$ means one step clockwise, $n = -1$ means one step counterclockwise, $n = 2$ means two steps clockwise and so on), cf. Fig. 3a.
3. A movement along the new orientation of the particle is chosen with probability $w_+ = 25/30$, and other directions are chosen with probability $w_t = 1/30$ each mimicking translational diffusion, cf. Fig. 3b.
4. If the target lattice site is empty the move is accepted, otherwise the move is rejected. This ensures that each lattice site is either unoccupied or occupied by exactly one particle.
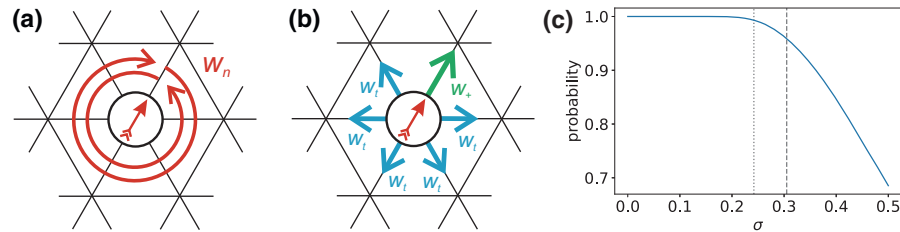
Fig. 3 Sketch to illustrate serial model I on a hexagonal lattice. **a** First, the orientation (arrow) of the particle is updated drawing a random number from a Gaussian distribution. **b** Then, a move along the particle's orientation is attempted with rate w_+, diffusion along another direction is attempted with rate w_t each. **c** Probability to keep the current orientation as a function of σ (as given by the integral over the Gaussian distribution from -0.5 to 0.5). Dashed and dotted lines correspond to critical values for model I on the hexagonal ($\sigma_c \simeq 0.3048$) and square lattice ($\sigma_c \simeq 0.2415$)
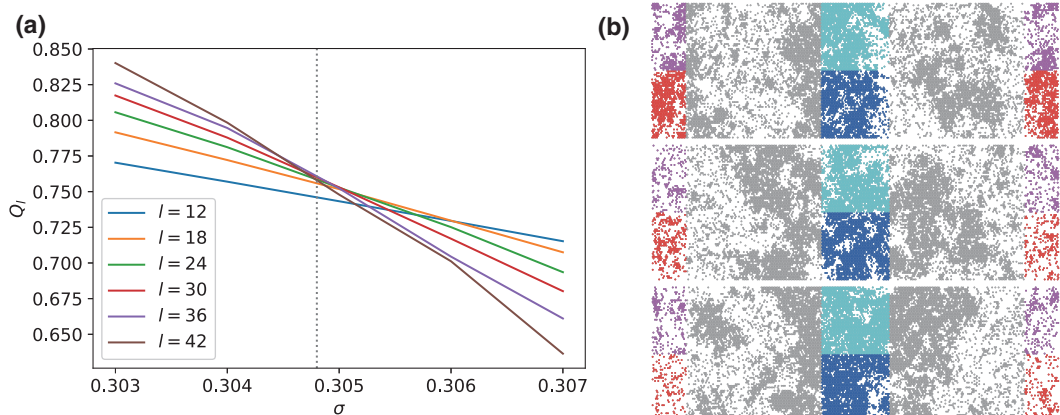
Fig. 4 **a** Cumulant ratios Q_l for model I on the hexagonal lattice. The dotted line indicates the estimated critical value $\sigma_c \simeq 0.3048$ as the mean crossing point for $l = 24, 30, 36, 42$ excluding the two smallest system sizes. Note that each tick on the x-axis corresponds to one simulation point. **b** Snap-shots for the largest system of $l = 42$ below the critical point at $\sigma = 0.307$ (top), at the critical point at $\sigma = 0.3048$ (middle) and above the critical point at $\sigma = 0.303$ (bottom). Particles are colored according to the subbox they are in

Note that the adjustment of orientation in step 2 is always accepted and a translation does not change the orientation of the particle. Since w_+ and w_t are fixed, the "activity" of the system is solely adjusted via the rotational diffusion, which is defined by the width σ of the Gaussian distribution. A low value for σ corresponds to low rotational diffusion and therefore highly persistent motion [see Fig. 3c]. Note that the probability to keep the current orientation is not linear in σ, especially not around the estimated values for the critical points. It is also important to note that in contrast to model II discussed below, rotation (step 2) and translation (step 4) are always performed in series.

3.2 Analysis and results

By closely following the analysis described in Sec. 2.2, we determine the critical point $\sigma_{cr,I} \simeq 0.3048$ as the average of the cumulant ratio crossings (Fig. 4) for the four largest system sizes under consideration ($l = 24, 30, 36, 42$). This value is in agreement with the

results published in Ref. [7], which has analyzed systems of comparable system sizes. Excluding the two smallest boxes ($l = 12, 18$)[1], the cumulant ratios for the bigger boxes cross within a small interval as expected for critical scaling.

Figure 5a–c shows results for the order parameter, the susceptibility and the derivative of the cumulant ratio. Fitting power laws yields the following exponents

$$\beta \simeq 0.1567(3), \quad \gamma/\nu \simeq 1.678(2), \quad 1/\nu \simeq 1.03(2) \tag{7}$$

and thus $\nu \simeq 0.97$ and $\gamma \simeq 1.63$. While the agreement with the corresponding 2d Ising values is reasonable for ν ($\nu_{\text{Ising}} = 1.0$) and γ ($\gamma_{\text{Ising}} = 1.75$), the exponent β differs by more than 25% from $\beta_{\text{Ising}} = 0.125$. This disagreement is also clearly visible in Fig. 5a.

---

[1] The fact that only intermediate box sizes cross is common for block density distribution methods also in passive systems [42].
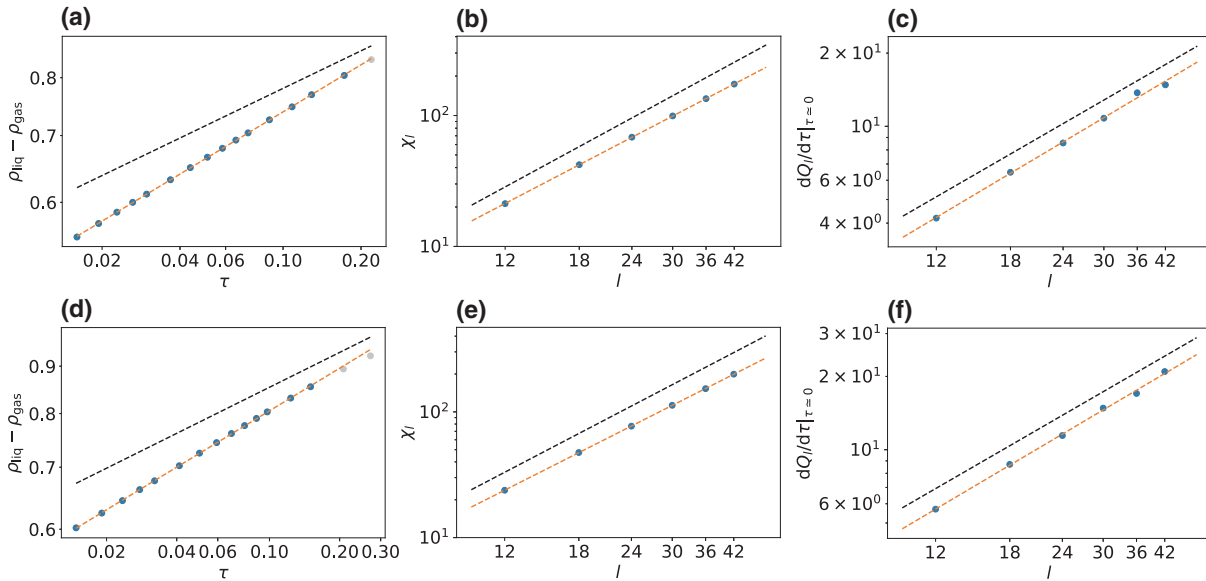
Fig. 5 **a**–**c** Estimating the critical exponents for model I. Plotted are (a) the order parameter $\rho_{\mathrm{liq}} - \rho_{\mathrm{gas}}$, **b** the susceptibility χ_l and **c** the slope of the cumulant ratio at the critical point. **d**–**f** Corresponding determination for model I but on a square lattice with $\sigma_c \simeq 0.2415$. Gray dots in (a) and (d) were excluded from the analysis. The black dashed lines show the slopes with the critical exponents for the 2d Ising system

To test the influence of the underlying lattice geometry, we have also performed an analogous investigation of the model on a square lattice with $w_+ = 17/20$ for movements along the particles current orientation and $w_t = 1/20$ for the three remaining directions. The results are shown in Fig. 5d–f with exponents

$$\beta \simeq 0.1528(1), \quad \gamma/\nu \simeq 1.695(3), \quad 1/\nu \simeq 1.023(8)$$
(8)

and thus $\nu \simeq 0.98$ and $\gamma \simeq 1.66$. These critical exponents are very similar to the hexagonal case and within numerical uncertainties, indicating that the influence of the underlying lattice is negligible as one would expect.

4 Model II: concurrent rotation/translation

4.1 Model description

The second model is based on a square lattice and has been proposed in Ref. [34]. As illustrated in Fig. 6, there are now six possible moves: either rotation of the particle orientation clockwise or counterclockwise by 90° with weight w_1 [Fig. 6a], or translation along the orientation with weight w_+ or any of the three other directions with weight w_t [Fig. 6b]. In contrast to model I, the weight $w_1 = 0.1$ for rotation is now kept constant and we vary w_+ with $w_t = 1$. Moreover, in each MC step one of the moves is selected according to its weight. Hence, the particle can either rotate or move in one time step, which we term concurrent.
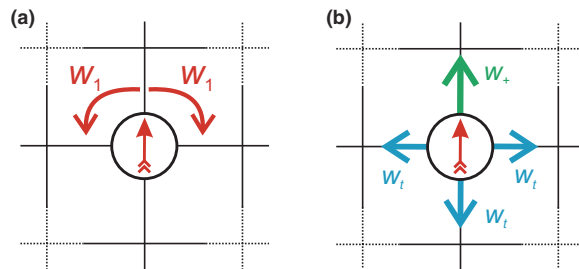

Fig. 6 Sketch to illustrate model II on a square lattice. **a** The particle orientation is turned clockwise or counterclockwise by 90° with rate w_1. **b** A move along the orientation is attempted with rate w_+, diffusion into any other direction with rate w_t each. Note that only one of these moves is attempted in each time step. The probability for each move is given by the respective rate divided by the sum of all rates

4.2 Analysis and results

Figure 7 shows the crossings of the cumulant ratios Q_l for different box lengths l. The crossings start to converge for the bigger boxes with $l \geq 24$. Hence, we only take these system sizes into account and determine the critical point to be at $w_{+,\mathrm{cr}} \simeq 4.76$. Corresponding results for the critical exponents are displayed in Fig. 8, for which we find

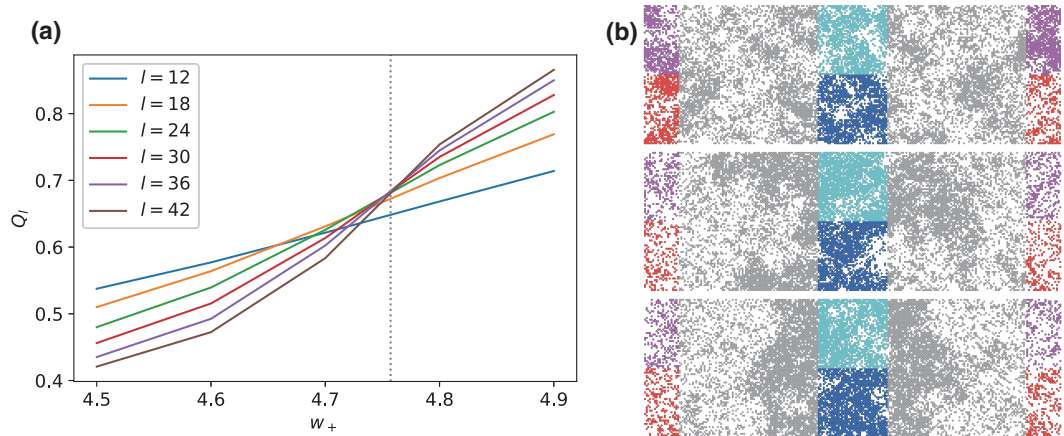$$\beta \simeq 0.2208(1), \quad \gamma/\nu \simeq 1.649(1), \quad 1/\nu \simeq 1.021(7).$$
(9)

Fig. 7 **a** Cumulant crossing for model II yielding a critical point at $w_{+,\mathrm{cr}} \simeq 4.76$ as determined by the mean crossing point for $= 24, 30, 36, 42$ (dotted line). Note that each tick on the x-axis represents a w_+ at which simulations for the various system sizes took place. **b** Snapshots for the largest system of $l = 42$ below the critical point at $w_+ = 4.5$ (top), at the critical point at $w_+ = 4.76$ (middle) and above the critical point at $w_+ = 4.9$ (bottom). Particles are colored according to the subbox they are in
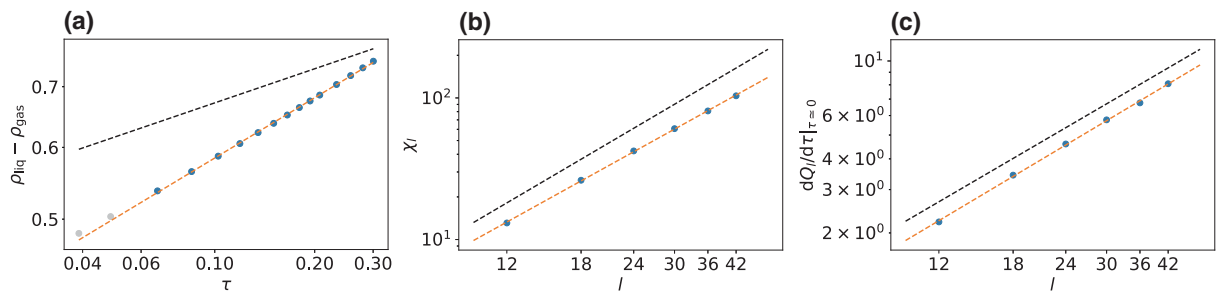
Fig. 8 Critical exponents for model II, cf. Fig. 5. Note that for (a) the gray points were not considered for the fit as slabs started to dissolve, resulting in an ill-defined plateau of the density profiles. In (b) $w_+ = 4.76$ has been used. For comparison, the black dashed lines indicate the 2d Ising critical exponents

While $\gamma \simeq 1.68$ and $\nu \simeq 0.98$ again exhibit reasonable agreement with 2d Ising values (1.75 and 1, respectively), $\beta = 0.221$ exceeds the corresponding value (0.125) by almost a factor of two. Note that β needs to be measured further from the critical point than in model I because the density profiles lose their stability faster. This indicates that fluctuations are stronger and the slab in the 1:3 simulation box stays less stable in the vicinity of the critical point for model II.

5 Alternative determination of β

The accuracy of measuring the exponent β from the density difference is limited by the fact that it becomes more and more difficult to reliably estimate this difference as we approach the critical point. For the Ising model (cf. Fig. 2), this has led to a noticeable deviation from the known analytical value. There is an alternative method using the density fluctuations $\langle (\rho_l - \langle \rho_l \rangle)^2 \rangle \sim l^{-2\beta'/\nu}$ at the critical point which is equivalent to (and

therefore not independent from) how γ/ν is determined from χ_l, see also Ref. [8]. The densities for the subboxes are given by $\rho_l = N_l/l^2$. This analysis is shown in Fig. 9. For the 2d Ising model we now obtain $2\beta'/\nu \simeq 0.249(1)$, which is in excellent agreement with the analytical value. The values for the other models are included in Table 1, but it is clear that they substantially deviate from 2d Ising universality.

6 Discussion and conclusions

Our results for the critical exponents are summarized in Table 1. We have also added the corresponding values for active Brownian particles as determined in Ref. [5]. For all lattice models studied here, we find values for ν that are in very good agreement with Ising universality ($< 3\%$ smaller) and values for γ/ν that are in good agreement ($< 5\%$ smaller). These values are in agreement with plots shown in Ref. [7], which concludes that Ising universality holds. This conclusion seems
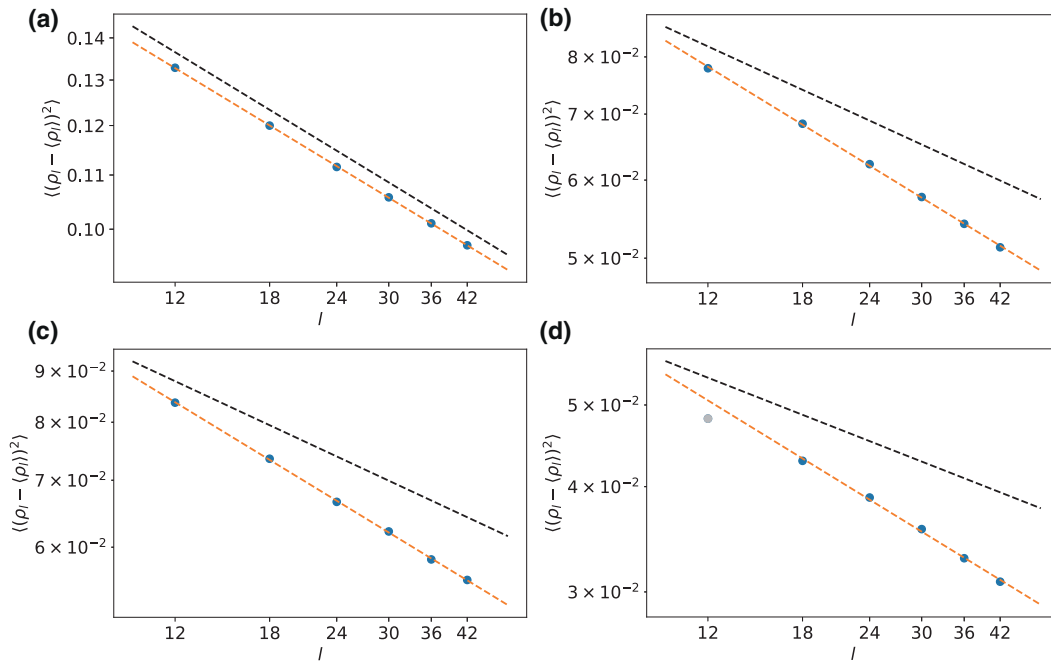
Fig. 9 Alternative determination of β. Plotted is the slope of $\langle(\rho_l - \langle\rho_l\rangle)^2\rangle$ for the different system sizes at the critical point, which yields $-2\beta'/\nu$. For comparison, the black dashed lines indicate the analytical 2d Ising slope of $-1/4$. Fits are shown for: **a** 2d Ising model, **b** model I on hexagonal lattice, **c** model I on square lattice and **d** model II. For model II, there is a noticeable bending and the gray dot in (d) was excluded from the analysis

Table 1 Comparison of critical exponents

Model	β	γ/ν	$1/\nu$	$\gamma/\nu + 2\beta/\nu$	$2\beta'/\nu$
2d Ising	0.125	1.75	1	2	0.25
2d Ising (sim.)	0.113(1)	1.751(2)	0.97(3)	1.97	0.249(1)
ABPs [5]	0.45	1.47	0.67	2.07	–
Model I (hex.)	0.1567(3)	1.678(2)	1.03(2)	2.00	0.334(2)
Model I (sq.)	0.1528(1)	1.695(3)	1.023(8)	2.00	0.327(4)
Model II (sq.)	0.2208(1)	1.649(1)	1.021(7)	2.10	0.391(6)

The first three columns are the estimated values. The fourth column is the hyperscaling relation Eq. (4), which is approximately obeyed by all models. The last column shows results for the alternative determination of β' (cf. Sec. 5). Errors refer to statistical errors obtained by splitting respective data sets into three parts and calculating the standard error of the mean

questionable when taking the exponent β into account, which deviates substantially. Indeed, the determination of β is technically the most challenging. However, note that the hyperscaling relation Eq. (4) places a strong constraint on the exponents. From $\gamma/\nu \simeq 1.68$ and $\nu \simeq 0.98$, we can obtain an estimate for $\beta \simeq 0.157$ that is in excellent agreement with the numerically estimated values for model I on both lattice geometries, supporting that reduction of γ (and ν) is not a statistical effect but systematic. In our analysis, we cannot completely exclude the possibility that the system sizes under consideration are still too small and larger sizes would lead to a slightly shifted critical point. This

could in principle also shift the critical exponents, particularly β/ν, while the influence on β and $1/\nu$ is less pronounced.

The value for β estimated for model II is even larger. However, in this case the hyperscaling relation is only fulfilled approximately, which might indicate that β is too large. We have observed that obtaining "good" crossings of the cumulant ratio in this model is more challenging, which might be because the speed is changed in contrast to the rotational diffusion in model I. Moreover, the distance to the critical point is larger since the determination of $\rho_{\text{liq}} - \rho_{\text{gas}}$ requires stable liquid slabs with a well defined plateau of the

density profile. The alternative method of Sec. 5 yields a smaller $\beta' \simeq 0.19$. We notice that the ratio γ/ν has become even smaller, moving away from the Ising value. While this seems to indicate an influence of the different dynamic rules on the critical behavior, we cannot rule out that the scaling closer to the critical point changes (but note that the smaller value of γ/ν accommodates a larger β). Even further from Ising universality are off-lattice active Brownian particles, where also the exponent ν now changes substantially from $\nu = 1$ to $\nu \simeq 1.5$. Still, the hyperscaling relation is again approximately fulfilled, indicating that the exponents are consistent. We cannot exclude the possibility that corrections to scaling are relevant and modify these exponents in a way that is compatible with scaling relations [43].

Based on our numerical results, we find the general conclusion from Ref. [7] that MIPS belongs to the 2d Ising universality class to be somewhat premature. Our results even cast some serious doubts on the weaker claim that model I exhibits 2d Ising behavior. At this point, we would like to emphasize that the numerical evidence presented in Ref. [7] is based on figures similar to our Figs. 5(b) and (c) in which the slopes for the 2d Ising values were drawn on top of the simulation values suggesting excellent agreement. However, the authors neither provide values for γ or ν, nor did they mention the discrepancy for the exponent β.

Instead, we see mounting evidence that the critical behavior for models exhibiting MIPS is at least to some degree model-dependent. Whether or not there is an underlying Ising universality or any universality at all, and to which extent deviations occur and why still remains an interesting and challenging question for simulations and theory alike.

Author contribution statement

PV and TS designed the research. FD wrote and performed the simulations and analyzed the data. All authors contributed to writing the manuscript.

A Hyperscaling relation

The scaling relation Eq. (4) is typically derived from a free energy following arguments originally developed by Widom [44]. Since active matter is steadily driven away from thermal equilibrium, its behavior is not governed by such a free energy. However, the property of the free energy that is mostly exploited in deriving scaling laws is that of a *generating function*, and some of the results can be transferred to non-equilibrium systems.

To this end, consider the cumulant generating function

$$\phi(\tau, h) = \ln \sum_{\mathcal{C}} p(\mathcal{C}; \tau) e^{h\hat{m}(\mathcal{C})} \tag{10}$$

for the order parameter $\hat{m} = \hat{m}(\mathcal{C})$ summing over all possible configurations $\mathcal{C}$ with probability $p(\mathcal{C}; \tau)$ depending on the control parameter τ. The auxiliary field h allows to obtain the average m and susceptibility χ as

$$m = \left.\frac{\partial \phi}{\partial h}\right|_{h=0} = \langle \hat{m} \rangle, \qquad \chi = \left.\frac{\partial^2 \phi}{\partial h^2}\right|_{h=0} = \langle \hat{m}^2 \rangle - m^2. \tag{11}$$

A system with linear extend l and correlation length ξ in d dimensions can be viewed as $n \simeq (l/\xi)^d$ independent systems, for which the joint probability $p(\mathcal{C}) = \prod_{i=1}^n p_\xi(\mathcal{C}_i)$ becomes a product of probabilities $p_\xi(\mathcal{C}'; \tau)$ for the configuration in a smaller system with linear extend ξ. With $\hat{m}(\mathcal{C}) = \sum_{i=1}^n \hat{m}(\hat{C}_i)$ we have

$$\phi(\tau, h) \simeq \ln \left[\sum_{\mathcal{C}'} p_\xi(\mathcal{C}') e^{h\hat{m}(\mathcal{C}')} \right]^n \simeq (l/\xi)^d \tilde{\phi}(h/|\tau|^\Delta). \tag{12}$$

In the second step, we invoke the usual scaling hypothesis positing a scaling function $\tilde{\phi}(x)$ of the combined argument $h/|\tau|^\Delta$ with gap exponent Δ. With $\xi \sim \tau^{-\nu}$ we thus find $m \sim \tau^{d\nu - \Delta} \sim \tau^\beta$ and $\chi \sim \tau^{d\nu - 2\Delta} \sim \tau^{-\gamma}$. Eliminating $\Delta = d\nu - \beta$ leads to $\gamma + 2\beta = d\nu$ [Eq. (4)]. Hence, this scaling relation only requires extensivity and homogeneity of the generating function, two properties that are not restricted to equilibrium.

B Critical slowing down

As mentioned above, the statistical quality of the data obtained for the active lattice models is way better than that obtained for the 2d Ising model, despite comparable simulation run time. We determine the autocorrelation function for $N - \langle N \rangle$ in order to estimate effects of critical slowing
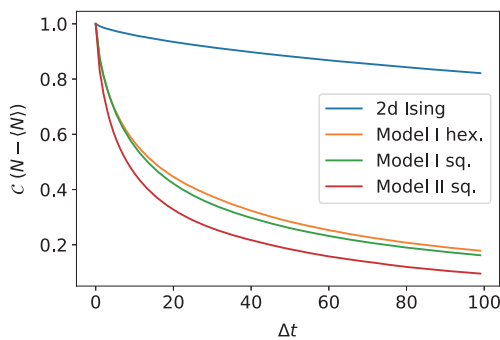
Fig. 10 Autocorrelation of the density fluctuations $N - \langle N \rangle$ for the different models plotted for the largest system size of $l = 42$ and at the respective critical point. Averaged over all individual subboxes and all simulation data available

Table 2 Amount of simulation data for the biggest simulation box ($l = 42$) at each respective critical point

Model	Run time	MC steps per individual run	Number of individual runs
2d Ising	15 days	ca. 1,230,000,000	20
Model I (hex.)	15 days	ca. 170,000,000	12
Model I (sq.)	15 days	ca. 175,000,000	12
Model II (sq.)	15 days	ca. 285,000,000	12

A comparable amount of data is used for each of the other simulation points. The same run time is applied to the smaller simulation boxes, therefore more data is available for these systems. The difference in MC steps performed is a result of different computational effort for the particular models. The equilibration time is not included

down. The strongest effects can be found for the biggest systems; therefore, Fig. 10 only shows the results for $l = 42$ (simulation box of size 84×252). Each model is evaluated at its respective critical point. The autocorrelation function is calculated for each individual subbox separately and then averaged over all subboxes and all simulation data obtained. The time lag Δt is given in units of 1,000 Monte Carlo (MC) steps. For each MC step, each lattice site is on average picked once. So in total $\Delta t = 1$ is in this case equivalent to performing 21,168,000 simulation steps. Table 2 provides an overview of the total amount of simulation data evaluated for this work.

Figure 10 shows that the correlation for the 2d Ising model is quiet persistent, indicating critical slowing down. On the other hand, the correlations decay rather quickly for the active lattice models and are more or less gone after $\Delta t = 100$. Consequently, critical slowing down is not an issue for the active lattice models. The main reason for these differences is the acceptance schemes in the models. For the Ising model, the metropolis criterion has to be fulfilled for a spin swap. In comparison, each move to a free lattice site is accepted for the active lattice models and there is no interaction except for hard repulsion.

References

1. T. Vicsek, A. Zafeiris, Phys. Rep. **517**(3–4), 71 (2012)
2. C. Bechinger, R. Di Leonardo, H. Löwen, C. Reichhardt, G. Volpe, G. Volpe, Rev. Mod. Phys. **88**(4) (2016)
3. G. Gompper, R.G. Winkler, T. Speck, A. Solon, C. Nardini, F. Peruani, H. Loewen, R. Golestanian, U.B. Kaupp, L. Alvarez, T. Kioerboe, E. Lauga, W. Poon, A.D. Simone, F. Cichos, A. Fischer, S.M. Landin, N. Soeker, R. Kapral, P. Gaspard, M. Ripoll, F. Sagues, J. Yeomans, A. Doostmohammadi, I. Aronson, C. Bechinger, H. Stark, C. Hemelrijk, F. Nedelec, T. Sarkar, T. Aryaksama, M. Lacroix, G. Duclos, V. Yashunsky, P. Silberzan, M. Arroyo, S. Kale, J. Phys. Condens. Matter **32** (2020)
4. M.E. Cates, J. Tailleur, Annu. Rev. Condens. Matter Phys. **6**, 219 (2015)
5. J.T. Siebert, F. Dittrich, F. Schmid, K. Binder, T. Speck, P. Virnau, Phys. Rev. E **98** (2018)
6. F. Caballero, C. Nardini, M.E. Cates, J. Stat. Mech.: Theory Exp **2018**(12) (2018)
7. B. Partridge, C.F. Lee, Phys. Rev. Lett. **123** (2019)
8. C. Maggi, M. Paoluzzi, A. Crisanti, E. Zaccarelli, N. Gnan, arXiv:2007.12660 (2020)
9. Y. Fily, M.C. Marchetti, Phys. Rev. Lett. **108** (2012)
10. G.S. Redner, M.F. Hagan, A. Baskaran, Phys. Rev. Lett. **110** (2013)
11. J. Stenhammar, A. Tiribocchi, R.J. Allen, D. Marenduzzo, M.E. Cates, Phys. Rev. Lett. **111** (2013)
12. J. Stenhammar, D. Marenduzzo, R.J. Allen, M.E. Cates, Soft Matter **10**, 1489 (2014)
13. A. Wysocki, R.G. Winkler, G. Gompper, EPL (Europhys. Lett.) **105**(4), 48004 (2014)
14. J. Bialké, T. Speck, H. Löwen, J. Non-Cryst, Solids **407**, 367 (2015)
15. J.T. Siebert, J. Letz, T. Speck, P. Virnau, Soft Matter **13**(5), 1020–1026 (2017)
16. P. Digregorio, D. Levis, A. Suma, L.F. Cugliandolo, G. Gonnella, I. Pagonabarraga, Phys. Rev. Lett. **121**, (2018)
17. F. Turci, N.B. Wilding, arXiv:2012.10365 (2020)
18. A.K. Omar, K. Klymko, T. GrandPre, P.L. Geissler, arXiv:2012.09803 (2020)
19. P.C. Hohenberg, B.I. Halperin, Rev. Mod. Phys. **49**, 435 (1977)
20. C. Nardini, E. Fodor, E. Tjhung, F. van Wijland, J. Tailleur, M.E. Cates, Phys. Rev. X **7** (2017)
21. E. Tjhung, C. Nardini, M.E. Cates, Phys. Rev. X **8** (2018)
22. V. Prymidis, S. Paliwal, M. Dijkstra, L. Filion, J. Chem. Phys. **145**(12) (2016)
23. J. Zausch, P. Virnau, K. Binder, J. Horbach, R.L. Vink, J. Chem. Phys. **130**(6) (2009)
24. T. Vicsek, A. Czirók, E. Ben-Jacob, I. Cohen, O. Shochet, Phys. Rev. Lett. **75**, 1226 (1995)
25. S.K. Das, S.A. Egorov, B. Trefz, P. Virnau, K. Binder, Phys. Rev. Lett. **112** (2014)
26. B. Trefz, S.K. Das, S.A. Egorov, P. Virnau, K. Binder, J. Chem. Phys. **144**(14) (2016)
27. B. Trefz, J.T. Siebert, T. Speck, K. Binder, P. Virnau, J. Chem. Phys. **146**(7) (2017)
28. A.G. Thompson, J. Tailleur, M.E. Cates, R.A. Blythe, J. Stat. Mech. 02029 (2011)

29. R. Soto, R. Golestanian, Phys. Rev. E **89** (2014)
30. K.R. Pilkiewicz, J.D. Eaves, Phys. Rev. E **89** (2014)
31. A.P. Solon, J. Tailleur, Phys. Rev. E **92** (2015)
32. A. Manacorda, A. Puglisi, Phys. Rev. Lett. **119**, (2017)
33. M. Kourbane-Houssene, C. Erignoux, T. Bodineau, J. Tailleur, Phys. Rev. Lett. **120** (2018)
34. S. Whitelam, K. Klymko, D. Mandal, J. Chem. Phys. **148**(15), (2018)
35. L. Onsager, Phys. Rev. **65**(3–4), 117 (1944)
36. C.N. Yang, Phys. Rev. **85**(5), 808 (1952)
37. T.T. Wu, B.M. McCoy, C.A. Tracy, E. Barouch, Phys. Rev. B **13**, 316 (1976)
38. K. Binder, Zeitschrift für Physik B Condensed Matter **43**(2), 119 (1981)
39. K. Binder, Ferroelectrics **73**(1), 43 (1987)
40. S. Paliwal, J. Rodenburg, R. van Roij, M. Dijkstra, New J. Phys. **20**(1) (2018)
41. A.P. Solon, J. Stenhammar, M.E. Cates, Y. Kafri, J. Tailleur, Phys. Rev. E **97** (2018)
42. H. Watanabe, N. Ito, C.K. Hu, J. Chem. Phys. **136**(20) (2012)
43. A. Aharony, M.E. Fisher, Phys. Rev. Lett. **45**, 679 (1980)
44. B. Widom, J. Chem. Phys. **43**(11), 3892 (1965)

Author Contributions

"SD and PV designed the research. FD wrote and performed the simulations. FD analyzed the data with the help of JM. JM prepared all the plots and fitted the data. All authors contributed to writing the manuscript."

Personal impact

For this work I wrote and performed all simulations regarding active systems. I used the HOOMD-blue toolkit to do the simulations of the ABPs and wrote Python code to set up and run the simulations. In an effort to perform the lattice simulations, I altered the simulations I previously wrote for publication [A1].

In order to analyze the trajectories acquired from the simulations, I used calculation scripts provided by J. Midya and S. Das. J. Midya further evaluated and plotted the output data from these calculation scripts. He also provided simulation scripts for running the 2D Ising simulations shown for comparison in the SI.

To enhance the original idea of looking into the dynamical behavior of ABPs for quenches to state points inside the miscibility gaps, I suggested extending that investigation to active lattice systems as well as to quenches to the critical point.

I made substantial contributions to writing the methods part of the script and minor contributions to writing the other parts. Furthermore, I provided the snapshots shown.

Growth and aging in a few phase-separating active matter systems

Florian Dittrich,[1] Jiarul Midya [ORCID],[2,3] Peter Virnau,[1,*] and Subir K. Das [ORCID][4,†]

[1]*Institute of Physics, Johannes Gutenberg University Mainz, 55128 Mainz, Germany*
[2]*Theoretical Physics of Living Matter, Forschungszentrum Jülich, 52425 Jülich, Germany*
[3]*School of Basic Sciences, Indian Institute of Technology, Bhubaneswar 752050, India*
[4]*Theoretical Sciences Unit and School of Advanced Materials,*
Jawaharlal Nehru Centre for Advanced Scientific Research, Jakkur P.O., Bangalore 560064, India

Via computer simulations we study evolution dynamics in systems of continuously moving active Brownian particles. The obtained results are discussed against those from the passive 2D Ising case. Following sudden quenches of random configurations to state points lying within the miscibility gaps and to the critical points, we investigate the far-from-steady-state dynamics by calculating quantities associated with structure and characteristic length scales. We also study aging for quenches into the miscibility gap and provide a quantitative picture for the scaling behavior of the two-time order-parameter correlation function. The overall structure and dynamics are consistent with expectations from the Ising model. This remains true for certain active lattice models as well, for which we present results for quenches to the critical points.

I. INTRODUCTION

Nonequilibrium models of self-propelled or active particles describe a multitude of phenomena ranging from the movement of bacteria and artifical microswimmers to macroscopic flocks of birds [1–3]. Some of these systems exhibit cooperative phenomena such as motility-induced phase separation (MIPS) [4] that resembles the passive liquid-gas phase separation but occurs in absence of any attractive interactions: At large propulsion speeds and low rotational diffusion, artificial microswimmers can self-trap and form clusters. The resulting phase diagram shows a binodal curve of coexisting densities that ends in a critical point. Computationally, artificial microswimmers are often studied with continuously moving active Brownian particles (ABPs) [5–13] or variants thereof, but recently active lattice models have gained attention as well [14–16].

Whether the phase behavior in the vicinity of a nonequilibrium critical point is unique, and if it belongs to any standard universality class is a question of fundamental interest and has sparked an ongoing controversy [15–22]. For ABPs, a determination of the critical point and its associated critical exponents revealed results incompatible with any known universality class [17], while active Ornstein-Uhlenbeck particles appear to be compatible with 2D-Ising behavior [19,21,22]. Similarly, active lattice models exhibit exponents close to the 2D-Ising values [15] even though small model-dependant deviations remain [16]. For the description of static critical behavior first theoretical approaches have appeared recently which may reconcile some of these discrepancies [18,20].

In this manuscript we focus on dynamical aspects of active systems. Understanding of nonequilibrium dynamics following quenches of homogeneous systems to the critical point, as well as to state points inside the coexistence region, is of fundamental as well as practical relevance [23,24]. In the context of passive matter systems associated phenomena received much attention. In this broad area, recent focus has been on active matter systems [25–31]. In a class of studies the objective is to understand the scaling behaviors related to structure, growth, and aging [23,26,32–36]. Below we provide brief descriptions of these nonequilibrium aspects.

Typically, growth in such nonequilibrium situations, following quenches inside the coexistence region, occurs in a power-law fashion, viz., average size of domains, rich or poor in particles of a particular type, ℓ, grows with time (t) as [23]

$$\ell \sim t^\alpha. \tag{1}$$

Such a growth is usually self-similar in nature, i.e., the domain patterns at two different times are different from each other only via a change in ℓ. This property is reflected in the scaling behavior of the two-point equal time correlation function [23],

$$C(r, t) = \langle \psi(\vec{r}, t)\psi(0, t) \rangle - \langle \psi(\vec{r}, t) \rangle \langle \psi(0, t) \rangle, \tag{2}$$

as [23]

$$C(r, t) \equiv \tilde{C}(r/\ell). \tag{3}$$

Here ψ is a space- ($\vec{r}$) and time-dependent order parameter. Another important property associated with such nonequilibrium systems is the aging phenomena. This can be captured in the relaxation behavior of the two-time order-parameter auto-correlation function [32]

$$C_{ag}(t, t_w) = \langle \psi(\vec{r}, t)\psi(\vec{r}, t_w) \rangle - \langle \psi(\vec{r}, t) \rangle \langle \psi(\vec{r}, t_w) \rangle, \tag{4}$$

024609-1

where t_w $(< t)$ is a waiting time, also referred to as the age of the system. As opposed to the equilibrium systems, the time translation invariance in growing systems is not obeyed. Note that the rate of relaxation is expected to be different for different ages of a system. Thus, C_{ag} does not exhibit collapse of data from different values of t_w when plotted versus $t - t_w$, but is reported to exhibit collapse when plotted as a function of t/t_w [32], with the scaling form

$$C_{ag} \sim \left(\frac{t}{t_w} \right)^{-\alpha\lambda}, \tag{5}$$

λ being referred to as an aging exponent. With the increase of the exponent λ, the decay of $C(t, t_w)$ becomes generally faster. In the domain of kinetics of phase transitions, λ is a key quantity for the determination of the universality classes.

Similar interest exists for quenches to the critical point. In this case the correlation in the system is expected to grow with time as [29,37,38]

$$\xi(t) \sim t^{1/z}, \tag{6}$$

z being a dynamic critical exponent. Note that in the long time limit values of ξ diverge with the approach to the critical point in a power-law fashion with an exponent ν [39].

Obtaining the values of α, λ, and z are of fundamental importance in the domain of dynamics of phase transitions. Understanding of these are quite advanced for various lattice systems in the case of passive matter. For fluids, the status is reasonably poor. In the case of active matter systems, such interest is very recent. In this work, we intend to obtain these quantities for phase-separating systems consisting of active Brownian particles [4,17]. In addition, we also study active lattice systems [14,15] as they are computationally less demanding and thus yield statistically better data. These systems did show interesting deviations in steady-state critical behavior from ABPs in prior work [16]. Therefore, a comparative analysis of dynamical behavior adds further understanding toward the uniqueness of active matter systems.

Note that self-propelled particles forming nonequilibrium active systems offer a wide range of interesting behavior and applications [1–3,40,41]. While phase transition and the overall nonequilibrium behavior in these systems constitute a broad field of ongoing research [5–12,17], we add an additional aspect of nonequilibrium behavior by quenching uncorrelated homogeneous active systems to correlated or phase separated states.

II. METHODS

A. Model and simulations: Active Brownian particles

Systems of active Brownian particles in two dimensions consist of hard disks which are actively propelled along their orientation (see below). Periodic boundary conditions are applied in both dimensions and equations of motion are given by [17]

$$\dot{\mathbf{r}}_k = -\frac{D_t}{k_B T} \nabla_k U + v_0 \begin{pmatrix} \cos\varphi_k \\ \sin\varphi_k \end{pmatrix} + \sqrt{2D_t}\mathbf{R}_k, \tag{7}$$

where $\mathbf{R}_k$ is normal distributed Gaussian noise, D_t the translational diffusion constant, and U arises from a purely
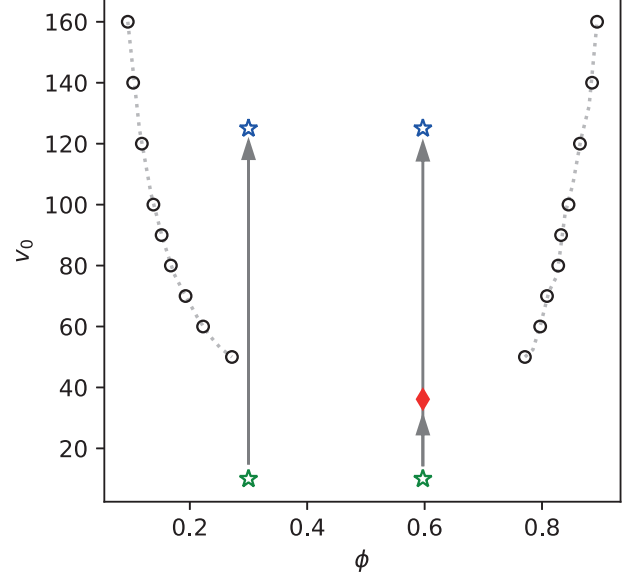

FIG. 1. Phase diagram for ABPs as shown in Ref. [17]. The green stars at the bottom mark the initialization points from where the systems were quenched at constant packing fractions $\phi = 0.597$ and $\phi = 0.3$ into the phase separated region (blue stars at the top) and to the critical point (red diamond). Dotted lines were only drawn to guide the eye.

repulsive Weeks-Chandler-Andersen (WCA) potential between disks with $\epsilon = 100$ and $\sigma = 1$ as in Ref. [17]. If not mentioned otherwise, then units are from now on omitted and correspond to standard simulation units. Furthermore, D_t is set to 1. With a cutoff distance of $r = 2^{1/6}$ we obtain an effective hard disk Barker-Henderson diameter $d_{\text{BH}} \approx 1.10688$. A particle's orientation is described by the angle φ_k, which undergoes free rotational diffusion with diffusion coefficient D_r, i.e. $\dot{\varphi}_k = \sqrt{2D_r}R_r$, where R_r is Gaussian distributed, has unit variance and is neither correlated between particles nor in time. Each particle is propelled along its orientation with constant speed v_0. GPU-based simulations were performed using HOOMD-blue [42] applying a Brownian integrator with a time step of 10^{-6}. Temperature was set to 1, and simulations were performed at fixed volumes and particle numbers. If the rotational diffusion D_r (set to $3D_t/d_{\text{BH}}^2 \approx 2.45$ throughout this work) is small with respect to the active velocity v_0, then a self-trapping mechanism can be observed [4,43]. Particles that form an emerging cluster require more time to orient away from the cluster than it takes for other particles to reach and enlarge it. This leads to a separation into a dense and a dilute phase and a nonequilibrium phase diagram with a critical point (Fig. 1) [17] even in the absence of explicit attractions.

In the present work we have performed several quenches into the phase-separated region and to the critical point. All simulations started in a mixed state with $v_0 = 10$ and were first equilibrated for 2×10^7 time steps (corresponding to 20 MD times). For the quenches into the phase-separated region the final active velocity was set to $v_0 = 125$. Critical density ($\phi = 0.597$ [17]) was established in a system of size 1024×1024 with 649 636 particles [Fig. 2(b)], while the quench to the low-density branch (at $\phi = 0.3$) [Fig. 2(a)]
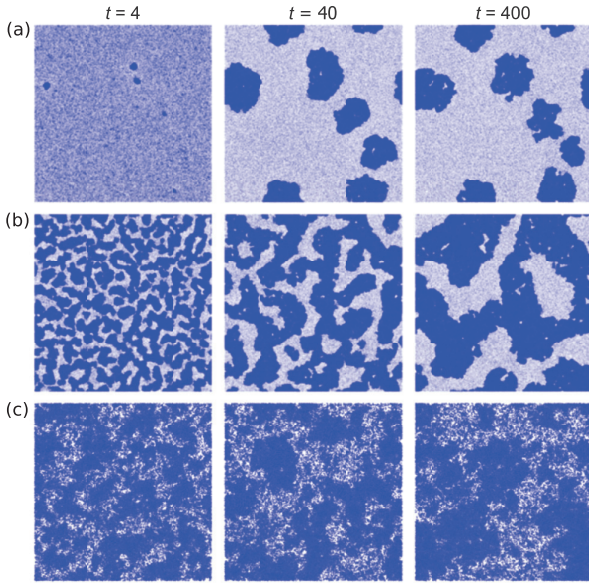
FIG. 2. Snapshots obtained during the evolutions of the ABP model, at three different times, after the quenches took place. Time t is given in MD units. (a) For density $\phi = 0.3$, we have simulated system size 1024×1024 following quench to $v_0 = 125$. (b) For critical density $\phi = 0.597$, we have system size 1024×1024 and quench was to $v_0 = 125$. (c) For critical density $\phi = 0.597$, system size was 256×256 and quench was to the critical $v_0 = 40/d_{BH} \approx 36.14$.

was realized with 314 573 particles. To improve statistics we averaged over 10 independent runs each.

For quenches to the critical point [Fig. 2(c)] the final active velocity was set to $v_0 = 40/d_{BH} \approx 36.14$ [17]. To study the scaling of the steady-state correlation length ξ_{max} with system size, different system sizes had to be realized. In particular, 100 independent runs for size 64×64 containing 2500 particles each, 50 runs for size 128×128 with 10 000 particles, and 15 runs for size 256×256 containing 40 401 particles each were performed.

B. Model and simulations: Active lattice systems

Quenches to the critical points were also performed for three active lattice models which are described in detail in Ref. [16]. In contrast to ABPs [17], these systems are already reported to exhibit steady-state critical exponents close to the 2D-Ising values [16]. From a computational point of view they are also less demanding, and superior statistics can be achieved in a straightforward implementation on CPUs.

Rotational diffusion and active propulsion are handled similarly to ABPs, but parameters are probabilities or rates in Monte Carlo (MC) simulations. Each particle can occupy a single site and is oriented toward one of its neighboring sites. Density is defined as the number of occupied divided by the total number of sites. Again, all simulations were performed with a fixed number of particles in 2D with periodic boundary conditions. One Monte Carlo time unit consists of as many individual Monte Carlo attempts as there are lattice spaces in the system. A rotation move only changes the orientation of

the particle. In a translation move, a particle attempts to move to a neighboring site, which is always accepted if the targeted space is empty and rejected otherwise. To implement activity, movements along the particles' orientation were chosen with higher probability. Other directions were also allowed with reduced probability to account for translational diffusion.

As in Ref. [16] Model I [15] on a hexagonal (hex.) and a square (sq.) lattice were investigated to study the influence of lattice geometry on emerging dynamical properties. In each simulation step, the program attempts to change the orientation of a particle first: A Gaussian distributed random number (having standard deviation σ_{rot} and zero mean) is chosen and rounded to the nearest integer. The current orientation is adjusted by that integer, and the move is accepted with probability 1. As indicated, the rotational diffusion parameter σ_{rot} governs the width of the Gaussian distribution and hence the activity of the model: A low value for σ_{rot} corresponds to a low probability for orientation adjustments and thus enhanced activity and vice versa. Afterwards, a translation move is attempted with the same particle and accepted if the destination location is empty. The direction for the move is chosen at random, with probability w_+ along the particle's current orientation and with probability w_t for any of the remaining directions. For the hexagonal lattice probabilities are set to $w_+ = 25/30$ and $w_t = 1/30$ [15], for the square lattice $w_+ = 17/20$ and $w_t = 1/20$ [16].

In Model II [14] either a rotation or a translation move is attempted in an individual simulation step on the square lattice. A clockwise or anticlockwise rotation is performed with rate $w_1 = 0.1$, an attempted move along the current orientation is undertaken with rate w_+ and in any other direction with $w_t = 1$. Activity is regulated by adjusting w_+. Probabilities for each move are obtained by dividing the individual rates by the sum of all rates, namely $(w_+ + 3w_t + 2w_1)$. For a more in-depth discussion of the lattice models including steady state critical exponents and visualizations of particle moves, the reader is referred to Ref. [16]. Note that model parameters for the three active lattice models (including w_+, w_t, and w_1) were all taken from the original publications in which the models were first introduced [14–16]. In general, parameters were chosen to balance active movement with regular diffusion and mimic off-lattice models such as active Brownian particles. Such choices are helpful in dealing with matters that are parts of debates.

All lattice systems were equilibrated at the corresponding critical densities (0.524 for Model I hex., 0.498 for Model I sq., and 0.527 for Model II [16]) for 5000 time units in a mixed state and then quenched to the critical points. For equilibration, activity in Model I was set to $\sigma_{rot} = 1$ and in Model II to $w_+ = 1.25$. Two hundred independent runs were performed for $L = 512$. The system size for the hexagonal lattice was increased by $2/\sqrt{3}$ to 592 in one direction to account for the hexagonal structure. Quenches to the critical points were simulated for five different system sizes. Four hundred independent runs were undertaken for $L = 64$ and $L = 128$ 200 runs for $L = 256$ and 512 and 50 for $L = 1024$. For the hexagonal lattices, one dimension was again adjusted as described above. Critical simulation parameters were taken from Ref. [16] as $\sigma_{rot} = 0.3048$ for Model I hex., $\sigma_{rot} = 0.2415$ for Model I sq. and $w_+ = 4.76$ for Model II sq.
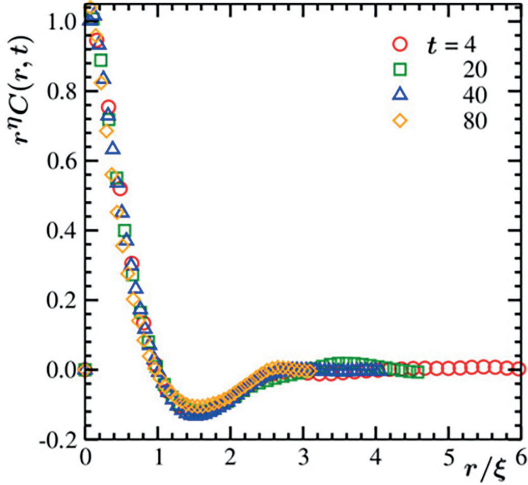
FIG. 3. Scaling plots of the correlation functions for the quench protocol of Fig. 2(c). Data from several different times are included for quenches of random initial configurations to the critical point, for the off-lattice model. The exponent η is set to 0.25, the 2D Ising value.

III. RESULTS AND DISCUSSION

As already stated, in Fig. 1 we show the phase diagram of the off-lattice model. The MIPS phase behavior resembles that of a vapor-liquid phase separation in passive systems rather closely. Nevertheless, it is not clear yet whether the critical behavior can be attributed to the Ising universality class. On the one hand, a study with the model used in this paper showed clear deviations from the 2D Ising universality class [17]. On the other hand, studies using other (somewhat similar) models concluded agreement with 2D Ising universality class [15,19] which resulted in a controversy. Recently, however, renormalization group studies of active matter models appeared [18,20] which could potentially reconcile these discrepancies and explain deviations from ideal Ising behavior. Apart from the Wilson-Fisher fixed point associated with the Ising universality, these studies find other points that limit the region in which the former dictates the phase transition. Even though little is known about the transitions described by these other points, they might potentially be connected to various forms of microphase separation observed, e.g., in Ref. [44].

In Fig. 2 we show snapshots from the evolution of our off-lattice ABP model system following a quench of random initial configurations to various state points. There, locations of particles are marked by dots. The frames under Figs. 2(a) and 2(b) are for quenches to state points inside the coexistence region (see Fig. 1). In Fig. 2(a) the overall density of particles is closer to the vapor branch of the coexistence curve. For this case, as expected, we observe formation and growth of disconnected clusters. In Fig. 2(b) we have included evolution snapshots corresponding to the critical value of $\phi = \phi_c$. In this case we observe an essentially bicontinuous structure. The snapshots in Fig. 2(c) are for quenches to the critical point, and the resulting fractal nature of the morphology can be appreciated. In the following we will only discuss Figs. 2(b) and 2(c) before moving to results from the lattice models.
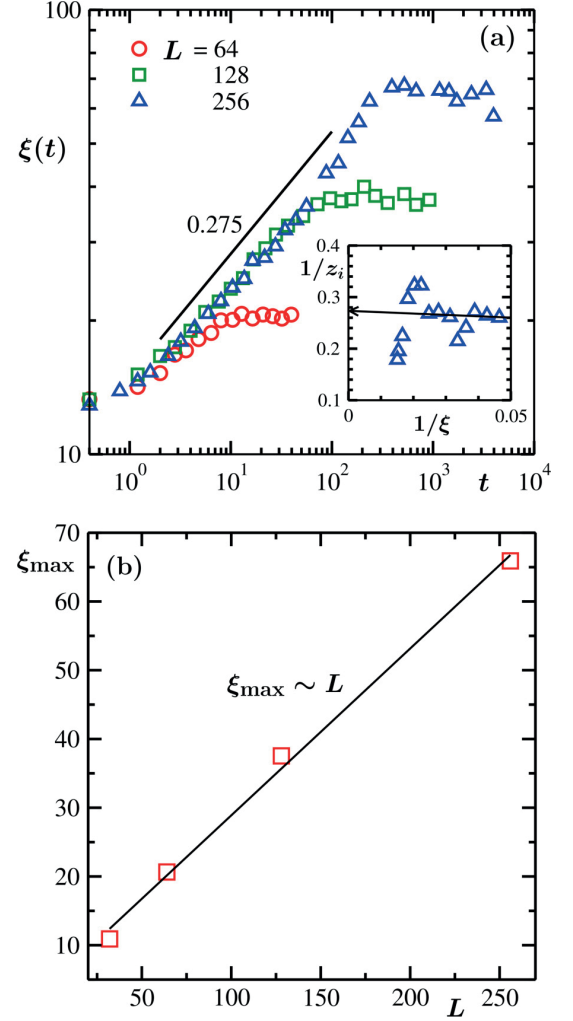

FIG. 4. (a) Results for growing correlation length are shown from different system sizes for quenches of random initial configurations to the critical point. The solid line is a power law, the value of the exponent mentioned next to it. Inset shows the plot of instantaneous exponent, $1/z_i$, as a function of $1/\xi$, for $L = 256$. (b) The steady state values of the correlation length, ξ_{max}, are plotted versus the system size L. These results are for the continuum model.

Note that in the case of Fig. 2(a), gathering meaningful data would require simulations of very large systems over long periods.

First we discuss the case of a quench to the critical point. In this case, due to the fractal nature of the structure the scaling property of Eq. (3) should be written as

$$C(r, t) \equiv r^{\Delta} \tilde{C}[r/\xi(t)], \qquad (8)$$

where Δ is a function of the space and the fractal dimensions. Recalling that the equilibrium (here steady-state) correlation function in the critical vicinity has the form [38,39]

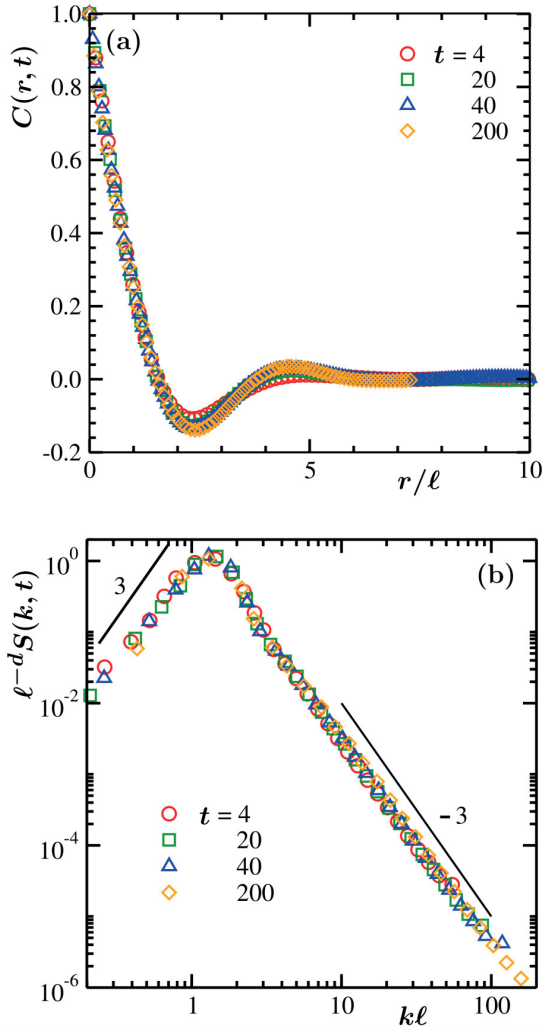$$r^{-p} e^{-r/\xi}; \; p = d - 2 + \eta, \qquad (9)$$

FIG. 5. Scaling plots of (a) $C(r, t)$ and (b) $S(k, t)$, for the quenching protocol described in Fig. 2(b). In panel (b) the solid lines represent power laws with exponent values mentioned in adjacent locations. These results are from the simulations of the off-lattice model.
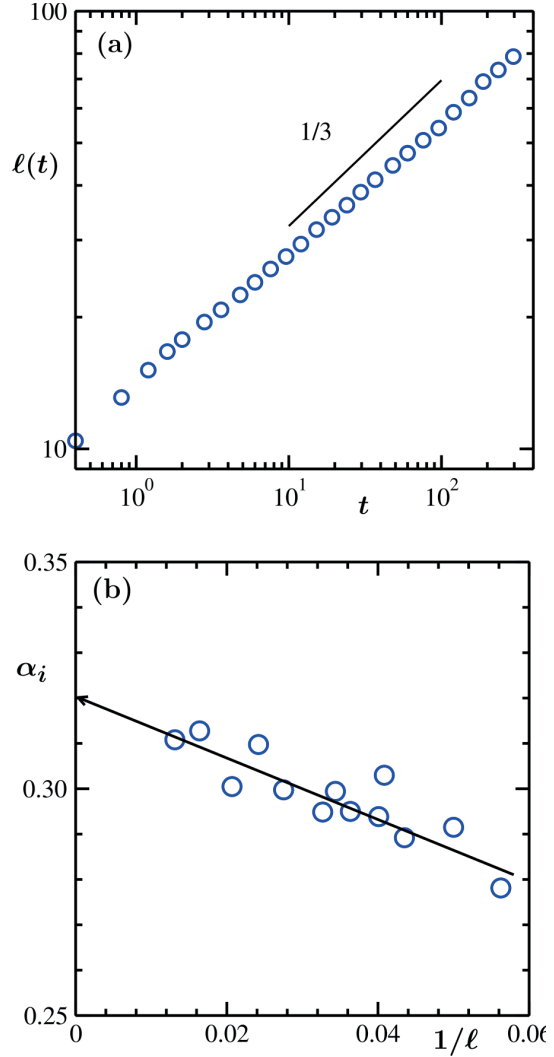

FIG. 6. (a) Plot of the average domain length as a function of time for the quenching protocol described in Fig. 2(b). (b) Instantaneous exponent corresponding to the growth in panel (a) is plotted versus $1/\ell$. These results are from the simulations of the continuum model.

we have the modified scaling form

$$r^{\eta} C(r, t) \equiv \tilde{C}[r/\xi(t)], \tag{10}$$

the critical exponent η being $1/4$ in space dimension $d = 2$ for the Ising class [39]. To confirm this scaling property we have plotted $r^{0.25} C(r, t)$ as a function of $r/\xi(t)$ in Fig. 3. Results from several different times have been included. Similar exercises were performed by replacing η by other numbers. The collapse for 0.25 appears the best.

The values of $\xi(t)$ obtained via the above discussed scaling analysis are plotted in Fig. 4(a), as a function of t. Data from different system sizes, as seen on the log-log scale, indicate a power-law growth with the exponent $\simeq 0.275$. This is consistent with $1/z$, with $z = 4 - \eta$, as expected for the 2D Ising class. In the inset we have shown the instantaneous

exponent [46–48]

$$1/z_i = \frac{d \ln \xi(t)}{d \ln t}, \tag{11}$$

as a function of $1/\xi(t)$. Asymptotically, a convergence toward 0.275 can be appreciated. In Fig. 4(b) we demonstrate that the maximum correlation length scales with the system size, as in the passive case, at the critical point. A more accurate study calls for an exercise where ξ_{max} for different system sizes L are calculated at the finite-size critical points. Now we discuss the case of Fig. 2(b).

To check for the self-similar nature of the evolving pattern we calculate $C(r, t)$. Scaling plots of this quantity are presented in Fig. 5(a). In this case we aim to validate the scaling form of Eq. (3). Data from a few different times
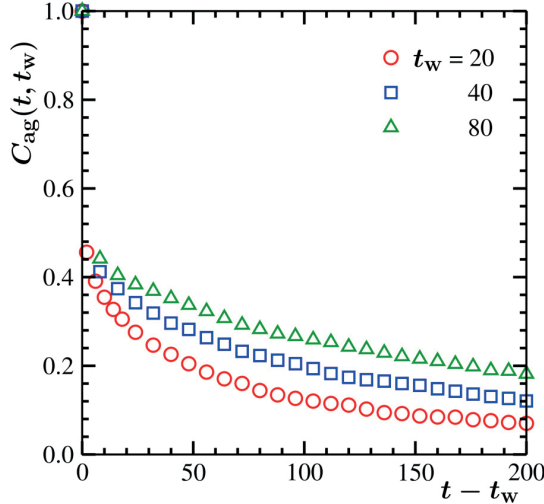
FIG. 7. Autocorrelation functions from the simulations of the off-lattice model are plotted versus the translated time $t - t_w$, for a few values of the waiting time t_w. These results are for the protocol of Fig. 2(b).

FIG. 9. The instantaneous aging exponent is plotted versus t_w/t for a value of t_w. The solid line is a guide to the eyes.

are shown. There, the distance axis is scaled by the average domain lengths at the corresponding times. Clearly, data from different times nicely collapse on top of each other, confirming self-similar growth. A scaling plot for the structure factor is presented in Fig. 5(b). There the power-law decay in the large wave vector (k) limit validates the Porod law [49]. The latter originates from scattering from sharp interfaces. We will discuss the small k power-law behavior later. Note that the presented scaling form for the structure factor $S(k, t)$ is a direct consequence of the fact that this quantity is the Fourier transform of $C(r, t)$.
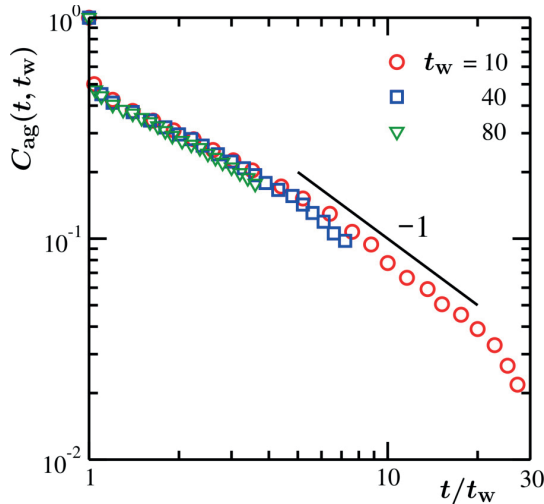
The average domain lengths are plotted in Fig. 6(a) as a function of time. The late time behavior is consistent with a power-law exponent $1/3$. The latter is expected for diffusive domain growth as seen in Lifshitz-Slyozov mechanism [35] and is realized in Monte Carlo simulations [29] of Ising model via Kawasaki exchange [50] kinetics that preserves the system integrated order parameter over time [23,29]. In Fig. 6(b) we show [46–48]

$$\alpha_i = \frac{d \ln \ell(t)}{d \ln t}, \qquad (12)$$

versus $1/\ell$. Clearly the asymptotic convergence ($\ell = \infty$ limit) is toward a value very close to $1/3$.

In Fig. 7 we present the autocorrelation function, $C_{ag}(t, t_w)$, versus the translated time $t - t_w$. Clearly, results from different t_w do not overlap, as expected for evolving systems. The same data sets are plotted versus t/t_w in Fig. 8. Good overlap is observed. There the deviations of the data points from the master curve, that occur at different abscissa values for different t_w, are due to finite size of the systems. These departures should not be considered while quantifying the decay in the thermodynamically large system size limit. At large values of t/t_w, prior to the appearance of the finite-size effects, it appears that C_{ag} decays in a power-law manner with an exponent 1. For an accurate estimate of the exponent, in Fig. 9 we show the corresponding instantaneous exponent [32,36] $-d \ln C_{ag}/d \ln(t/t_w)$ as a function of t_w/t. The convergence is toward 1.1, when analyzed by discarding the finite-size affected part, that appears when t_w/t is small. This implies $\lambda \simeq 3.3$ which is in agreement with the Ising value for conserved order parameter [36].

Depending upon the conservation of order-parameter during evolution, there exist important bounds on the aging exponent λ [32,34]. For nonconserved order-parameter dynamics, which is not relevant to the present problem, Fisher and Huse provided a lower bound, $\lambda \geqslant d/2$, that can be obtained from the well-known Ohta-Jasnow-Kawasaki (OJK) correlation function [52] involving two space points and two times. Later Yeung, Rao, and Desai (YRD) [34] provided a

FIG. 8. Same as Fig. 7 but here we show $C_{ag}(t, t_w)$ as a function of t/t_w. The solid line has a power-law decay. The value of the exponent is mentioned next to the line.

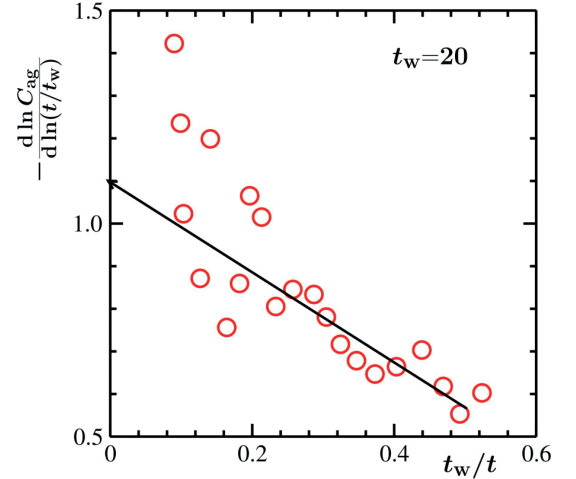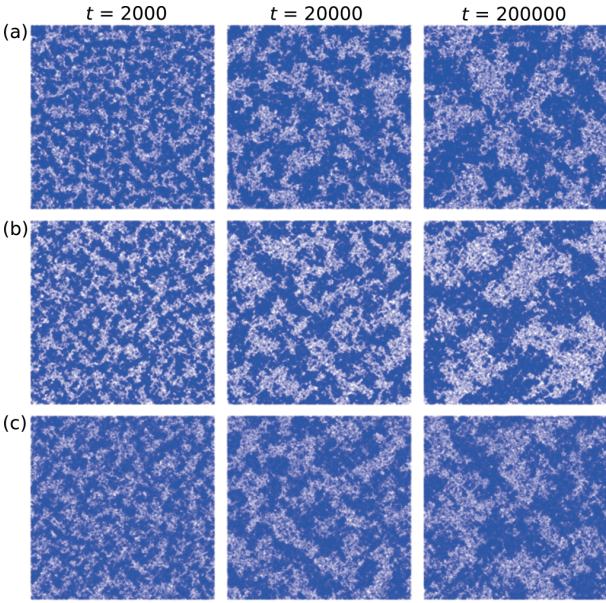FIG. 10. Snapshots obtained during the evolutions of the considered lattice models are presented for three different times after the quenches to the critical points took place. Time t is given in Monte Carlo steps. The locations of the particles are marked. (a) For Model I hex., a system at critical density 0.524, is quenched to $\sigma_{\rm rot} = 0.3048$. The system is of size 512×592, to adjust for the hexagonal lattice structure. (b) For Model I sq., a critical density (0.498) system is quenched to $\sigma_{\rm rot} = 0.2415$. The system is of size 512×512. (c) For Model II sq., a system with critical density 0.527 is quenched to $w_+ = 4.76$. System is of size 512×512. The comparison of the results with the 2D conserved Ising model is presented in Fig. S4, in the Supplemental Material [45].

more general lower bound, viz.,

$$\lambda \geqslant \frac{d + \beta}{2}, \qquad (13)$$

where β is the exponent characterizing the small wave-vector (k) power-law behavior [51],

$$S(k, t_w) \sim k^\beta. \qquad (14)$$

For Ising-type systems, for standard nonconserved dynamics [36,52] $\beta = 0$. Thus, the YRD bound matches with the lower bound of FH. However, for similar models with conserved order-parameter dynamics one should ideally have [51] $\beta = 4$. The latter type of dynamics is of relevance here [23,29]. In Fig. 5(b) we have shown a representative plot of the structure factor, as a function of k, on a double-log scale. The small k behavior is consistent with $\beta = 3$. In that case we have the YRD bound to be equal to 2.5, recalling that here $d = 2$. Our result in Fig. 9 satisfies the lower bound of YRD. Somewhat smaller value of β than 4 was realized in earlier works also [53].

Before concluding, we present results from growth in the lattice models. In Fig. 10 we show evolution snapshots for quenches to the critical points for different lattice models. In Fig. 11 we have shown the growth of ξ for these lattice models. The results are consistent with the Ising case. For
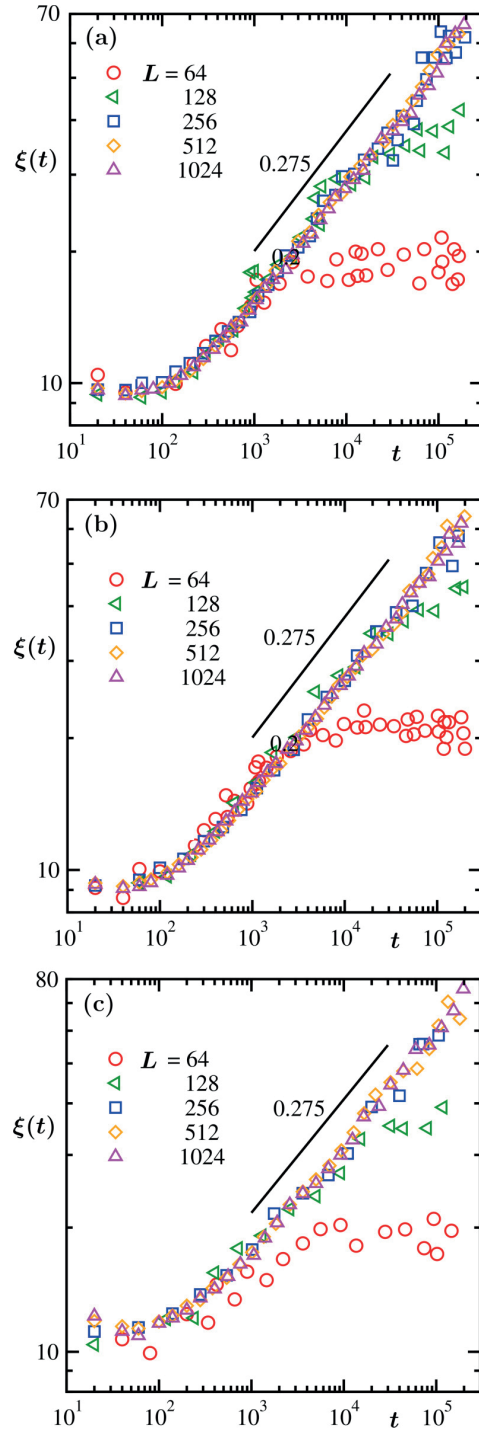

FIG. 11. Time-dependent correlation lengths are plotted for (a) square lattice using method-I, (b) hexagonal lattice using method-I, and (c) square lattice using method-II. The solid lines are power laws with mentioned value of the exponent. These results are for quenches of random initial configurations to the critical points.

quenches inside the coexistence regions, patterns obtained from the lattice models differ from the 2D conserved Ising model, and in the late stages the underlying lattice geometry becomes apparent. See Figs. S1 and S2 in the Supplemental Material [45]. The average domain length grows faster as well (Fig. S3) [45]. Further investigations, thus, are certainly warranted.

IV. CONCLUSION

We have studied critical and off-critical kinetics of vapor-liquid phase transition in a model system consisting of active Brownian particles [17]. Results are presented for structure, growth, and aging. Each of these aspects appear to be quite similar to those observed during phase separation in the Ising model with conserved order-parameter dynamics [23,29]. The growth of average domain size follows a power-law behavior with an exponent $\alpha = 1/3$, as expected for Lifshitz-Slyzov mechanism [35]. The aging exponent λ appears to have a value 3.3 that is in quite good agreement with two-dimensional conserved dynamics of Ising model [36] within 10%. The value of λ satisfies the Yeung-Rao-Desai bound [34]. The structure also matches Ising behavior.

Note that our results for ABPs are not necessarily in contradiction to the central claim of Ref. [17], namely that static critical exponents differ from the 2D Ising case. In our opinion, they merely indicate that critical behavior in nonequilibrium systems may still not be as well-understood as in the equilibrium case, and that future research in this field is certainly warranted. On a related note, inertia [54,55] and hydrodynamics [56] also appear to affect behavior of active particles in the phase separated region and beyond, and a thorough investigation of their influence on dynamics, particularly in the critical region would be interesting as well.

Finally, we have also presented results from a few lattice models [15] for quenches to the critical points. In these cases also the structure and dynamics, like in the case of the continuum model, are similar to those for the conserved Ising model in $d = 2$.

[1] T. Vicsek and A. Zafeiris, Phys. Rep. **517**, 71 (2012).

[2] C. Bechinger, R. Di Leonardo, H. Löwen, C. Reichhardt, G. Volpe, and G. Volpe, Rev. Mod. Phys. **88**, 045006 (2016).

[3] G. Gompper, R. G. Winkler, T. Speck, A. Solon, C. Nardini, F. Peruani, H. Loewen, R. Golestanian, U. B. Kaupp, L. Alvarez, T. Kioerboe, E. Lauga, W. Poon, A. D. Simone, F. Cichos, A. Fischer, S. M. Landin, N. Soeker, R. Kapral, P. Gaspard *et al.*, J. Phys.: Condens. Matter **32**, 193001 (2020).

[4] M. E. Cates and J. Tailleur, Annu. Rev. Condens. Matter Phys. **6**, 219 (2015).

[5] Y. Fily and M. C. Marchetti, Phys. Rev. Lett. **108**, 235702 (2012).

[6] G. S. Redner, M. F. Hagan, and A. Baskaran, Phys. Rev. Lett. **110**, 055701 (2013).

[7] J. Stenhammar, A. Tiribocchi, R. J. Allen, D. Marenduzzo, and M. E. Cates, Phys. Rev. Lett. **111**, 145702 (2013).

[8] J. Stenhammar, D. Marenduzzo, R. J. Allen, and M. E. Cates, Soft Matter **10**, 1489 (2014).

[9] A. Wysocki, R. G. Winkler, and G. Gompper, Europhys. Lett. **105**, 48004 (2014).

[10] J. Bialké, T. Speck, and H. Löwen, J. Non-Cryst. Solids **407**, 367 (2015).

[11] J. T. Siebert, J. Letz, T. Speck, and P. Virnau, Soft Matter **13**, 1020 (2017).

[12] P. Digregorio, D. Levis, A. Suma, L. F. Cugliandolo, G. Gonnella, and I. Pagonabarraga, Phys. Rev. Lett. **121**, 098003 (2018).

[13] L. Caprini, U. M. B. Marconi, C. Maggi, M. Paoluzzi, and A. Puglisi, Phys. Rev. Res. **2**, 023321 (2020).

[14] S. Whitelam, K. Klymko, and D. Mandal, J. Chem. Phys. **148**, 154902 (2018).

[15] B. Partridge and C. F. Lee, Phys. Rev. Lett. **123**, 068002 (2019).

[16] F. Dittrich, T. Speck, and P. Virnau, Eur. Phys. J. E **44**, 53 (2021).

[17] J. T. Siebert, F. Dittrich, F. Schmid, K. Binder, T. Speck, and P. Virnau, Phys. Rev. E **98**, 030601(R) (2018).

[18] F. Caballero, C. Nardini, and M. E. Cates, J. Stat. Mech. (2018) 123208.

[19] C. Maggi, M. Paoluzzi, A. Crisanti, E. Zaccarelli, and N. Gnan, Soft Matter **17**, 3807 (2021).

[20] T. Speck, Phys. Rev. E **105**, 064601 (2022).

[21] C. Maggi, N. Gnan, M. Paoluzzi, E. Zaccarelli, and A. Crisanti, Comm. Phys. **5**, 55 (2022).

[22] N. Gnan and C. Maggi, Soft Matter **18**, 7654 (2022).

[23] A. J. Bray, Adv. Phys. **51**, 481 (2002).

[24] V. Wadhawan and S. E. Puri, *Kinetics of Phase Transitions*, 1st ed. (CRC Press, Boca Raton, FL, 2009)

[25] P. Cremer and H. Löwen, Phys. Rev. E **89**, 022307 (2014).

[26] S. K. Das, J. Chem. Phys. **146**, 044902 (2017).

[27] K. Binder and P. Virnau, Soft Mater. **19**, 267 (2021).

[28] G. Grégoire and H. Chaté, Phys. Rev. Lett. **92**, 025702 (2004).

[29] D. P. Landau and K. Binder, *A Guide to Monte Carlo Simulations in Statistical Physics*, 2nd ed. (Cambridge University Press, Cambridge, UK, 2005).

[30] S. Chakraborty and S. K. Das, J. Chem. Phys. **153**, 044905 (2020).

[31] S. Paul, A. Bera, and S. K. Das, Soft Matter **17**, 645 (2021).

[32] D. S. Fisher and D. A. Huse, Phys. Rev. B **38**, 373 (1988).

[33] F. Liu and G. F. Mazenko, Phys. Rev. B **44**, 9185 (1991).

[34] C. Yeung, M. Rao, and R. C. Desai, Phys. Rev. E **53**, 3073 (1996).

[35] I. Lifshitz and V. Slyozov, J. Phys. Chem. Solids **19**, 35 (1961).

[36] J. Midya, S. Majumder, and S. K. Das, Phys. Rev. E **92**, 022124 (2015).

[37] P. C. Hohenberg and B. I. Halperin, Rev. Mod. Phys. **49**, 435 (1977).

[38] A. Onuki, *Phase Transition Dynamics* (Cambridge University Press, Cambridge, UK, 2002).

[39] M. E. Fisher, Rep. Prog. Phys. **30**, 615 (1967).

[40] S. K. Das, S. A. Egorov, B. Trefz, P. Virnau, and K. Binder, Phys. Rev. Lett. **112**, 198301 (2014).

[41] B. Trefz, S. K. Das, S. A. Egorov, P. Virnau, and K. Binder, J. Chem. Phys. **144**, 144902 (2016).

[42] J. A. Anderson, J. Glaser, and S. C. Glotzer, Comput. Mater. Sci. **173**, 109363 (2020).

[43] I. Buttinoni, J. Bialké, F. Kümmel, H. Löwen, C. Bechinger, and T. Speck, Phys. Rev. Lett. **110**, 238301 (2013).

[44] E. Tjhung, C. Nardini, and M. E. Cates, Phys. Rev. X **8**, 031080 (2018).

[45] See Supplemental Material at http://link.aps.org/supplemental/10.1103/PhysRevE.108.024609 for detailed results (Figs. S1–S4) on the active lattice models and their comparison with

two-dimensional Ising model with conserved order-parameter dynamics.

[46] D. A. Huse, Phys. Rev. B **34**, 7845 (1986).

[47] J. G. Amar, F. E. Sullivan, and R. D. Mountain, Phys. Rev. B **37**, 196 (1988).

[48] S. Majumder and S. K. Das, Phys. Rev. E **84**, 021110 (2011).

[49] G. Porod, *Small-angle X-ray Scattering*, edited by O. Glatter and O. Kratky (Academic Press, New York, NY, 1982).

[50] K. Kawasaki, *Phase Transitions and Critical Phenomena*, Vol. 2, edited by C. Domb and M. S. Green (Academic Press, New York, NY, 1972), p. 443.

[51] C. Yeung, Phys. Rev. Lett. **61**, 1135 (1988).

[52] T. Ohta, D. Jasnow, and K. Kawasaki, Phys. Rev. Lett. **49**, 1223 (1982).

[53] S. Ahmad, S. K. Das, and S. Puri, Phys. Rev. E **85**, 031140 (2012).

[54] H. Löwen, J. Chem. Phys. **152**, 040901 (2020).

[55] L. Caprini and U. Marini Bettolo Marconi, J. Chem. Phys. **154**, 024902 (2021).

[56] G. Negro, C. B. Caporusso, P. Digregorio, G. Gonnella, A. Lamura, and A. Suma, Eur. Phys. J. E **45**, 75 (2022).

52

Supplementary material

Growth and aging in a few phase-separating active matter systems

Florian Dittrich,[1] Jiarul Midya,[2,3] Peter Virnau,[1,*] and Subir K. Das[4,†]

[1]*Institute of Physics, Johannes Gutenberg-Universität, Mainz, Germany*

[2]*Theoretical Physics of Living Matter,*

Forschungszentrum Jülich, 52425 Jülich, Germany

[3]*School of Basic Sciences, Indian Institute of Technology, Bhubaneswar, 752050, India*

[4]*Theoretical Sciences Unit and School of Advanced Materials,*

Jawaharlal Nehru Centre for Advanced Scientific Research,

Jakkur P.O., Bangalore 560064, India

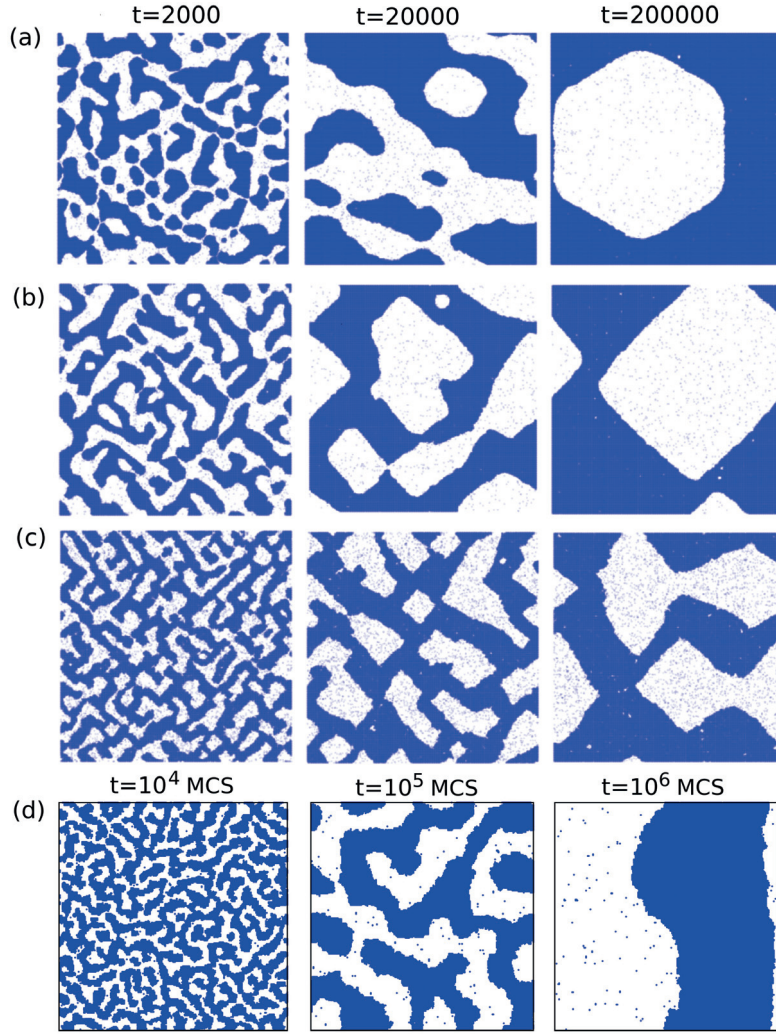[*] virnau@uni-mainz.de

[†] das@jncasr.ac.in

1

FIG. S1. Series of snapshots obtained during the evolutions of the ABP lattice models and conserved Ising model, for three different times, after the quenches to the miscibility gap took place. Time t is given in MC steps. The locations of the particles are marked. (a) For Model I hex., a system at critical density 0.524 is quenched to $\sigma_{\mathrm{rot}} = 0.15$. The system is of size 512×592, to adjust for the hexagonal lattice structure. (b) For Model I sq., a system of size 512×512, at critical density 0.498 is quenched to $\sigma_{\mathrm{rot}} = 0.15$. (c) For Model II sq., a system at critical density 0.527, having size 512×512, is quenched to $w_+ = 30$. (d) For conserved 2D Ising model a system with 50:50 composition and size 256×256, has been quenched to $T = 0.6T_{\mathrm{c}}$. Here $T_{\mathrm{c}} \simeq 2.269$ is the critical temperature.
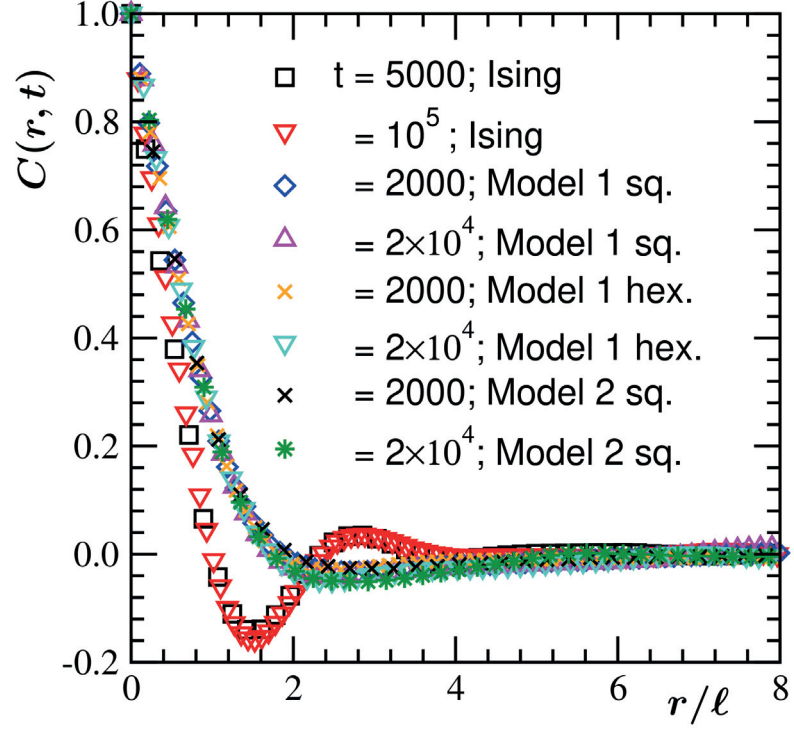
2

FIG. S2. Scaling plots of correlation function, $C(r,t)$, as a function of r/ℓ as obtained from the different active lattice models and the conserved 2D Ising model for the quenching protocols described in Fig. S1
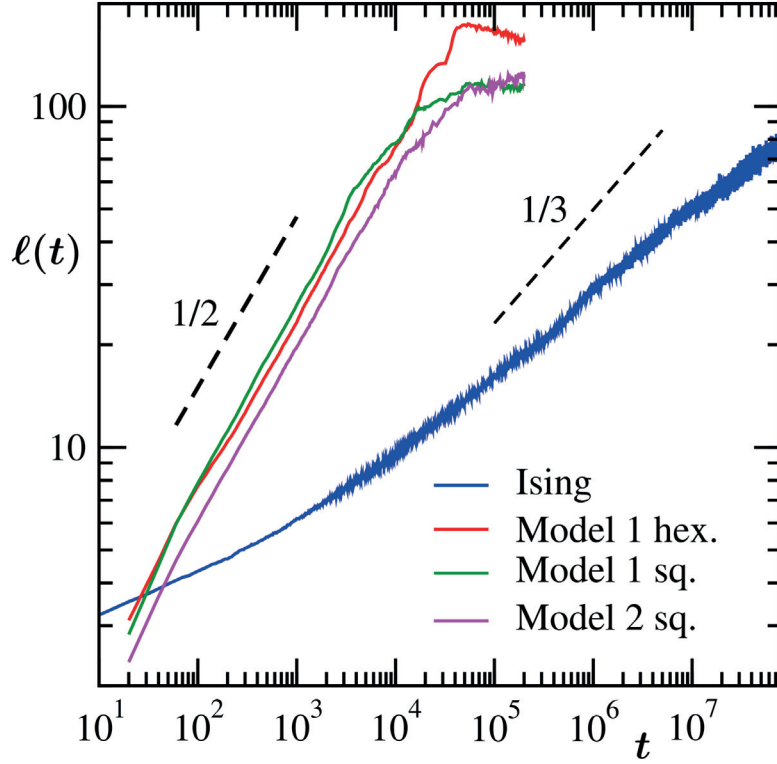
FIG. S3. Domain length ℓ, as a function of time t, obtained from the different active lattice models and the conserved $2D$ Ising model, for the quenching protocol described in Fig. S1, are shown. The black dashed lines correspond to power-laws. The exponent values are indicated next to them.
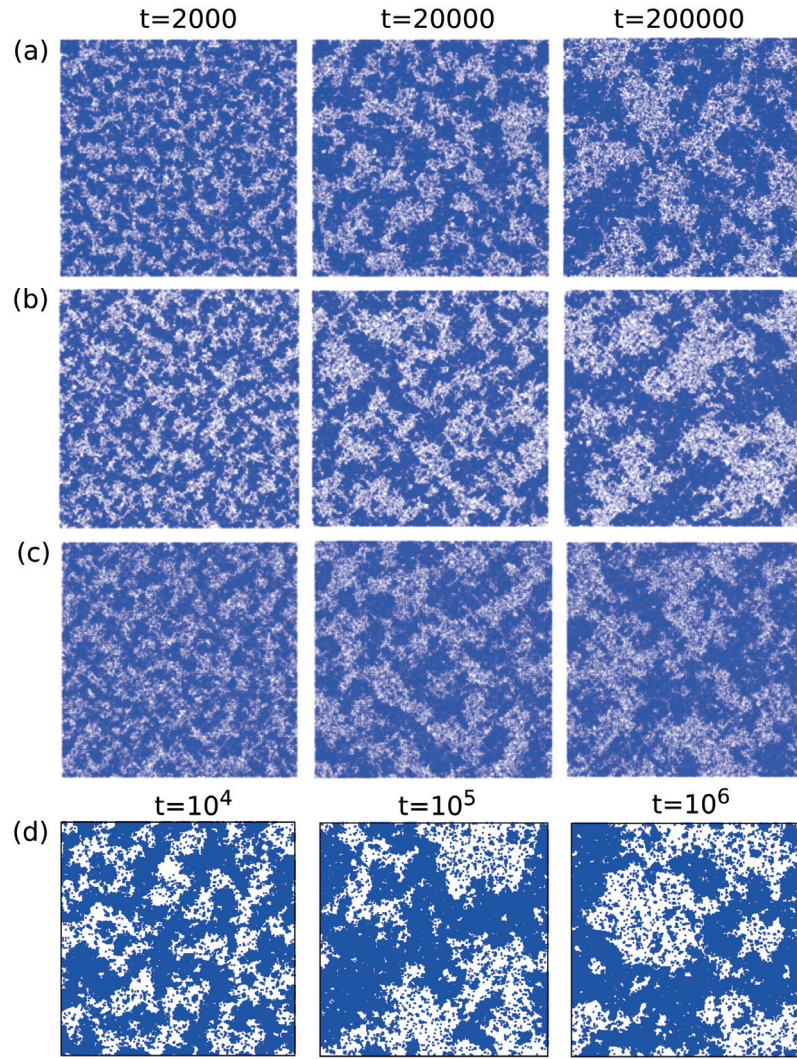
4

FIG. S4. Snapshots obtained during the evolutions of the ABP lattice models and conserved Ising model are shown from three different times after the quenches to the critical points took place. Time t is given in MC steps. The locations of the particles are marked. These are similar to Fig. S1, expect for the fact that in the former quenches were performed into the coexistence region.

5

„Skyrmion Lattice Phases in Thin Film Multilayer" (Adv. Funct. Mater. 2020, 30, 2004037)
J. Zázvorka, F. Dittrich, Y. Ge, N. Kerber, K. Raab, T. Winkler, K. Litzius, M. Veis, P. Virnau, M. Kläui

Author Contributions

"J.Z. and F.D. contributed equally to this work. M.K., P.V., and J.Z. proposed and supervised the study. J.Z. and N.K. fabricated and characterized the multilayer samples. J.Z., N.K., and K.R. prepared the measurement setup and conducted the experiments using the Kerr microscope. F.D., J.Z., Y.G., T.W., and N.K. evaluated the experimental data with the help of K.R., P.V., M.V., and K.L. F.D. and P.V. conducted theoretical simulations and comparison with the experimental results. J.Z. and F.D. prepared the manuscript with the help of M.V., P.V., and M.K. All authors commented on the manuscript."

Personal impact

This work can be divided into three parts: The experimental part, the evaluation of experimental data and the theoretical part.

I did not contribute to the experimental part, that generated Kerr microscope videos of the skyrmion lattices.

For the evaluation part, the Skyrmions in the videos had to be tracked first. I suggested and tested the toolkit Trackpy to do so. I also wrote the basic tracking script, that was later used to do the final tracking by Y. Ge. I subsequently analyzed the tracking results with self-written Python scripts. The data for all the plots was provided by me, the plotting was done by J. Zázvorka. I further contributed the snapshots in Fig. 3 & 5.

In order to perform the evaluation and the matching simulations, a lot of theoretical work had to be done (see SI, 4.-5.). This part was done entirely by me with the help of P. Virnau. I developed the procedure to determine the skyrmion potential form the pair correlation function by matching simulations. Moreover, I suggested the use of $\langle|\psi_6|\rangle$ as indicator and found its independence from the potential at the transition point. I used the HOOMD-blue toolkit to do the simulations and the freud library to evaluate the data. For that I wrote the Python code, ran all the simulations, evaluated the data and compared it with the experimental data.

I contributed to around half of the writing of the manuscript.

Skyrmion Lattice Phases in Thin Film Multilayer

Jakub Zázvorka, Florian Dittrich, Yuqing Ge, Nico Kerber, Klaus Raab, Thomas Winkler, Kai Litzius, Martin Veis, Peter Virnau,* and Mathias Kläui*

Phases of matter are ubiquitous with everyday examples including solids and liquids. In reduced dimensions, particular phases, such as the 2D hexatic phase and corresponding phase transitions occur. A particularly exciting example of 2D ordered systems are skyrmion lattices, where in contrast to previously studied 2D colloid systems, the skyrmion size and density can be tuned by temperature and magnetic fields. This allows for the system to be driven from a liquid phase to the onset of a hexatic phase as deduced from the analysis of the hexagonal order. Using coarse-grained molecular dynamics simulations of soft disks, the skyrmion interaction potentials are determined, and it is found that the simulations are able to reproduce the phase behavior. This shows that not only the static behavior of skyrmions is qualitatively well described in terms of a simple 2D model system but skyrmion lattices are versatile and tunable 2D model systems that allow for studying phases and phase transitions in reduced dimensions.

1. Introduction

Magnetic skyrmions, topologically stabilized whirls of magnetization, are in the focus of the scientific community due to their attractive properties for possible novel functional devices.[1–3] Using spin-transfer torque and spin–orbit torque,[4–7] skyrmions can be moved with high speeds at low current densities and can

even be stabilized with no external magnetic field applied,[7–9] which makes them potentially useful for memory and computer logic devices.[3,10] In addition to such devices based on the controlled operation of single skyrmions, also thermally activated skyrmions and skyrmion ensembles have been suggested for functional devices for non-conventional computing approaches: recently it was shown, that skyrmions, including ensembles, can be relevant for stochastic computing where a functional skyrmion reshuffler device was implemented.[11] And in particular for reservoir computing, we have suggested to use ensembles of many skyrmions where the skyrmion interaction and collective behavior is of key importance.[12] Thus advanced functionality in nanoscale devices is enabled if the properties of ensembles of skyrmions can be understood and controlled. Periodic ensembles called skyrmion lattices have been found widely in bulk materials with B20 symmetry, where the topological structures are stabilized due to bulk Dzyaloshinskii–Moriya interaction (DMI).[4,5,13,14] However, in bulk systems the skyrmions are mostly not 2D like, as the "skyrmion tube" length can easily exceed the skyrmion diameter or even the skyrmion-skyrmion distance. In advanced thin film systems, skyrmions down to sub-nm thickness and diameters in the range of micrometers are stabilized, making them prime candidates for perfectly 2D systems. While skyrmion lattices have been studied theoretically in such systems, only recently first experimental reports of thin film lattices have been reported, albeit with systems where the relatively large (≈100 nm) film thickness is similar to the lateral skyrmion size making these systems not necessarily 2D.[13,15–17] Thus to experimentally probe the rich phase behavior of 2D systems[18–20] akin to colloids in the past,[21–23] 2D skyrmion lattices occurring in ultra-thin film stacks might be an ideal model system.[24] The nature of phase transitions in 2D systems of hard and soft disks has been a grand challenge in statistical physics, which has recently been numerically treated.[18] Apart from a liquid at low and a solid phase at high density, a third intermediate phase may emerge: The hexatic phase is characterized by short range translational and quasi-long range orientational order, and there is a clear need for experimental 2D systems to probe this unique phase behavior. This calls for studying 2D skyrmion lattices and analysis of their phase behavior with numerical simulations based on coarse-grained models from Statistical Mechanics to identify possibly unique 2D properties as well as gauge the suitability of these systems to study the exciting 2D phase behavior.

Dr. J. Zázvorka, F. Dittrich, Y. Ge, N. Kerber, K. Raab, T. Winkler,
Dr. K. Litzius, Dr. P. Virnau, Prof. M. Kläui
Institute of Physics
Johannes Gutenberg-Universität Mainz
Staudingerweg 7, Mainz 55128, Germany
E-mail: virnau@uni-mainz.de; klaeui@uni-mainz.de

Dr. J. Zázvorka, Dr. M. Veis
Institute of Physics
Faculty of Mathematics and Physics
Charles University
Ke Karlovu 5, Prague 12116, Czech Republic

N. Kerber, Dr. K. Litzius, Dr. P. Virnau, Prof. M. Kläui
Graduate School of Excellence Materials Science in Mainz
Johannes Gutenberg-Universität Mainz
Staudingerweg 9, Mainz 55128, Germany

Dr. K. Litzius
Modern Magnetic Systems
Max Planck Institute for Intelligent Systems
Heisenbergstrasse 3, Stuttgart 70569, Germany

**ADVANCED
SCIENCE NEWS**
www.advancedsciencenews.com

**ADVANCED
FUNCTIONAL
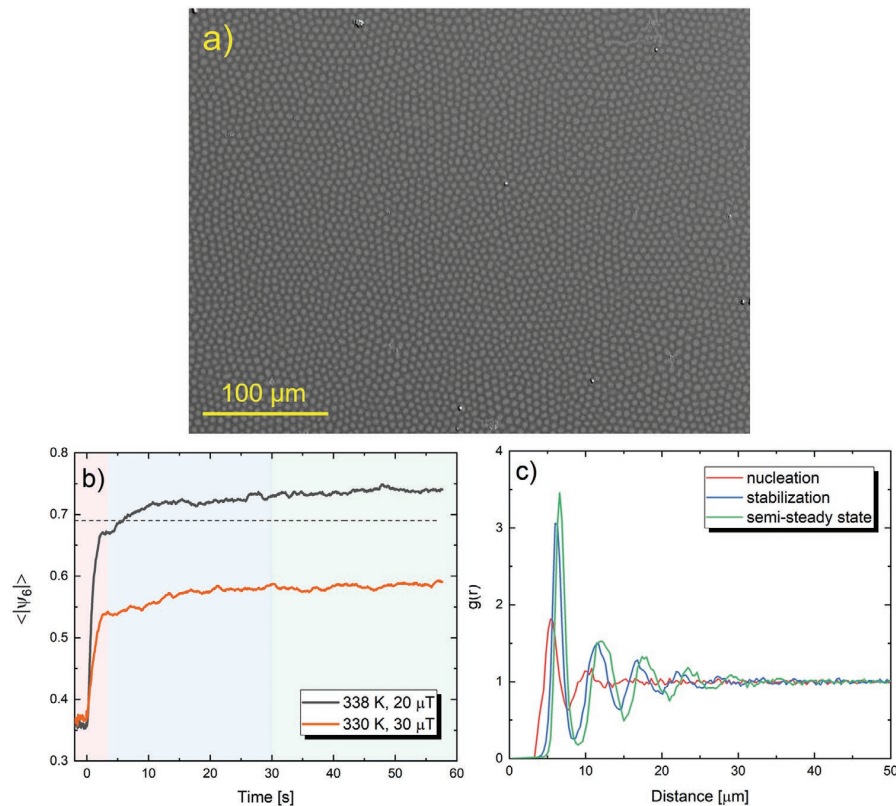MATERIALS**
www.afm-journal.de

Figure 1. Picture of skyrmion lattice and evolution of phase quantifiers. a) Kerr image of a skyrmion lattice at 335 K with μm sized skyrmions. b) The evolution of $\langle|\psi_6|\rangle$ averaged over all skyrmions in one frame in dependence of time after nucleation. The red, blue, and green backgrounds depict the nucleation, stabilization, and a semi-steady skyrmion state, respectively. $\langle|\psi_6|\rangle$ is dependent on the temperature and the applied out-of-plane field. c) Pair correlation function $g(r)$ right after nucleation, in the stabilization phase and in the semi-steady state for temperature 338 K and 20 μT applied out-of-plane field. After switching off the in-plane field and the resulting skyrmion nucleation, the red pair correlation function (in (c)) emerges and indicates typical nearest and next-nearest neighbor distances. Blue and green curves show the pair correlation function $g(r)$ in the relaxation and semi-steady state of the lattice, respectively. In the stabilization process, the correlation function is noisier, whereas in the semi-steady state the function has a finer distribution.

Thus, in this work, we use a sub-nm thick CoFeB-based multilayer system to study the emergence of skyrmion lattices as well as their response to tuning external parameters such as temperature and field. Since the skyrmion diameter (**Figure 1**a) is three orders of magnitudes larger than its thickness (0.9 nm), and as the thickness of the magnetic layer is much smaller than the exchange length so that the magnetization texture is uniform along the z-direction, this system could be considered to be inherently 2D. This is distinctly different from previous reports on topologically trivial bubbles for instance in yttrium iron garnet (YIG) films that are >μm thick and where no sizeable DMI is found. By experimentally ascertaining the phase transitions, we demonstrate the 2D nature of the system as well as its suitability as a model system to probe 2D phase behavior.

2. Results and Discussion

Using Kerr microscopy imaging we investigated a low-pinning multilayer stack $Ta(5)/Co_{20}Fe_{60}B_{20}(0.9)/Ta(0.08)/MgO(2)/Ta(5)$ similar to a material previously characterized in which the

skyrmions show thermally activated diffusion at low skyrmion densities.[11] The studied material exhibits perpendicular magnetic anisotropy (PMA) and interfacial DMI.[11] Using out-of-plane magnetic field sweeps, stripe domains, and a low density of skyrmions are present in the sample. Upon fixing the out-of-plane field and a subsequent saturation of the sample using an in-plane field in any direction, a high density of skyrmions is nucleated in the sample when the in-plane field is reduced back to zero abruptly by switching off the power supply to the in-plane coil. Due to the interfacial DMI and concluded from current induced motion experiments, the observed skyrmions were topologically stabilized, with a fixed chirality, and rotational symmetry and a topological charge $Q = 1$. This is desired for our further investigation as there are no reports indicating phase transitions with spatially ordered $Q = 0$ magnetic bubbles that are not rotationally symmetric. The density and the mean radius of the skyrmions is controlled by the values of the out-of-plane magnetic field applied and the temperature. For details on the MOKE hysteresis loops and skyrmion lattice nucleation, see Supporting Information. By varying the out-of-plane field, the size and as a result also the skyrmion lattice density and

**ADVANCED
SCIENCE NEWS**
www.advancedsciencenews.com

**ADVANCED
FUNCTIONAL
MATERIALS**
www.afm-journal.de

ordering is tuned, which is a unique handle compared to previously used systems, such as colloids with fixed sizes. Variations in temperatures are found to tune the amount of thermally activated motion but also the average skyrmion radius, as well as lattice density due to the changing magnetic properties.[11] To evaluate phases in 2D systems such as the skyrmion lattice phases (Figure 1a), we employ two quantifiers:

The local orientational order parameter[18,25] (Figure 1b)

$$\psi_6(k) = \frac{1}{n_k} \sum_{l=1}^{n_k} e^{i6\theta_{kl}} \qquad (1)$$

and the pair correlation function (Figure 1c)

$$g(r) = \frac{1}{2\pi r} \frac{1}{N\rho} \sum_{k=1}^{N} \sum_{k \neq l}^{N} \langle \delta(r - |r_k - r_l|) \rangle \qquad (2)$$

The local orientational order parameter is a standard measure to quantify the emergence of local hexagonal order.[18,25] θ_{kl} describes the angle of the connecting line between a (central) skyrmion k and the lth of its n_k nearest neighbors with respect to a fixed axis (here the *x*-axis).[18] The cut-off distance to find the nearest neighbors was selected to be the position of the first minimum in the corresponding pair correlation function $g(r)$. A strict cut is implemented, so the number of neighbors n_k will usually but not necessarily be 6. For a perfect (periodic) triangular lattice, the contribution of all six neighbors yields $|\psi_6| = 1$.

The 1D pair correlation function $g(r)$ (Equation (2)) contains basic information such as typical nearest and next-nearest neighbor distances and the general structure of a gas, liquid or crystal. Particularly, it allows us to quantify the local structure of a skyrmion lattice in area A by comparing it to a structureless, homogeneous fluid of area density $\rho = \frac{N}{A}$. Essentially, we count the number of particles located at a certain distance around each particle and divide this number by the expected number of particles in a fluid with no structure. In our modelling approach we use this quantifier to reproduce the basic structure of the system while keeping the fitting procedure manageable. Equation (2) is, however, not suited to visualize the emergence of hexagonal order like the 2D-pair correlation function, for example, used in ref. [18].

To study the evolution of the phases of the system, we take a video using the Kerr microscope after an in-plane magnetic field is switched off. The observed skyrmions are tracked, their positions are evaluated, and quantifiers are calculated for each frame in the video. Calculation of the correlation functions and individual skyrmion position evaluation is described in Section 4. The local orientational order parameter is calculated for every skyrmion in one frame except for those on the border of the frame. Note that in this context the expression "order parameter" refers to a parameter which quantifies the local orientational order of a system and is not to be understood in the classical sense as a parameter which characterizes second-order phase transitions. To obtain a quick indication of the state and the phase of the system, we introduce a heuristic parameter $\langle |\psi_6| \rangle$, which averages the absolute value of ψ_6 over all skyrmions for which ψ_6 was computed.[25] From simulations of a soft disc system we find that the liquid branch of the liquid to hexatic coexistence region is marked by $\langle |\psi_6| \rangle \approx 0.69$ irrespective of the exponent of the underlying

repulsive power-law potential used in the simulations. Larger values correspond to hexatic or solid phases (respectively their onsets), while smaller values are characteristic for liquid phases. For details, we refer the reader to Supporting Information.

Figure 1b shows $\langle |\psi_6| \rangle$ of the skyrmion lattice at fixed out-of-plane field and sample temperature as a function of time after the initial lattice nucleation. As visible, the angular ordering as well as translational ordering as quantified by the pair correlation function (Figure 1c) is not constant instantly after switching off the magnetic in-plane field: A local liquid-like structure emerges and becomes more pronounced as relaxation proceeds. Note that it is not possible to distinguish the 1D $g(r)$ of the hexatic phase from that of a dense liquid as pointed out above. Immediately after switching off this field, the skyrmions are nucleated on a timescale that is below the time resolution of the measurement setup (ms). This is then followed by a stabilization phase in the range of seconds to tens of seconds. The stabilization time frame is influenced by the energy landscape of the multilayer material and the diffusion parameter of the skyrmions to form an ordered structure that we term here in line with literature a skyrmion lattice. While the initial ordering occurs rather quickly in all cases, $\langle |\psi_6| \rangle$ is still increasing slightly over the course of our measurement (60 s) consistent with the expected prolonged equilibration times associated with the emergence of hexagonal order. We refer to the last 30s of the $\langle |\psi_6| \rangle(t)$ as the "semi-steady" state, which is a sufficiently long period to robustly measure quantifiers. The initial 4 s after switching off the in-plane field where the highest slope of $\langle |\psi_6| \rangle$ (t) is found and where the nucleated skyrmions form a lattice is referred to as the "nucleation" period. The "relaxation" period covers the remaining part of the time evolution. These criteria were chosen by comparing the obtained videos at every temperature and out-of-plane field combination for a comparable evaluation of the skyrmion lattice.

While as shown in Figure 1b, at 338 K the system orders with $\langle |\psi_6| \rangle > 0.69$ (indicating possibly a hexatic phase, see further below for a detailed discussion), at 330 K $\langle |\psi_6| \rangle$ only goes up to the value of 0.55, consistent with the formation of a more disordered dense liquid phase. Likewise, the pair correlation function also changes in the course of equilibration (Figure 1c). Fluctuations are related to the thermally activated movement of the skyrmions that occurs in the lattice. We observe that skyrmions repel each other and we do not see any significant skyrmion-skyrmion annihilation thus boding well to study the phase transitions. Having established the time evolution of $\langle |\psi_6| \rangle$, we now systematically study the dependence of the semi-steady state lattice properties on the external parameters, temperature and magnetic field to explore the tunability. The average $\langle |\psi_6^t| \rangle$ is obtained from all frames after 30 s of equilibration and shown in **Figure 2**. With reducing temperature, the range of out-of-plane field where skyrmions can be stabilized becomes narrower and a monotonic trend of higher hexagonal order with higher temperature is observed. The highest temperature achievable was limited by the measurement temperature control as well as the spatial resolution since the skyrmion diameter depends on temperature. At too low out-of-plane fields, after in-plane field sweeps, not only skyrmions are stabilized but also elongated chiral domains are present. These effectively distort the lattice and hinder its higher ordering so
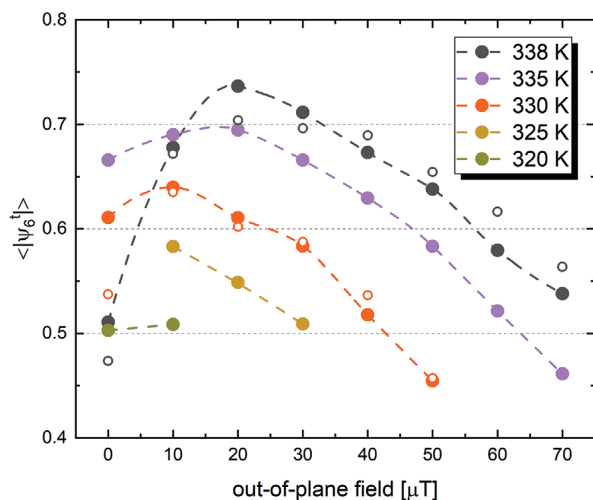
**ADVANCED
SCIENCE NEWS**

www.advancedsciencenews.com

**ADVANCED
FUNCTIONAL
MATERIALS**

www.afm-journal.de

Figure 2. Time averaged $\langle |\psi_6^t| \rangle$ for different out-of-plane fields in the temperature range 325–338 K. The field and temperature ranges are limited by the stability of a pure skyrmion lattice as well as the minimum size of skyrmions that can be detected. The highest ordering achieved is at 338 K with 20 µT. $\langle |\psi_6^t| \rangle$ was calculated from the skyrmion position in the sample in the semi-steady state part of the skyrmion lattice formation (after 30 s since the skyrmion nucleation). Empty circles are simulation results corresponding to $T = 338$ K and $T = 330$ K and were determined after 10^6 simulation time steps. Dashed lines serve as guidelines between points only.

that we have focused on parameter combinations where we have only skyrmions. A decreasing tendency of angular order is found at increased out-of-plane field values for every studied temperature. This can result from higher skyrmion-skyrmion distances, where the thermal movement of the magnetic textures is more pronounced and thus hinders the ordering of the lattice. A maximum value of $\langle |\psi_6^t| \rangle$ of around 0.73 is obtained at the highest investigated temperature and 20 µT out-of-plane field when also the highest observable skyrmion density is reached.

As the onset of the hexatic (or even solid) phase is directly visible in the spatially resolved map of the local orientational order parameter, we study this at the maximum value of $\langle |\psi_6^t| \rangle$ (338 K, 20 µT): **Figure 3**a shows the hexatic skyrmion domains with coincident orientation of ψ_6 as measured by the angle θ (Euler angle of the complex number ψ_6 divided by 6 as explained in Section 4). The average domain size is of the order of 50 µm, corresponding to roughly 100 skyrmions. In particular we see a homogenous distribution of $|\psi_6|$ in Figure 3c.

For comparison, we also show the corresponding liquid phase results for $T = 330$ K and B = 40 µT in Figure 3b,d. Note that skyrmions are much larger under these conditions and domains of similar orientation are of the order of 10 particles or less. In this liquid phase, there is no homogeneous distribution of $|\psi_6|$ as shown by the irregular colors in Figure 3d. To understand our results and draw robust conclusions about the phases and the 2D nature of the studied system, we support the experimental results with numerical simulations using a model of soft particles which interact with each other via a repulsive power-law potential r^{-n}. This choice is purely empirical but allows us to describe the strong short range repulsive interaction studied previously.[26] At the same time, the chosen potential benefits from the availability of exact phase diagrams for a wide range of n.[18] For $n \geq 6$ (which includes the hard disk scenario) the transition from the liquid to the hexatic phase was shown to be of first order followed by a continuous transition to
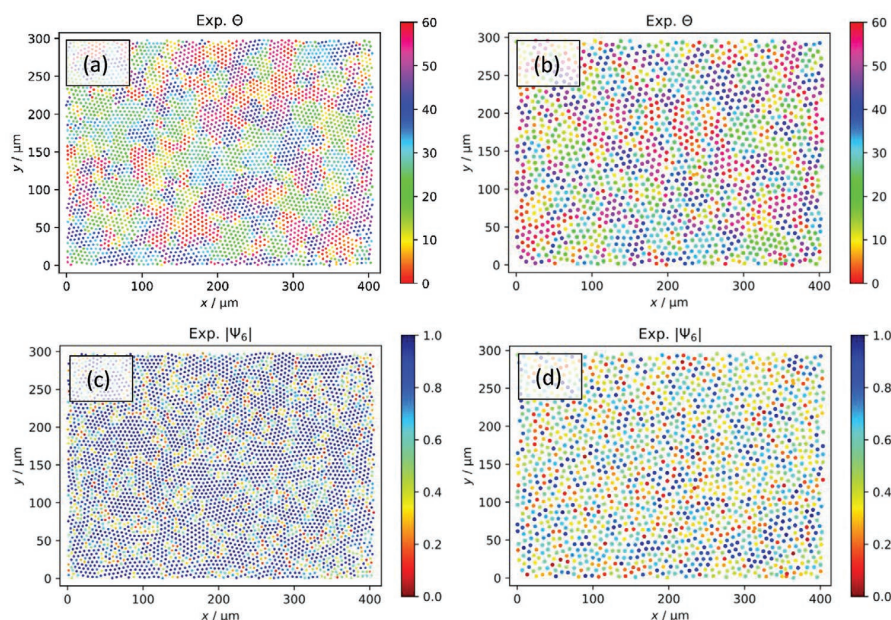
Figure 3. Spatial distribution of the local orientational order parameter ψ_6 of individual skyrmions. (a) and (c) were evaluated at 338 K and an out-of-plane field value of 20 µT. This represents the state with the highest value of $\langle |\psi_6^t| \rangle$ in Figure 2. (a) visualizes the orientation of ψ_6, that is, the orientation angle θ, while (c) visualizes the absolute value of ψ_6. (b) and (d) are corresponding figures for 330 K and 40 µT.

**ADVANCED
SCIENCE NEWS**

www.advancedsciencenews.com

**ADVANCED
FUNCTIONAL
MATERIALS**

www.afm-journal.de
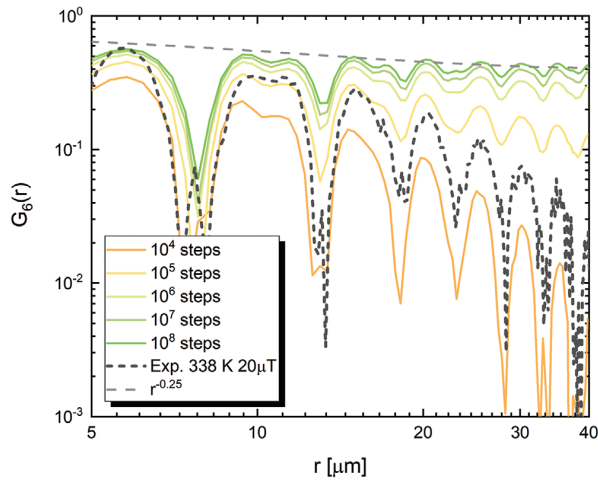
Figure 4. Decay of the spatial correlation function G_6 for the experimental system (338 K, 20 µT, averaged over frames 300–960) and matching simulations after different runtimes (single snapshot of a quadratic simulation box containing 40 000 particles).

the solid phase.[18] For smaller values of n, the transition from the liquid to the hexatic phase becomes continuous and of the Kosterlitz-Thouless–Halperin–Nelson–Young (KTHNY) type.[27]

In the following, we want to ascertain to which extent skyrmion lattices can be used as generic model systems to explore the phase behavior of 2D systems akin to colloids.[21–23] At the same time, we want to gauge if a coarse phenomenological model from statistical physics is actually able to describe the bulk macroscopic behavior of skyrmions accurately. Building upon expansive numerical work, which has determined the phase behavior of soft disks with great accuracy, Molecular Dynamics simulations of this model were performed and mapped onto our skyrmion system.[18,28–30] Parameters were adjusted to match the pair correlation function of skyrmions for a given density. Note that fixing n (to, e.g., 6 to represent interactions between dipoles) will generally lead to a worse agreement with the experimental $g(r)$. For a detailed discussion of the mapping procedure, see Section 4 and Supporting Information.

Using this ansatz, we have reproduced the experimentally observed behavior of $\langle |\psi_6^t| \rangle$ for $T = 338$ K and $T = 330$ K

(Figure 2). Qualitative agreement between simulations and experiments is found. However, one should note that $\langle |\psi_6| \rangle$ is very sensitive to the details of the mapping (e.g., if all details or only parts of $g(r)$ are used). Another caveat for both simulations and experiments at $T = 338$ K is the time after which $\langle |\psi_6| \rangle$ is measured as it increases during the course of equilibration. Nevertheless, considering that our mapping is purely based on basic structural information (namely density and the 1D $g(r)$), the qualitative agreement shows that static properties of skyrmion interactions can indeed be captured by a coarse-grained phenomenological model.

A more quantitative approach relies on the decay of the spatial correlation function G_6 which can also be used to distinguish phases in 2D systems:[21,22]

$$G_6(r) = \frac{1}{n_r} \sum_{|r_k - r_l| = r} \psi_6(r_k) \psi_6^*(r_l) \qquad (3)$$

Here, we sum over all n_r particle pairs whose distance is r. In **Figure 4**, we compare the decay of G_6 from experiment at $T = 338$ K and $B = 20$ µT and simulation. While this correlation function decays exponentially in the liquid phase, quasi-long range orientational order is expected to emerge in the hexatic phase.[27] Depending on the equilibration time after which the correlation function is measured in the simulation, the envelope of G_6 increases toward an algebraic decay. We also observe that the experimental data (black dashed curve) is still decaying exponentially and is likely not fully equilibrated, yet, in line with our observations in Figure 3a.

The effect of equilibration can also be seen in simulation snapshots. While after 10^4 equilibration steps the distribution of θ in **Figure 5**a (as well as the decay of G_6) is similar to the corresponding experimental plot (Figure 3a), the domains of similar orientation continue to grow as indicated by a snapshot taken after 10^8 equilibration steps (Figure 5b).

3. Conclusions

Based on our numerical simulations, we conclude that the observation of multiple domains in the experiment (Figure 3) is likely the result of an incomplete equilibration process as equilibration times are notoriously large in an emergent hexatic (or solid) phase. This is corroborated by the observation that
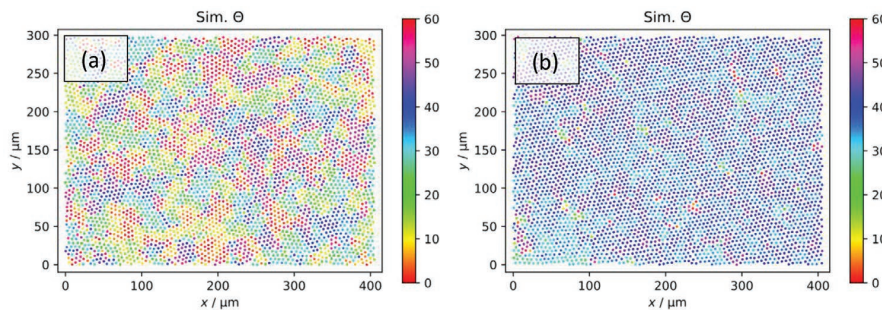

Figure 5. Spatial distribution of θ in a simulation corresponding to a sample temperature of 338 K and an out-of-plane field of 20 µT after a) 10^4 and b) 10^8 equilibration steps. Only a small part of the simulation box is shown to make plots comparable to Figure 3a.

2004037 (5 of 8)

**ADVANCED
SCIENCE NEWS**

www.advancedsciencenews.com

**ADVANCED
FUNCTIONAL
MATERIALS**

www.afm-journal.de

the sizes of the experimental domains continue to grow up to the maximum time which can be measured (that is limited by the setup stability). Additionally, we occasionally see structural defects that pin certain skyrmions that are thus not ordered locally and remain unordered potentially leading to artificial domain wall pinning.

In conclusion, we have analyzed the phases of skyrmion lattices to identify the reduced dimensionality of this μm sized but sub-nm thick system. We have shown that by using the pair correlation function and local orientational order parameter we can characterize the skyrmion lattice system, which allows us to investigate 2D phase transitions. Temperature and out-of-plane field impact density and mean skyrmion-skyrmion distance and translate to different nucleation dynamics and hexagonal ordering of the observed lattice. We find that the hexagonal order increases with higher temperature and field values in the range of 10–30 μT. Above 338 K, the skyrmion lattice cannot be resolved with the optical microscope setup. For the majority of the selected parameters, we observe behavior consistent with a 2D, dense liquid. However, we also find that for selected conditions, our system is in an emergent hexatic (or even solid) phase showing its 2D nature. As expected for the hexatic phase, we find that the equilibration in this phase is very slow. By comparison with theory, we were able to reproduce qualitatively the experimentally observed phase behavior using computer simulations with a simple phenomenological model based on soft disks by matching density and the 1D pair correlation function. We thus demonstrate that static behavior of skyrmion ensembles may be described by a simple 2D model system highlighting that our skyrmion lattices can indeed be used as 2D model systems with major advantages in terms of tunability and speed compared to conventionally used 2D model systems such as colloids.

4. Experimental Section

Sample Parameters: The sample was prepared using magnetron sputtering in a Singulus Rotaris sputtering tool. The base pressure during the growth process was less than 3×10^{-8} mbar. The composition of the single stack was $Ta(5)/Co_{20}Fe_{60}B_{20}(0.9)/Ta(0.08)/MgO(2)/Ta(5)$, with the thickness of individual layers given in nanometers in parentheses. With the used deposition system, the thickness of the individual layers can be tuned in the stack in a controlled manner with high accuracy. The stack is similar to the one reported on previously where it was found that the very thin Ta layer on top of the CoFeB plays a key role in setting the effective anisotropy.[1] The sample was characterized using the magneto-optical Kerr effect (MOKE) measurement. Single skyrmions can be stabilized in the ferromagnetic layer using out-of-plane field sweeping, meaning applying an oscillating out-of-plane field over several oscillation periods. This procedure moves the domains and eventually they break into smaller domains and in this case can form skyrmions. Elongated domains and skyrmions exhibit thermally activated diffusion. The hysteresis loop in applied out-of-plane field shows an hour-glass shape, typical for material with the presence of skyrmions (see Supporting Information). With higher temperature, the hysteresis loop is tilted toward larger applied fields. This indicates a change of the anisotropy of the material with temperature. The lowest investigated temperature is determined by the ability to stabilize the skyrmion lattice. Below 325 K, only stripe domains were nucleated by the saturation of the sample with an in-plane field. The highest achievable temperature for the lattice investigation was determined by the resolution of the microscope and the thermally activated motion of skyrmions. Above 338 K, the size of the skyrmions was comparable to the resolution of the Kerr microscope. The

skyrmions movement was also more rapid. Above this temperature, no reliable skyrmion tracking in this material system could be performed.

The DMI was measured by investigating the domain periodicity at zero magnetic field and by comparison with micromagnetic simulations. Using the measured parameters of magnetic anisotropy and saturation magnetization and an exchange parameter of $A = 10$ pJ m^{-1}, it was found that DMI is needed to stabilize skyrmion structures. The obtained DMI from comparing the measurement with the simulations is comparable to the value published previously for a similar stack ($D_I = 0.3 \pm 0.1$ mJ m^{-2}).[1] The DMI in the material is sufficiently strong so that only topologically non-trivial skyrmion spin structures are stable. The effect of the topology on the skyrmion lattice phases and phase transitions could be studied in a material where both topologically trivial bubbles and non-trivial skyrmions are stable, which however goes beyond the scope of the current work.

Measurement Setup: A commercial Evico GmbH MOKE microscope was used. The optical spatial resolution is approximately 400 nm. The temporal resolution remains the same at any temperature and magnetic field and is 62.5 ms. At higher temperatures, the skyrmions become much smaller and their diffusion is enhanced and thus faster. This hinders the reliable tracking to identify the position given the time resolution. Therefore, the threshold where skyrmions can be tracked is determined by both the temporal and spatial resolution of the microscope setup. The in-plane field coil was supplied from the microscope manufacturer. The highest achievable in-plane field was 300 mT. The coil for the out-of-plane field application was custom built at the University of Mainz. The coil was designed to have negligible coercivity and to be able to supply the sample with very small controlled fields in orders of μT. A current versus magnetic field calibration was performed using a Gaussmeter in the position of the sample and used during the measurement along different directions. The calibration for the Earth magnetic field was done using the hysteresis loop of the material. The residual Earth field caused an offset in the *x*-axis of the *M-H* loop. The authors compensated for this offset in the coil calibration. The calibration of all stray-fields and resulting offsets in the field values was performed before every measurement and no changes were observed during the timescale of the measurement. Adjustment of the in-plane field coil was done the same way. When the coil was tilted or set in a way that a cross field between the out-of-plane and in-plane field was present, the *M-H* loop of the material was shifted. The in-plane field coil was adjusted so that the hysteresis loop is the same as without the coil, only with out-of-plane field. A stage with two HighTech QuickCool QC-32-0.6.1.2 Peltier elements was used for the temperature change of the sample in the range of 280–350 K. The temperature was externally controlled by measurement of resistivity of a Pt100 resistor, which was placed next to the multilayer sample. The stability of the set temperature was measured to be within 0.3 K. The frame rate of the microscope camera was 16 frames s^{-1}; therefore, the time resolution of the microscope measurement was 62.5 ms.

Skyrmion Tracking: Skyrmion lattices are visualized using a Magneto-Optical Kerr-Microscope. In the pictures the out-of-plane magnetization is represented by a grey scale, so that the skyrmions appear as light blobs on a dark(er) background. Videos recorded that way were consecutively analyzed using the Trackpy[3] package. In a first stage, it locates the skyrmions by detecting Gaussian-like blobs in the grey scale movies. It was ensured that the software finds all skyrmions in the individual video frames. Several parameters are set to optimize the recognition for reliable results. Most importantly, the mask-parameter sets a rough estimate for the pixel-diameter of the features to be found. During the evaluation, it is set slightly above the average skyrmion diameter determined by simple binarization of the frame. The separation-parameter enforces a minimum separation between the recognized features, this way over-recognition in defective areas is prevented. A safe value for the recognition is several pixels lower than the average skyrmion distance. The percentile-parameter depends on the contrast of the video and indicates to which extend the features are expected to be brighter than the surrounding area. The noise-parameter is a measure for the "sharpness" of the features to be detected and can vary between

**ADVANCED
SCIENCE NEWS**

www.advancedsciencenews.com

**ADVANCED
FUNCTIONAL
MATERIALS**

www.afm-journal.de

measurement videos with different external parameters. Most of the skyrmion diameters are in a range from 7 to 13 pixels, corresponding to 4.5–8.5 μm. For example, at the temperature of 338 K and the out-of-plane field of 20 μT, we set the mask to 9, the separation to 4, and the noise to 0.15.

Quantifiers for Phase Transitions in 2D Systems: The pair correlation function (PCF) (Equation (2)) determines the probability of finding two skyrmions at a distance **r** from each other. The position of the first peak assesses the mean nearest neighbor distance and deep in the solid phase characteristic sharp peaks resulting from the underlying lattice appear. It is, however, impossible to distinguish $g(r)$ of liquid, hexatic and solid phases close to the phase transition and other identifiers need to be considered. Since the disk-shaped skyrmions develop hexagonal order as the bulk density increases, one can resort to the local orientational order parameter ψ_6 (Equation (1)).[27] This complex parameter measures deviations from hexagonal order. The absolute value $|\psi_6| = 1$ for a perfect triangular lattice and decreases to 0 with increasing disorder. In addition to the absolute value of ψ_6 one can also extract the local orientation angle of neighboring skyrmions, that is, the Euler angle of ψ_6 divided by 6. Note that the orientation of a hexagonally ordered cluster consisting of the central particle and its six neighbors is essentially determined by the angle between the x-axis and the vector of the central particle and its neighbor in the range of 0–60°. The factor of six in the definition of ψ_6 projects all vectors between the central particle and its neighbors on top of each other and ψ_6 averages over these projections. The orientation angle (ranging from 0° to 60°) is therefore a gauge for the local orientation of the cluster with respect to the x-axis. This parameter is well-suited to visualize clusters of equal orientation. In simulations of soft disks, it was also noticed empirically that the mean $|\psi_6|$ is roughly $\langle|\psi_6|\rangle \approx 0.69$ at the liquid branch of the liquid to hexatic phase transition (see Supporting Information), and this parameter was used as an additional indicator for the transition. For computing $g(r)$ and ψ_6, the MD analysis program FREUD was employed.[17]

Molecular Dynamics Simulations of Soft Disks: Molecular Dynamics simulations of soft disks were performed using the model of Kapfer and Krauth with the HOOMD Molecular Dynamics package and a Langevin integrator:[18,32]

$$V(r) = \left(\frac{\sigma}{r}\right)^n \tag{4}$$

In this coarse, phenomenological model for the bulk behavior of skyrmions, σ roughly corresponds to the mean skyrmion distance, and n denotes the steepness of the potential. By running MD simulations at the experimentally determined skyrmion density, the authors were able to adjust the simulation potential so that the pair correlation for the simulated soft disks matches the pair correlation of the skyrmions. In order not to overparameterize the mapping to the experimentally measured PCFs, the authors only adjusted n and set σ constant. Even though the position of the first peak of the PCFs is not necessarily identical with the σ of the simulation potential, this approximation turns out to be sufficiently accurate for the examined densities. Therefore, σ was set in the simulations to be the position of the first peak of the experimentally determined PCFs. Simulations were then run for varying n in the range between 6 and 12 with 0.1 resolution. The matching of the simulated and experimental PCFs is determined as mean squared deviation measured up to the fourth maximum. This deviation shows a smooth dependence of n and a clear minimum which were taken as best match to the experiment. The optimal n is typically around 10 (for $T = 338$ K) and somewhat lower for lower temperatures. The determined density, σ and n allow running simulations mapped closely to the experiment and the estimated underlying experimental potential. For these mapped simulations, the mean absolute value $\langle|\psi_6|\rangle$ were determined, which is to some extent, dependent on the equilibration time of the simulations. If not mentioned otherwise, the system was equilibrated for 10^6 time steps before measurements were taken. It should also be noted that the simulations employ a Langevin dynamics thermostat with a time step of 10^{-3} and could be further improved by including additional specific

terms to account for gyrotropic dynamics.[33–35] It is not expected that the current static equilibrium results are affected because such terms do not contribute to the energy of the system and thus do not break detailed balance.[35] However, to analyze the dynamics of the system evolution in the future, such terms need to be considered.

Data Availability

The data that support the plots within this paper and other findings of this study are available from the corresponding author upon reasonable request.

Supporting Information

Supporting Information is available from the Wiley Online Library or from the author.

Conflict of Interest

The authors declare no conflict of interest.

Author Contributions

J.Z. and F.D. contributed equally to this work. M.K., P.V., and J.Z. proposed and supervised the study. J.Z. and N.K. fabricated and characterized the multilayer samples. J.Z., N.K., and K.R. prepared the measurement setup and conducted the experiments using the Kerr microscope. F.D., J.Z., Y.G., T.W., and N.K. evaluated the experimental data with the help of K.R., P.V., M.V., and K.L. F.D. and P.V. conducted theoretical simulations and comparison with the experimental results. J.Z. and F.D. prepared the manuscript with the help of M.V., P.V., and M.K. All authors commented on the manuscript.

[1] A. Fert, N. Reyren, V. Cros, *Nat. Rev. Mater.* **2017**, *2*, 17031.

[2] G. Finocchio, F. Büttner, R. Tomasello, M. Carpentieri, M. Kläui, *J. Phys. D. Appl. Phys.* **2016**, *49*, 423001.

[3] X. Zhang, M. Ezawa, Y. Zhou, *Sci. Rep.* **2015**, *5*, 9400.

**ADVANCED
SCIENCE NEWS**

www.advancedsciencenews.com

**ADVANCED
FUNCTIONAL
MATERIALS**

www.afm-journal.de

[4] F. Jonietz, S. Mühlbauer, C. Pfleiderer, A. Neubauer, W. Münzer, A. Bauer, T. Adams, R. Georgii, P. Böni, R. A. Duine, K. Everschor, M. Garst, A. Rosch, *Science* **2010**, *330*, 1648.

[5] X. Z. Yu, N. Kanazawa, W. Z. Zhang, T. Nagai, T. Hara, K. Kimoto, Y. Matsui, Y. Onose, Y. Tokura, *Nat. Commun.* **2012**, *3*, 988.

[6] W. Jiang, P. Upadhyaya, W. Zhang, G. Yu, M. B. Jungfleisch, F. Y. Fradin, J. E. Pearson, Y. Tserkovnyak, K. L. Wang, O. Heinonen, S. G. E. E. te Velthuis, A. Hoffmann, *Science* **2015**, *349*, 283.

[7] S. Woo, K. Litzius, B. Krüger, M.-Y. Im, L. Caretta, K. Richter, M. Mann, A. Krone, R. M. Reeve, M. Weigand, P. Agrawal, I. Lemesh, M.-A. Mawass, P. Fischer, M. Kläui, G. S. D. D. Beach, *Nat. Mater.* **2016**, *15*, 501.

[8] I. Lemesh, K. Litzius, M. Böttcher, P. Bassirian, N. Kerber, D. Heinze, J. Zázvorka, F. Büttner, L. Caretta, M. Mann, M. Weigand, S. Finizio, J. Raabe, M. Im, H. Stoll, G. Schütz, B. Dupé, M. Kläui, G. S. D. Beach, *Adv. Mater.* **2018**, *30*, 1805461.

[9] F. Zheng, H. Li, S. Wang, D. Song, C. Jin, W. Wei, A. Kovács, J. Zang, M. Tian, Y. Zhang, H. Du, R. E. Dunin-Borkowski, *Phys. Rev. Lett.* **2017**, *119*, 197205.

[10] K. Everschor-Sitte, J. Masell, R. M. Reeve, M. Kläui, *J. Appl. Phys.* **2018**, *124*, 240901.

[11] J. Zázvorka, F. Jakobs, D. Heinze, N. Keil, S. Kromin, S. Jaiswal, K. Litzius, G. Jakob, P. Virnau, D. Pinna, K. Everschor-Sitte, L. Rózsa, A. Donges, U. Nowak, M. Kläui, *Nat. Nanotechnol.* **2019**, *14*, 658.

[12] D. Prychynenko, M. Sitte, K. Litzius, B. Krüger, G. Bourianoff, M. Kläui, J. Sinova, K. Everschor-Sitte, *Phys. Rev. Appl.* **2018**, *9*, 014034.

[13] T. Nakajima, H. Oike, A. Kikkawa, E. P. Gilbert, N. Booth, K. Kakurai, Y. Taguchi, Y. Tokura, F. Kagawa, T. Arima, *Sci. Adv.* **2017**, *3*, e1602562.

[14] S. Mühlbauer, B. Binz, F. Jonietz, C. Pfleiderer, A. Rosch, A. Neubauer, R. Georgii, P. Böni, *Science* **2009**, *323*, 915.

[15] P. Huang, T. Schönenberger, M. Cantoni, L. Heinen, A. Magrez, A. Rosch, F. Carbone, H. M. Rønnow, *Nat. Nanotechnol.* **2020**, *1*, https://doi.org/10.1038/s41565-020-0716-3.

[16] S. A. Díaz, C. J. O. Reichhardt, D. P. Arovas, A. Saxena, C. Reichhardt, *Phys. Rev. B* **2017**, *96*, 085106.

[17] V. Ramasubramani, B. D. Dice, E. S. Harper, M. P. Spellings, J. A. Anderson, S. C. Glotzer, *Comput. Phys. Commun.* **2020**, *254*, 107275.

[18] S. C. Kapfer, W. Krauth, *Phys. Rev. Lett.* **2015**, *114*, 035702.

[19] M. Engel, J. A. Anderson, S. C. Glotzer, M. Isobe, E. P. Bernard, W. Krauth, *Phys. Rev. E* **2013**, *87*, 042134.

[20] E. P. Bernard, W. Krauth, *Phys. Rev. Lett.* **2011**, *107*, 155704.

[21] K. Zahn, R. Lenke, G. Maret, *Phys. Rev. Lett.* **1999**, *82*, 2721.

[22] K. Zahn, G. Maret, *Phys. Rev. Lett.* **2000**, *85*, 3656.

[23] P. Keim, G. Maret, H. H. Von Grünberg, *Phys. Rev. E* **2007**, *75*, 031402.

[24] Y. Nishikawa, K. Hukushima, W. Krauth, *Phys. Rev. B* **2019**, *99*, 064435.

[25] P. Dillmann, G. Maret, P. Keim, *J. Phys. Condens. Matter* **2012**, *24*, 464118.

[26] U. K. Rößler, A. A. Leonov, A. N. Bogdanov, *J. Phys. Conf. Ser.* **2011**, *303*, 012105.

[27] D. R. Nelson, B. I. Halperin, *Phys. Rev. B* **1979**, *19*, 2457.

[28] J. Zausch, P. Virnau, K. Binder, J. Horbach, R. L. Vink, *J. Chem. Phys.* **2009**, *130*, 064906.

[29] D. Winter, J. Horbach, P. Virnau, K. Binder, *Phys. Rev. Lett.* **2012**, *108*, 028303.

[30] S. K. Das, S. A. Egorov, B. Trefz, P. Virnau, K. Binder, *Phys. Rev. Lett.* **2014**, *112*, 198301.

[31] Trackpy, https://github.com/soft-matter/trackpy (accessed: July 2019).

[32] J. A. Anderson, C. D. Lorenz, A. Travesset, *J. Comput. Phys.* **2008**, *227*, 5342.

[33] A. A. Thiele, *Phys. Rev. Lett.* **1973**, *30*, 230.

[34] B. L. Brown, U. C. Täuber, M. Pleimling, *Phys. Rev. B* **2018**, *97*, 020405.

[35] B. L. Brown, U. C. Täuber, M. Pleimling, *Phys. Rev. B* **2019**, *100*, 024410.

ADVANCED FUNCTIONAL MATERIALS

Supporting Information

for *Adv. Funct. Mater.,* DOI: 10.1002/adfm.202004037

Skyrmion Lattice Phases in Thin Film Multilayer

Jakub Zázvorka, Florian Dittrich, Yuqing Ge, Nico Kerber, Klaus Raab, Thomas Winkler, Kai Litzius, Martin Veis, Peter Virnau,* and Mathias Kläui*

Skyrmion Lattice Phases in Thin Film Multilayer.

Jakub Zázvorka[1,2, +], Florian Dittrich[1, +], Yuqing Ge[1], Nico Kerber[1,3], Klaus Raab[1], Thomas Winkler[1], Kai Litzius[1,3,4], Martin Veis[2], Peter Virnau[1,3,*], Mathias Kläui[1,3,*].

1. Institut für Physik, Johannes Gutenberg-Universität Mainz, Mainz, Germany.

2. Charles University, Faculty of Mathematics and Physics, Institute of Physics, Ke Karlovu 5, CZ-121 16, Prague 2, Czech Republic.

3. Graduate School of Excellence Materials Science in Mainz, Mainz, Germany.

4. Max Planck Institute for Intelligent Systems, Stuttgart, Germany.

[+]*These authors contributed equally.*

[*] Corresponding authors: Klaeui@uni-mainz.de, Virnau@uni-mainz.de

Supplementary Information

1. MOKE Loops

Magnetization hysteresis loops using the Kerr microscope were investigated with respect to an out-of-plane field. No in-plane field was applied. The measurements were performed to determine the range of the out-of-plane field which can be applied to stabilize domains and magnetic textures in the sample. The MOKE signal is evaluated as the overall grayscale contrast averaged over the whole picture frame. **Figure S1** shows the gradual change of the

hysteresis loops at different temperatures. Whereas at 300 K a sharp switching was observed and no skyrmions could be nucleated using field sweeping, at 325 K the sample shows a "hourglass-shaped" loop. In this configuration, using an out-of-plane field, a low density of skyrmions is nucleated together with elongated worm-like domains. At higher temperatures, the loop tilts towards higher field and skyrmions are nucleated at those field values. However, the nucleation of skyrmion lattices was only achieved using in-plane field sweeping.
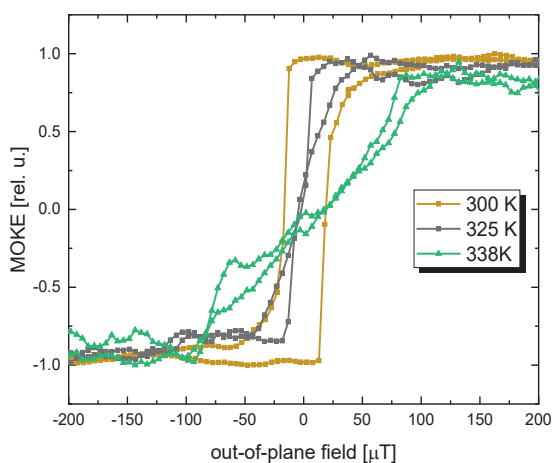

Figure S1. Magnetization hysteresis loops at various temperatures measured using the Kerr microscope. The hysteresis loops transform from rectangular sharp switching at temperature 300 K to a butterfly-shaped loop at temperatures around 330 K. At those temperatures, the skyrmion lattices are nucleated and investigated.

2. Magnetization with Temperature

The temperature dependence of the magnetization was determined using the superconducting quantum interference device (SQUID). Measurements were performed to

investigate the change of magnetization in the range of temperatures used in the study. The substrate contribution was obtained by measuring the magnetization loops and subtracting the diamagnetic background. Magnetization dependence was fitted using the Bloch's law. The Curie temperature was determined at $T_C \approx 448\ K$. This indicates that the temperature range used for the skyrmion lattice ordering is far enough from the critical temperature.
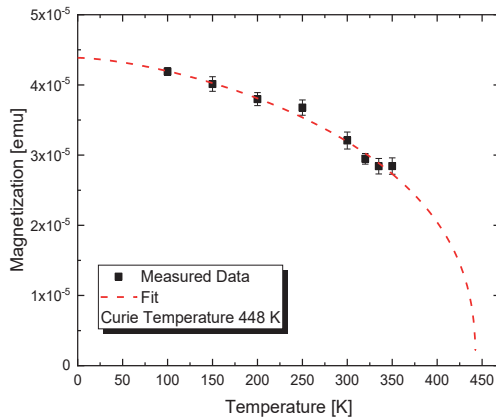

Figure S2. Temperature dependence of the magnetization of the studied material.

3. Skyrmion Nucleation

The studied material exhibited perpendicular magnetic anisotropy. Using out-of-plane field sweeping, only stripe domains and a low density of skyrmions are present in the sample. Upon saturation of the sample using an in-plane field (not depending on the field orientation in the hard plane) and after discontinuation of the in-plane field, a high density of skyrmions is nucleated in the sample. The density and the mean radius of the skyrmions is controlled by simultaneous application of the out-of-plane field additional to the nucleation in-plane field. Depending on the interplay between the out-of-plane field and the

material magnetic anisotropy, the nucleated skyrmions expand to worm domains or shrink in their size down to a complete annihilation. The magnetic state before and after the application of the in-plane field sweeping is shown in **Figure S3**. As it has been previously shown that skyrmion nucleation occurs in the time scale of nanoseconds and the time needed for the in-plane field to be fully switched in our setup is in the range of milliseconds, we cannot resolve the skyrmion nucleation by itself. However, we focus on the formation and effects of the skyrmion lattice which lie within the resolution of our setup. To evaluate the skyrmion lattice, videos of the domain state have been taken using the Kerr microscope. The starting point was after the application of the desired out-of-plane field and when the sample was fully saturated with the in-plane field. Afterwards, videos with the duration of one minute with the frame resolution of 16 fps (62.5 ms) have been taken for various out-of-plane field settings and several temperatures.
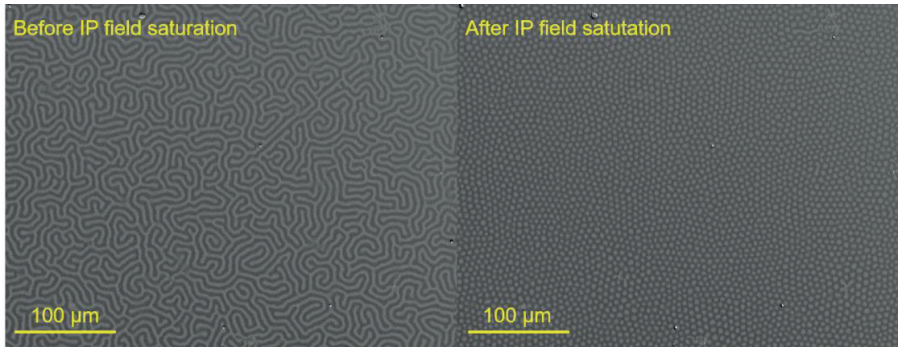

Figure S3. Effect of in-plane sweeping on the skyrmion nucleation at temperature 335 K and constant out-of-plane field of 20 µT. On the left is the domain state after application of the out-of-plane field. No skyrmions are present in this state. After in-plane (IP) field application and discontinuation, a high density of skyrmion is nucleated in the sample, as seen on the right.

4. Matching of Experiment and Simulation

The matching of simulations to experiments was outlined in the Experimental Section and here we address more details.

To match a certain experimental measurement the positional data of the measured skyrmions are evaluated first. The pair correlation function is calculated averaging over the last 30s of the measurement video. The position of the (first) maximum of the so obtained $g(r)$ sets the σ of our simulation potential (**Equation 4**). The skyrmion density is also calculated by averaging over the last 30s of the measurement video. For each frame, the number of detected skyrmions is divided by the detection area (given by the minimum and maximum of detected positions in x and y direction) and then averaged. This way the size of the unit cell of the simulation is given by the square root of the density. In different simulations with different exponents n in the potential, the deviation of the simulated $g(r)$ from the experimental $g(r)$ is calculated as described in the Experimental Section. A plot of this deviation in dependence of n can be seen in **Figure S4a**. It shows a clear minimum, from which n was determined. The simulated $g(r)$ for this best match and the experimental one can be seen in **Figure S4b**.

In general, this matching method works better for lower densities and higher out-of-plane fields. This is likely because the assumption that the position of the first peak roughly equals σ is more exact for these densities.
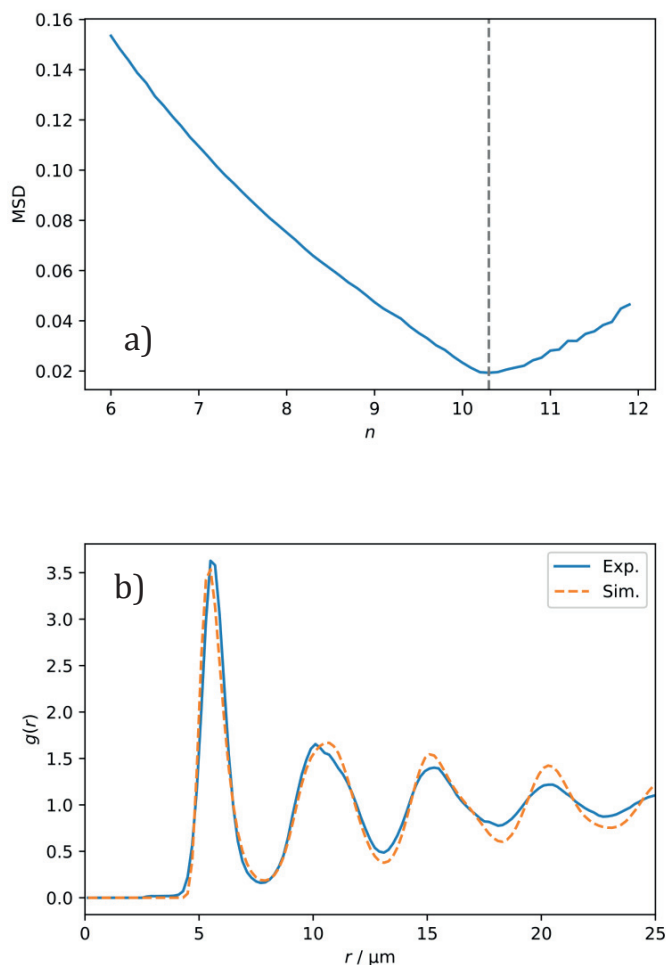
Figure S4. Matching theoretical simulations to experimental results. a) The mean squared deviation of the simulated pair correlation function and the experimental one, measured up to the 4th maximum in dependence of n (T = 338 K and 20 µT). The minimum is marked by the dashed line at n = 10.3. b) Experimental and matched pair correlation function (for T = 338 K and 20 µT), simulated with n = 10.3 as determined in **Figure S4a**. The experimental pair correlation function is less pronounced in the higher order peaks, likely due to interfaces. Note that the matching works better for less dense systems. The experimental

pair correlation function shows a small discontinuity at around 3 μm which corresponds to the cutoff of our tracking software. The slight increase for r>3 μm is likely due to defects.

5. Equilibration towards the Hexatic Phase

In order to better understand the equilibration process of the experimental data, we simulated the experimental data set at T = 338 K and 20 μT with corresponding mapped potential. As we showed before in **Figure 1** the formation of the skyrmion lattice is taking place rather quickly (about 30s) which is indicated by the measurements of $\langle|\psi_6|\rangle$ and the pair correlation function. Measurements of $\langle|\psi_6|\rangle$ however continue to grow slowly, indicating that equilibrium is not reached yet. **Figure 4** suggests, that the 60s of experimental measurements roughly correspond to something between 10^4 to 10^5 simulation steps for T = 338 K and 20 μT. **Figure S5** shows the evolution of $\langle|\psi_6|\rangle$ for the same simulation in dependence of simulation steps. It shows that the equilibration towards the hexatic phase is still not reached for 10^6 simulation steps and continues even further. This is in good agreement with the corresponding evolution of the spatial correlation functions shown in **Figure 4**. Between 10^4 to 10^5 simulation steps $\langle|\psi_6|\rangle$ for the simulation is below the experimental $\langle|\psi_6|\rangle$. This might indicate that the mapped potential is a bit too soft due to the above-mentioned problems of finding the correct σ. In conclusion one can estimate, that a fully equilibrated skyrmion lattice at this experimental setup is deeper in the hexatic phase than the measured $\langle|\psi_6|\rangle$ and spatial correlation functions do indicate for now.
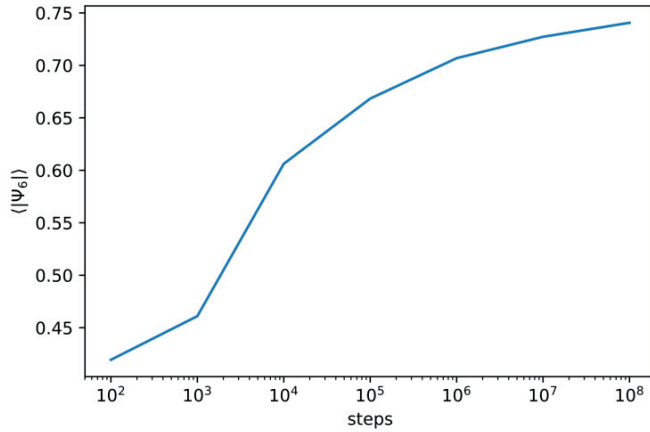
Figure S5. Time evolution of the mean absolute value $\langle|\psi_6|\rangle$ for a simulation matching the experimental 338 K, 20 µT system. Simulation took place in a quadratic box containing 40000 particles.

6. Analysis of $\langle|\psi_6|\rangle$ for Soft Disks

$\langle|\psi_6|\rangle$ for soft disks depends on the potential (i.e. *n*) and weakly depends on the system size. It turns out to be mostly independent of these parameters around the phase transition, namely the transition from the liquid phase to the liquid-hexatic-coexistence phase. This phase transition is the relevant one for us to mark the transition to the hexatic phase. **Figure S6** visualizes the properties of $\langle|\psi_6|\rangle$ described above and shows that $\langle|\psi_6|\rangle$ is around 0.69 when the phase transition to the hexatic phase starts. [18]
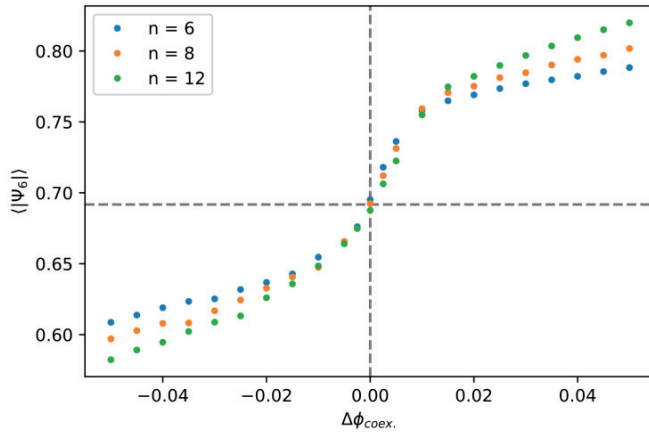
Figure S6. Shows that the mean absolute value $\langle|\psi_6|\rangle$ does not differ at the transition point and closely below for different potentials (with n= 6, 8 and 12). Same applies for different system sizes. Above points are the results of individual simulations of quadratic boxes containing 40000 particles each. X-Axis is linearly shifted to match the liquid-to-liquid-hexatic-coexistence phase transition points as determined in Ref. [18]. (dashed vertical line). The points in [-0.005...0.005] had 10^8 steps equilibration time and were measured over the course of 10^9 steps. All other points had $5 \cdot 10^6$ steps equilibration time and were measured over the course of 10^8 steps.

[1] A. Fert, N. Reyren, V. Cros, *Nat. Rev. Mater.* **2017**, *2*, 17031.

[2] G. Finocchio, F. Büttner, R. Tomasello, M. Carpentieri, M. Kläui, *J. Phys. D. Appl. Phys.* **2016**, *49*, 423001.

[3] X. Zhang, M. Ezawa, Y. Zhou, *Sci. Rep.* **2015**, *5*, 9400.

[4] F. Jonietz, S. Mühlbauer, C. Pfleiderer, A. Neubauer, W. Münzer, A. Bauer, T. Adams, R.

Georgii, P. Böni, R. A. Duine, K. Everschor, M. Garst, A. Rosch, *Science* **2010**, *330*, 1648.

[5] X. Z. Yu, N. Kanazawa, W. Z. Zhang, T. Nagai, T. Hara, K. Kimoto, Y. Matsui, Y. Onose, Y. Tokura, *Nat. Commun.* **2012**, *3*, 988.

[6] W. Jiang, P. Upadhyaya, W. Zhang, G. Yu, M. B. Jungfleisch, F. Y. Fradin, J. E. Pearson, Y. Tserkovnyak, K. L. Wang, O. Heinonen, S. G. E. E. te Velthuis, A. Hoffmann, *Science* **2015**, *349*, 283.

[7] S. Woo, K. Litzius, B. Krüger, M.-Y. Im, L. Caretta, K. Richter, M. Mann, A. Krone, R. M. Reeve, M. Weigand, P. Agrawal, I. Lemesh, M.-A. Mawass, P. Fischer, M. Kläui, G. S. D. D. Beach, *Nat. Mater.* **2016**, *15*, 501.

[8] I. Lemesh, K. Litzius, M. Böttcher, P. Bassirian, N. Kerber, D. Heinze, J. Zázvorka, F. Büttner, L. Caretta, M. Mann, M. Weigand, S. Finizio, J. Raabe, M. Im, H. Stoll, G. Schütz, B. Dupé, M. Kläui, G. S. D. Beach, *Adv. Mater.* **2018**, *30*, 1805461.

[9] F. Zheng, H. Li, S. Wang, D. Song, C. Jin, W. Wei, A. Kovács, J. Zang, M. Tian, Y. Zhang, H. Du, R. E. Dunin-Borkowski, *Phys. Rev. Lett.* **2017**, *119*, 197205.

[10] K. Everschor-Sitte, J. Masell, R. M. Reeve, M. Kläui, *J. Appl. Phys.* **2018**, *124*, 240901.

[11] J. Zázvorka, F. Jakobs, D. Heinze, N. Keil, S. Kromin, S. Jaiswal, K. Litzius, G. Jakob, P. Virnau, D. Pinna, K. Everschor-Sitte, L. Rózsa, A. Donges, U. Nowak, M. Kläui, *Nat. Nanotechnol.* **2019**, *14*, 658.

[12] D. Prychynenko, M. Sitte, K. Litzius, B. Krüger, G. Bourianoff, M. Kläui, J. Sinova, K. Everschor-Sitte, *Phys. Rev. Appl.* **2018**, *9*, 014034.

[13] T. Nakajima, H. Oike, A. Kikkawa, E. P. Gilbert, N. Booth, K. Kakurai, Y. Taguchi, Y. Tokura, F. Kagawa, T. Arima, *Sci. Adv.* **2017**, *3*, e1602562.

[14] S. Mühlbauer, B. Binz, F. Jonietz, C. Pfleiderer, A. Rosch, A. Neubauer, R. Georgii, P.

Böni, *Science* **2009**, *323*, 915.

[15] P. Huang, M. Cantoni, A. Magrez, F. Carbone, H. M. Rønnow, *arXiv* **2018**, *1807*, 08352.

[16] S. A. Díaz, C. J. O. Reichhardt, D. P. Arovas, A. Saxena, C. Reichhardt, *Phys. Rev. B* **2017**, *96*, 085106.

[17] V. Ramasubramani, B. D. Dice, E. S. Harper, M. P. Spellings, J. A. Anderson, S. C. Glotzer, *Comput. Phys. Commun.* **2020**, *254*, 107275.

[18] S. C. Kapfer, W. Krauth, *Phys. Rev. Lett.* **2015**, *114*, 035702.

[19] M. Engel, J. A. Anderson, S. C. Glotzer, M. Isobe, E. P. Bernard, W. Krauth, *Phys. Rev. E* **2013**, *87*, 042134.

[20] E. P. Bernard, W. Krauth, *Phys. Rev. Lett.* **2011**, *107*, 155704.

[21] K. Zahn, R. Lenke, G. Maret, *Phys. Rev. Lett.* **1999**, *82*, 2721.

[22] K. Zahn, G. Maret, *Phys. Rev. Lett.* **2000**, *85*, 3656.

[23] P. Keim, G. Maret, H. H. Von Grünberg, *Phys. Rev. E - Stat. Nonlinear, Soft Matter Phys.* **2007**, *75*, 031402.

[24] Y. Nishikawa, K. Hukushima, W. Krauth, *Phys. Rev. B* **2019**, *99*, 064435.

[25] P. Dillmann, G. Maret, P. Keim, *J. Phys. Condens. Matter* **2012**, *24*, 464118.

[26] U. K. Rößler, A. A. Leonov, A. N. Bogdanov, *J. Phys. Conf. Ser.* **2011**, *303*, 012105.

[27] D. R. Nelson, B. I. Halperin, *Phys. Rev. B* **1979**, *19*, 2457.

[28] J. Zausch, P. Virnau, K. Binder, J. Horbach, R. L. Vink, *J. Chem. Phys.* **2009**, *130*, 3253.

[29] D. Winter, J. Horbach, P. Virnau, K. Binder, *Phys. Rev. Lett.* **2012**, *108*, 028303.

[30] S. K. Das, S. A. Egorov, B. Trefz, P. Virnau, K. Binder, *Phys. Rev. Lett.* **2014**, *112*, 198301.

[31] J. A. Anderson, C. D. Lorenz, A. Travesset, *J. Comput. Phys.* **2008**, *227*, 5342.

[32]   A. A. Thiele, *Phys. Rev. Lett.* **1973**, *30*, 230.

[33]   B. L. Brown, U. C. Täuber, M. Pleimling, *Phys. Rev. B* **2018**, *97*, 020405.

[34]   B. L. Brown, U. C. Täuber, M. Pleimling, *Phys. Rev. B* **2019**, *100*, 024410.

Conclusion and Outlook

This work touched on many aspects of phase behavior in non-equilibrium systems and provided valuable insights and methods. Even though no final answer on the nature of universality in active matter systems could be provided yet, the understanding of such systems has been significantly improved. Nevertheless, there is still a long way to go towards a comprehensive theory of non-equilibrium systems.

There are clear indications that MIPS in 2D active matter systems does not show all the properties associated with the concept of universality known from equilibrium systems. The deviations documented in this work should not occur otherwise, especially there should be no model dependence if MIPS was a truly universal phenomenon. The combined results from [B1] and [A1] show these model dependent results for the critical exponents even clearer, besides using the very same measuring methods. In equilibrium, universality is not influenced by the underlying structure, e.g., whether the model is discrete or continuous, but solely based on the nature of the interaction potential and the dimensionality of the system. The continuous two-dimensional Lennard-Jones fluid for example yields the same critical exponents as the discrete two-dimensional Ising model.

Of course, one can argue that the measuring methods might cause the model dependence. Maybe they are working more exact in one model than in the other. However, the applied methods have not shown such deviations from model to model in equilibrium systems (2D Ising vs. Lennard-Jones fluid for example). Therefore, the discovered deviations clearly seem to be a highly interesting phenomenon unique to active matter either way.

A possible explanation is given in ref. [55]: When connecting the ABPs to field theories, the coupling between density and polarization in the particle current is a key ingredient. Close to two dimensions the renormalization flow exhibits a pair of perturbative fixed points that limit the attractive basin of the Wilson-Fisher fixed point. As a consequence, the critical behavior of active Brownian particles in two dimensions is governed by a strong-coupling fixed point different from Wilson-Fisher. A deviation from the Wilson-Fisher fixed point however can correspond to a deviation from Ising universality. Possibly, the amount of deviation can also be linked to the exact implementation of activity and other parameters, thus explaining some sort of model dependence.

Back in my diploma thesis I tested a slight modification of the 2D Ising model: First of all, a direction is assigned to all particles (spin up) and continuously updated to the direction of the last attempted movement of that particle, i.e., a Kawasaki move switching the spin with the next nearest lattice space. The Kawasaki move is furthermore preferably attempted in that direction with a

certain probability, hence introducing activity to the system. Since the spin-spin-interaction is kept in place, this model is not governed by MIPS, but by the 2D Ising phase separation. The introduced activity did only shift the critical temperature: The higher the activity, the lower the critical temperature and vice versa. This means, that the activity only introduced some additional energy to the system. However, the critical exponents measured deviated a bit from the ones measured for a pure 2D Ising system with no activity. The deviation increased with the amount of activity. Back then I attributed this to a lack in measurement accuracy. With the findings from the current work, it might be worth rethinking this assumption and having a second look.

In this context a closer look on possible influences of implementation parameters for ABPs (e.g., repulsive potential, setting of rotational diffusion and active propulsion, etc.) could provide more insights. Especially MIPS at very high rotational diffusion and active propulsion and vice versa might show interesting behavior. Unfortunately, improved measurement accuracy is key to these investigations. As discussed before, this is quite a challenge. The straightforward brute force approach of multiplying the computational resources is possible but not necessarily wise.

One idea is to further improve the subbox method to yield more and better statistics. Going back to the original subbox method of sampling the whole simulation box and finding another way to exclude the surface contributions might be a strategy. I came up with the idea of dynamically excluding only the subboxes that contain a certain amount of surface contributions. This can for example be realized by determining the density gradient in each subbox and excluding all subboxes that show a greater gradient than a certain threshold. If the subbox is in the dense or dilute phase, the gradient would be low. The same applies for a subbox in the homogenous phase, i.e., in a system without phase separation below MIPS. These subboxes would not be excluded. Only for subboxes that contain both phases (dilute and dense) with a more or less sharp dividing surface show a significant gradient and would be excluded. Developing such an approach requires a big amount of time for testing different implementations and verifying results. This can be done best within the well-known 2D Ising system. Unfortunately, I came up with that idea towards the end of my thesis so that there was no time left to explore it. Nevertheless, this is probably a promising route to go.

Regarding the dynamical properties of active systems, we did not find notable deviations from 2D Ising behavior for the quenches to the critical point in [A2]. The supposed effect of activity on the universal behavior seems to affect different critical exponents with a different magnitude. This is consistent with [A1] where the results for the critical exponent β show the biggest deviations from 2D Ising universality. However, some deviations for

the quenches of the active lattice models deep inside the phase separated regime have been encountered and shown in the SI of [A2]. They are not discussed any further, since a more detailed investigation is required to understand this matter.

On the skyrmion topic, new analysis methods have been developed and established. The iterative fitting of pair-correlation functions from simulations to experiment is a powerful tool to probe the underlying interaction potential. Knowledge of the interaction potential for skyrmion lattices facilitated further research about the behavior in confined geometries, which is fundamental to developing new probabilistic computing applications, as examined in [B3]. The introduced parameter $\langle|\psi_6|\rangle$ and its determined threshold value of 0.69 for repulsive power law potentials provides a handy indication of whether the examined system is experiencing a liquid, hexatic or solid phase state. This kind of analysis was also applied in [B2] and complemented the experimental findings. Last but not least [A3] demonstrated, that skyrmion lattices are great experimental realization of two-dimensional soft disks. Compared to conventionally used two-dimensional model systems, colloids for example, they show major advantages in terms of tunability and speed.

Besides all that, my work at the intersection between soft and hard matter has led to a long-term successful collaboration between the group of apl. Prof. Dr. Peter Virnau and the group of Prof. Dr. Mathias Kläui. This collaboration has so far resulted in two master's theses and two doctoral students who are continuing and further developing this kind of simulations. Thus, apart from [B2] and [B3] there has been more follow up work that is based on the previously performed work in [A3]. My colleague Jan Rothörl for example added a magnus force (as described by the Thiele equation) to the soft disks of our coarse-grained skyrmion lattice simulations in order to check for the limits of the modelling done in [A3]. As expected he found that for the examined densities, there is no relevant correction towards the more coarse-grained modelling by pure soft disks with respect to static behavior. Furthermore, he refined the matching of pair-correlation functions between experiment and simulations by implementing an enhanced iterative Boltzmann inversion that is iterated throughout a series of BD simulations. Thereby previously encountered limitations due to low resolution of the experimentally measured pair-correlation function and high-density artefacts are bypassed. With this enhancement, it was possible to determine the skyrmion-skyrmion interaction potential more exactly and additionally the skyrmion-wall interaction potential for skyrmions in a confined geometry [119]. This is yet another nice example how methods from soft matter can be transferred and applied to hard matter problems. Additional follow up works include, e.g., studies of pinning-effects, enhanced diffusion and applications in the field of non-conventional computing [104], [123]–[126].

Obviously, the field of non-equilibrium systems remains a highly interesting subject with many opportunities to gain additional insights and develop new applications. A fundamental understanding of processes in these very systems will be key to future advances. This work was intended to, and did, create some part of that fundamental understanding.

Acknowledgement

References

[1]   F. Dittrich, T. Speck, and P. Virnau, "Critical behavior in active lattice models of motility-induced phase separation," *The European Physical Journal E*, vol. 44, no. 4, p. 53, Apr. 2021, doi: 10.1140/epje/s10189-021-00058-1.

[2]   F. Dittrich, J. Midya, P. Virnau, and S. K. Das, "Growth and aging in a few phase-separating active matter systems," *Phys Rev E*, vol. 108, no. 2, p. 024609, Aug. 2023, doi: 10.1103/PhysRevE.108.024609.

[3]   J. Zázvorka *et al.*, "Skyrmion Lattice Phases in Thin Film Multilayer," *Adv Funct Mater*, vol. 30, no. 46, p. 2004037, Nov. 2020, doi: 10.1002/adfm.202004037.

[4]   J. T. Siebert, F. Dittrich, F. Schmid, K. Binder, T. Speck, and P. Virnau, "Critical behavior of active Brownian particles," *Phys Rev E*, vol. 98, no. 3, p. 030601, Sep. 2018, doi: 10.1103/PhysRevE.98.030601.

[5]   A. v. Ognev *et al.*, "Magnetic Direct-Write Skyrmion Nanolithography," *ACS Nano*, vol. 14, no. 11, pp. 14960–14970, Nov. 2020, doi: 10.1021/acsnano.0c04748.

[6]   C. Song *et al.*, "Commensurability between Element Symmetry and the Number of Skyrmions Governing Skyrmion Diffusion in Confined Geometries," *Adv Funct Mater*, vol. 31, no. 19, p. 2010739, May 2021, doi: 10.1002/adfm.202010739.

[7]   J. Palacci, S. Sacanna, A. P. Steinberg, D. J. Pine, and P. M. Chaikin, "Living Crystals of Light-Activated Colloidal Surfers," *Science (1979)*, vol. 339, no. 6122, pp. 936–940, Feb. 2013, doi: 10.1126/science.1230020.

[8]   G. Brunner, "Applications of Supercritical Fluids," *Annu Rev Chem Biomol Eng*, vol. 1, no. 1, pp. 321–342, Jun. 2010, doi: 10.1146/annurev-chembioeng-073009-101311.

[9]   V. Reddy and M. Saharay, "Solubility of Caffeine in Supercritical CO_2 : A Molecular Dynamics Simulation Study," *J Phys Chem B*, vol. 123, no. 45, pp. 9685–9691, Nov. 2019, doi: 10.1021/acs.jpcb.9b08351.

[10]   J. R. Baylis *et al.*, "Self-propelled particles that transport cargo through flowing blood and halt hemorrhage," *Sci Adv*, vol. 1, no. 9, Oct. 2015, doi: 10.1126/sciadv.1500379.

[11]   S. T. Chang, V. N. Paunov, D. N. Petsev, and O. D. Velev, "Remotely powered self-propelling particles and micropumps based on miniature diodes," *Nat Mater*, vol. 6, no. 3, pp. 235–240, Mar. 2007, doi: 10.1038/nmat1843.

[12]   V. Magdanz, S. Sanchez, and O. G. Schmidt, "Development of a Sperm-Flagella Driven Micro-Bio-Robot," *Advanced Materials*, vol. 25, no. 45, pp. 6581–6588, Dec. 2013, doi: 10.1002/adma.201302544.

[13]   L. Alvarez *et al.*, "The rate of change in Ca2+ concentration controls sperm chemotaxis," *Journal of Cell Biology*, vol. 196, no. 5, pp. 653–663, Mar. 2012, doi: 10.1083/jcb.201106096.

[14]   W. Kang, Y. Huang, X. Zhang, Y. Zhou, and W. Zhao, "Skyrmion-Electronics: An Overview and Outlook," *Proceedings of the IEEE*, vol. 104, no. 10, pp. 2040–2061, Oct. 2016, doi: 10.1109/JPROC.2016.2591578.

[15]   P.-J. Hsu, A. Kubetzka, A. Finco, N. Romming, K. von Bergmann, and R. Wiesendanger, "Electric-field-driven switching of individual magnetic skyrmions," *Nat Nanotechnol*, vol. 12, no. 2, pp. 123–126, Feb. 2017, doi: 10.1038/nnano.2016.234.

[16]   W. Nolting, *Grundkurs Theoretische Physik 6*. Berlin, Heidelberg: Springer Berlin Heidelberg, 2014. doi: 10.1007/978-3-642-25393-5.

[17]   F. Schwabl, *Statistische Mechanik*. in Springer-Lehrbuch. Berlin/Heidelberg: Springer-Verlag, 2006. doi: 10.1007/3-540-31097-5.

[18]   M. E. Fisher, "Correlation Functions and the Critical Region of Simple Fluids," *J Math Phys*, vol. 5, no. 7, pp. 944–962, Jul. 1964, doi: 10.1063/1.1704197.

[19]   C. N. Yang, "The Spontaneous Magnetization of a Two-Dimensional Ising Model," *Physical Review*, vol. 85, no. 5, pp. 808–816, Mar. 1952, doi: 10.1103/PhysRev.85.808.

[20]   L. Onsager, "Crystal Statistics. I. A Two-Dimensional Model with an Order-Disorder Transition," *Physical Review*, vol. 65, no. 3–4, pp. 117–149, Feb. 1944, doi: 10.1103/PhysRev.65.117.

[21]   J. T. Siebert, "Computer simulations of active Brownian particles," Dissertation, Johannes Gutenberg-Universität Mainz, Mainz, 2018. doi: 10.25358/openscience-3854.

[22]   J. W. Essam and M. E. Fisher, "Padé Approximant Studies of the Lattice Gas and Ising Ferromagnet below the Critical Point," *J Chem Phys*, vol. 38, no. 4, pp. 802–812, Feb. 1963, doi: 10.1063/1.1733766.

[23]   B. Widom, "Equation of State in the Neighborhood of the Critical Point," *J Chem Phys*, vol. 43, no. 11, pp. 3898–3905, Dec. 1965, doi: 10.1063/1.1696618.

[24]   G. S. Rushbrooke, "On the Thermodynamics of the Critical Region for the Ising Problem," *J Chem Phys*, vol. 39, no. 3, pp. 842–843, Aug. 1963, doi: 10.1063/1.1734338.

[25]   D. R. Nelson and B. I. Halperin, "Dislocation-mediated melting in two dimensions," *Phys Rev B*, vol. 19, no. 5, pp. 2457–2484, Mar. 1979, doi: 10.1103/PhysRevB.19.2457.

[26]   S. C. Kapfer and W. Krauth, "Two-Dimensional Melting: From Liquid-Hexatic Coexistence to Continuous Transitions," *Phys Rev Lett*, vol. 114, no. 3, p. 035702, Jan. 2015, doi: 10.1103/PhysRevLett.114.035702.

[27]   M. Engel, J. A. Anderson, S. C. Glotzer, M. Isobe, E. P. Bernard, and W. Krauth, "Hard-disk equation of state: First-order liquid-hexatic transition in two dimensions with three simulation methods," *Phys Rev E*, vol. 87, no. 4, p. 042134, Apr. 2013, doi: 10.1103/PhysRevE.87.042134.

[28]   E. P. Bernard and W. Krauth, "Two-Step Melting in Two Dimensions: First-Order Liquid-Hexatic Transition," *Phys Rev Lett*, vol. 107, no. 15, p. 155704, Oct. 2011, doi: 10.1103/PhysRevLett.107.155704.

[29]   C. Alba-Simionesco *et al.*, "Effects of confinement on freezing and melting," *Journal of Physics: Condensed Matter*, vol. 18, no. 6, pp. R15–R68, Feb. 2006, doi: 10.1088/0953-8984/18/6/R01.

[30]   K. J. Strandburg, "Two-dimensional melting," *Rev Mod Phys*, vol. 60, no. 1, pp. 161–207, Jan. 1988, doi: 10.1103/RevModPhys.60.161.

[31]   H. P. Zhang, A. Be'er, E.-L. Florin, and H. L. Swinney, "Collective motion and density fluctuations in bacterial colonies," *Proceedings of the National Academy of Sciences*, vol. 107, no. 31, pp. 13626–13630, Aug. 2010, doi: 10.1073/pnas.1001651107.

[32]   H. H. Wensink and H. Löwen, "Emergent states in dense systems of active rods: from swarming to turbulence," *Journal of Physics: Condensed Matter*, vol. 24, no. 46, p. 464130, Nov. 2012, doi: 10.1088/0953-8984/24/46/464130.

[33]   G. H. Koenderink *et al.*, "An active biopolymer network controlled by molecular motors," *Proceedings of the National Academy of Sciences*, vol. 106, no. 36, pp. 15192–15197, Sep. 2009, doi: 10.1073/pnas.0903974106.

[34]   V. Schaller, C. Weber, C. Semmrich, E. Frey, and A. R. Bausch, "Polar patterns of driven filaments," *Nature*, vol. 467, no. 7311, pp. 73–77, Sep. 2010, doi: 10.1038/nature09312.

[35]   T. Sanchez, D. T. N. Chen, S. J. DeCamp, M. Heymann, and Z. Dogic, "Spontaneous motion in hierarchically assembled active matter," *Nature*, vol. 491, no. 7424, pp. 431–434, Nov. 2012, doi: 10.1038/nature11591.

[36]   Y. Katz, K. Tunstrøm, C. C. Ioannou, C. Huepe, and I. D. Couzin, "Inferring the structure and dynamics of interactions in schooling fish," *Proceedings of the National Academy of Sciences*, vol. 108, no. 46, pp. 18720–18725, Nov. 2011, doi: 10.1073/pnas.1107583108.

[37]   M. Ballerini *et al.*, "Interaction ruling animal collective behavior depends on topological rather than metric distance: Evidence from a field study," *Proceedings of the National Academy of Sciences*, vol. 105, no. 4, pp. 1232–1237, Jan. 2008, doi: 10.1073/pnas.0711437105.

[38]   C. Bechinger, R. di Leonardo, H. Löwen, C. Reichhardt, G. Volpe, and G. Volpe, "Active Particles in Complex and Crowded Environments," *Rev Mod Phys*, vol. 88, no. 4, p. 045006, Nov. 2016, doi: 10.1103/RevModPhys.88.045006.

[39]   W. F. Paxton *et al.*, "Catalytic Nanomotors: Autonomous Movement of Striped Nanorods," *J Am Chem Soc*, vol. 126, no. 41, pp. 13424–13431, Oct. 2004, doi: 10.1021/ja047697z.

[40]   J. Palacci, C. Cottin-Bizonne, C. Ybert, and L. Bocquet, "Sedimentation and Effective Temperature of Active Colloidal Suspensions," *Phys Rev Lett*, vol. 105, no. 8, p. 088304, Aug. 2010, doi: 10.1103/PhysRevLett.105.088304.

[41]   Y. Hong, N. M. K. Blackman, N. D. Kopp, A. Sen, and D. Velegol, "Chemotaxis of Nonbiological Colloidal Rods," *Phys Rev Lett*, vol. 99, no. 17, p. 178103, Oct. 2007, doi: 10.1103/PhysRevLett.99.178103.

[42]   H.-R. Jiang, N. Yoshinaga, and M. Sano, "Active Motion of a Janus Particle by Self-Thermophoresis in a Defocused Laser Beam," *Phys Rev Lett*, vol. 105, no. 26, p. 268302, Dec. 2010, doi: 10.1103/PhysRevLett.105.268302.

[43]   S. Herminghaus, C. C. Maass, C. Krüger, S. Thutupalli, L. Goehring, and C. Bahr, "Interfacial mechanisms in active emulsions," *Soft Matter*, vol. 10, no. 36, pp. 7008–7022, 2014, doi: 10.1039/C4SM00550C.

[44]   K. Peddireddy, P. Kumar, S. Thutupalli, S. Herminghaus, and C. Bahr, "Solubilization of Thermotropic Liquid Crystal Compounds in Aqueous Surfactant Solutions," *Langmuir*, vol. 28, no. 34, pp. 12426–12431, Aug. 2012, doi: 10.1021/la3015817.

[45]   A. Reinmüller, H. J. Schöpe, and T. Palberg, "Self-Organized Cooperative Swimming at Low Reynolds Numbers," *Langmuir*, vol. 29, no. 6, pp. 1738–1742, Feb. 2013, doi: 10.1021/la3046466.

[46]   R. Dreyfus, J. Baudry, M. L. Roper, M. Fermigier, H. A. Stone, and J. Bibette, "Microscopic artificial swimmers," *Nature*, vol. 437, no. 7060, pp. 862–865, Oct. 2005, doi: 10.1038/nature04090.

[47]   I. Buttinoni, G. Volpe, F. Kümmel, G. Volpe, and C. Bechinger, "Active Brownian motion tunable by light," *Journal of Physics: Condensed Matter*, vol. 24, no. 28, p. 284129, Jul. 2012, doi: 10.1088/0953-8984/24/28/284129.

[48]   I. Buttinoni, J. Bialké, F. Kümmel, H. Löwen, C. Bechinger, and T. Speck, "Dynamical Clustering and Phase Separation in Suspensions of Self-Propelled Colloidal Particles," *Phys Rev Lett*, vol. 110, no. 23, p. 238301, Jun. 2013, doi: 10.1103/PhysRevLett.110.238301.

[49]   G. Volpe, I. Buttinoni, D. Vogt, H.-J. Kümmerer, and C. Bechinger, "Microswimmers in patterned environments," *Soft Matter*, vol. 7, no. 19, p. 8810, 2011, doi: 10.1039/c1sm05960b.

[50]   C. Maggi, M. Paoluzzi, A. Crisanti, E. Zaccarelli, and N. Gnan, "Universality class of the motility-induced critical point in large scale off-lattice simulations of active particles," *Soft Matter*, vol. 17, no. 14, pp. 3807–3812, 2021, doi: 10.1039/D0SM02162H.

[51]   F. Caballero, C. Nardini, and M. E. Cates, "From bulk to microphase separation in scalar active matter: a perturbative renormalization group analysis," *Journal of Statistical Mechanics: Theory and Experiment*, vol. 2018, no. 12, p. 123208, Dec. 2018, doi: 10.1088/1742-5468/aaf321.

[52]   B. Partridge and C. F. Lee, "Critical Motility-Induced Phase Separation Belongs to the Ising Universality Class," *Phys Rev Lett*, vol. 123, no. 6, p. 068002, Aug. 2019, doi: 10.1103/PhysRevLett.123.068002.

[53]   A. K. Omar, K. Klymko, T. GrandPre, and P. L. Geissler, "Phase Diagram of Active Brownian Spheres: Crystallization and the Metastability of Motility-Induced Phase

Separation," *Phys Rev Lett*, vol. 126, no. 18, p. 188002, May 2021, doi: 10.1103/PhysRevLett.126.188002.

[54]   F. Turci and N. B. Wilding, "Phase Separation and Multibody Effects in Three-Dimensional Active Brownian Particles," *Phys Rev Lett*, vol. 126, no. 3, p. 038002, Jan. 2021, doi: 10.1103/PhysRevLett.126.038002.

[55]   T. Speck, "Critical behavior of active Brownian particles: Connection to field theories," *Phys Rev E*, vol. 105, no. 6, p. 064601, Jun. 2022, doi: 10.1103/PhysRevE.105.064601.

[56]   K. Binder, "Finite size scaling analysis of ising model block distribution functions," *Zeitschrift für Physik B Condensed Matter*, vol. 43, no. 2, pp. 119–140, Jun. 1981, doi: 10.1007/BF01293604.

[57]   R. C. Desai, D. W. Heermann, and K. Binder, "Finite-size scaling in a microcanonical ensemble," *J Stat Phys*, vol. 53, no. 3–4, pp. 795–823, Nov. 1988, doi: 10.1007/BF01014226.

[58]   M. Rovere, P. Nielaba, and K. Binder, "Simulation studies of gas-liquid transitions in two dimensions via a subsystem-block-density distribution analysis," *Zeitschrift für Physik B Condensed Matter*, vol. 90, no. 2, pp. 215–228, Jun. 1993, doi: 10.1007/BF02198158.

[59]   M. Rovere, D. W. Hermann, and K. Binder, "Block Density Distribution Function Analysis of Two-Dimensional Lennard-Jones Fluids," *Europhysics Letters (EPL)*, vol. 6, no. 7, pp. 585–590, Aug. 1988, doi: 10.1209/0295-5075/6/7/003.

[60]   K. Kaski, K. Binder, and J. D. Gunton, "Study of cell distribution functions of the three-dimensional Ising model," *Phys Rev B*, vol. 29, no. 7, pp. 3996–4009, Apr. 1984, doi: 10.1103/PhysRevB.29.3996.

[61]   K. Adachi and K. Kawaguchi, "Universality of active and passive phase separation in a lattice model," Dec. 2020.

[62]   J. Midya, S. A. Egorov, K. Binder, and A. Nikoubashman, "Phase behavior of flexible and semiflexible polymers in solvents of varying quality," *J Chem Phys*, vol. 151, no. 3, p. 034902, Jul. 2019, doi: 10.1063/1.5110393.

[63]   S. Whitelam, K. Klymko, and D. Mandal, "Phase separation and large deviations of lattice active matter," *J Chem Phys*, vol. 148, no. 15, p. 154902, Apr. 2018, doi: 10.1063/1.5023403.

[64]   J. T. Siebert, J. Letz, T. Speck, and P. Virnau, "Phase behavior of active Brownian disks, spheres, and dimers," *Soft Matter*, vol. 13, no. 5, pp. 1020–1026, 2017, doi: 10.1039/C6SM02622B.

[65]   J. Bialké, J. T. Siebert, H. Löwen, and T. Speck, "Negative Interfacial Tension in Phase-Separated Active Brownian Particles," *Phys Rev Lett*, vol. 115, no. 9, p. 098301, Aug. 2015, doi: 10.1103/PhysRevLett.115.098301.

[66] Y. Fily and M. C. Marchetti, "Athermal Phase Separation of Self-Propelled Particles with No Alignment," *Phys Rev Lett*, vol. 108, no. 23, p. 235702, Jun. 2012, doi: 10.1103/PhysRevLett.108.235702.

[67] A. P. Solon *et al.*, "Pressure and Phase Equilibria in Interacting Active Brownian Spheres," *Phys Rev Lett*, vol. 114, no. 19, p. 198301, May 2015, doi: 10.1103/PhysRevLett.114.198301.

[68] A. Wysocki, R. G. Winkler, and G. Gompper, "Cooperative motion of active Brownian spheres in three-dimensional dense suspensions," *EPL (Europhysics Letters)*, vol. 105, no. 4, p. 48004, Feb. 2014, doi: 10.1209/0295-5075/105/48004.

[69] D. Levis, J. Codina, and I. Pagonabarraga, "Active Brownian equation of state: metastability and phase coexistence," *Soft Matter*, vol. 13, no. 44, pp. 8113–8119, 2017, doi: 10.1039/C7SM01504F.

[70] G. S. Redner, M. F. Hagan, and A. Baskaran, "Structure and Dynamics of a Phase-Separating Active Colloidal Fluid," *Phys Rev Lett*, vol. 110, no. 5, p. 055701, Jan. 2013, doi: 10.1103/PhysRevLett.110.055701.

[71] J. Stenhammar, D. Marenduzzo, R. J. Allen, and M. E. Cates, "Phase behaviour of active Brownian particles: the role of dimensionality," *Soft Matter*, vol. 10, no. 10, pp. 1489–1499, 2014, doi: 10.1039/C3SM52813H.

[72] J. A. Anderson, J. Glaser, and S. C. Glotzer, "HOOMD-blue: A Python package for high-performance molecular dynamics and hard particle Monte Carlo simulations," *Comput Mater Sci*, vol. 173, p. 109363, Feb. 2020, doi: 10.1016/j.commatsci.2019.109363.

[73] J. A. Barker and D. Henderson, "Perturbation Theory and Equation of State for Fluids. II. A Successful Theory of Liquids," *J Chem Phys*, vol. 47, no. 11, pp. 4714–4721, Dec. 1967, doi: 10.1063/1.1701689.

[74] Yannik Muche, "Computersimulationen zum Phasenverhalten von aktiven Brownschen Teilchen," Bachelorarbeit, Johannes Gutenberg-Universität Mainz, Mainz, 2020.

[75] P. Cremer and H. Löwen, "Scaling of cluster growth for coagulating active particles," *Phys Rev E*, vol. 89, no. 2, p. 022307, Feb. 2014, doi: 10.1103/PhysRevE.89.022307.

[76] S. K. Das, "Pattern, growth, and aging in aggregation kinetics of a Vicsek-like active matter model," *J Chem Phys*, vol. 146, no. 4, p. 044902, Jan. 2017, doi: 10.1063/1.4974256.

[77] K. Binder and P. Virnau, "Phase transitions and phase coexistence: equilibrium systems versus externally driven or active systems - Some perspectives," *Soft Matter*, vol. 19, no. 3, pp. 267–285, Jul. 2021, doi: 10.1080/1539445X.2021.1906703.

[78] G. Grégoire and H. Chaté, "Onset of Collective and Cohesive Motion," *Phys Rev Lett*, vol. 92, no. 2, p. 025702, Jan. 2004, doi: 10.1103/PhysRevLett.92.025702.

[79] D. P. Landau and K. Binder, *A Guide to Monte Carlo Simulations in Statistical Physics*. Cambridge University Press, 2005. doi: 10.1017/CBO9780511614460.

[80]   S. Chakraborty and S. K. Das, "Relaxation in a phase-separating two-dimensional active matter system with alignment interaction," *J Chem Phys*, vol. 153, no. 4, p. 044905, Jul. 2020, doi: 10.1063/5.0010043.

[81]   S. Paul, A. Bera, and S. K. Das, "How do clusters in phase-separating active matter systems grow? A study for Vicsek activity in systems undergoing vapor–solid transition," *Soft Matter*, vol. 17, no. 3, pp. 645–654, 2021, doi: 10.1039/D0SM01762K.

[82]   S. Puri and V. Wadhawan, *Kinetics of Phase Transitions*. CRC Press, 2009. doi: 10.1201/9781420008364.

[83]   A. J. Bray, "Theory of phase-ordering kinetics," *Adv Phys*, vol. 43, no. 3, pp. 357–459, Jun. 1994, doi: 10.1080/00018739400101505.

[84]   D. S. Fisher and D. A. Huse, "Nonequilibrium dynamics of spin glasses," *Phys Rev B*, vol. 38, no. 1, pp. 373–385, Jul. 1988, doi: 10.1103/PhysRevB.38.373.

[85]   A. Onuki, *Phase Transition Dynamics*. Cambridge University Press, 2002. doi: 10.1017/CBO9780511534874.

[86]   P. C. Hohenberg and B. I. Halperin, "Theory of dynamic critical phenomena," *Rev Mod Phys*, vol. 49, no. 3, pp. 435–479, Jul. 1977, doi: 10.1103/RevModPhys.49.435.

[87]   M. E. Fisher, "The theory of equilibrium critical phenomena," *Reports on Progress in Physics*, vol. 30, no. 2, p. 306, Jul. 1967, doi: 10.1088/0034-4885/30/2/306.

[88]   K. Everschor-Sitte and M. Sitte, "Real-space Berry phases: Skyrmion soccer (invited)," *J Appl Phys*, vol. 115, no. 17, p. 172602, May 2014, doi: 10.1063/1.4870695.

[89]   T. H. R. Skyrme, "A non-linear theory of strong interactions," *Proc R Soc Lond A Math Phys Sci*, vol. 247, no. 1249, pp. 260–278, Sep. 1958, doi: 10.1098/rspa.1958.0183.

[90]   T. H. R. Skyrme, "A non-linear field theory," *Proc R Soc Lond A Math Phys Sci*, vol. 260, no. 1300, pp. 127–138, Feb. 1961, doi: 10.1098/rspa.1961.0018.

[91]   T. H. R. Skyrme, "A unified field theory of mesons and baryons," *Nuclear Physics*, vol. 31, pp. 556–569, Mar. 1962, doi: 10.1016/0029-5582(62)90775-7.

[92]   A. N. Bogdanov and U. K. Rößler, "Chiral Symmetry Breaking in Magnetic Thin Films and Multilayers," *Phys Rev Lett*, vol. 87, no. 3, p. 037203, Jun. 2001, doi: 10.1103/PhysRevLett.87.037203.

[93]   U. K. Rößler, A. N. Bogdanov, and C. Pfleiderer, "Spontaneous skyrmion ground states in magnetic metals," *Nature*, vol. 442, no. 7104, pp. 797–801, Aug. 2006, doi: 10.1038/nature05056.

[94]   B. Dupé, M. Hoffmann, C. Paillard, and S. Heinze, "Tailoring magnetic skyrmions in ultra-thin transition metal films," *Nat Commun*, vol. 5, no. 1, p. 4030, Jun. 2014, doi: 10.1038/ncomms5030.

[95] N. Romming *et al.*, "Writing and Deleting Single Magnetic Skyrmions," *Science (1979)*, vol. 341, no. 6146, pp. 636–639, Aug. 2013, doi: 10.1126/science.1240573.

[96] S. Mühlbauer *et al.*, "Skyrmion Lattice in a Chiral Magnet," *Science (1979)*, vol. 323, no. 5916, pp. 915–919, Feb. 2009, doi: 10.1126/science.1166767.

[97] R. Wiesendanger, "Nanoscale magnetic skyrmions in metallic films and multilayers: a new twist for spintronics," *Nat Rev Mater*, vol. 1, no. 7, p. 16044, Jun. 2016, doi: 10.1038/natrevmats.2016.44.

[98] I. Kézsmárki *et al.*, "Néel-type skyrmion lattice with confined orientation in the polar magnetic semiconductor GaV4S8," *Nat Mater*, vol. 14, no. 11, pp. 1116–1122, Nov. 2015, doi: 10.1038/nmat4402.

[99] X. Z. Yu *et al.*, "Real-space observation of a two-dimensional skyrmion crystal," *Nature*, vol. 465, no. 7300, pp. 901–904, Jun. 2010, doi: 10.1038/nature09124.

[100] A. Fert, V. Cros, and J. Sampaio, "Skyrmions on the track," *Nat Nanotechnol*, vol. 8, no. 3, pp. 152–156, Mar. 2013, doi: 10.1038/nnano.2013.29.

[101] F. Jonietz *et al.*, "Spin Transfer Torques in MnSi at Ultralow Current Densities," *Science (1979)*, vol. 330, no. 6011, pp. 1648–1651, Dec. 2010, doi: 10.1126/science.1195709.

[102] J. Masell, D. R. Rodrigues, B. F. McKeever, and K. Everschor-Sitte, "Spin-transfer torque driven motion, deformation, and instabilities of magnetic skyrmions at high currents," *Phys Rev B*, vol. 101, no. 21, p. 214428, Jun. 2020, doi: 10.1103/PhysRevB.101.214428.

[103] S. Woo *et al.*, "Spin-orbit torque-driven skyrmion dynamics revealed by time-resolved X-ray microscopy," *Nat Commun*, vol. 8, no. 1, p. 15573, May 2017, doi: 10.1038/ncomms15573.

[104] R. Gruber *et al.*, "Skyrmion pinning energetics in thin film systems," *Nat Commun*, vol. 13, no. 1, p. 3144, Jun. 2022, doi: 10.1038/s41467-022-30743-4.

[105] G. Chen, "Skyrmion Hall effect," *Nat Phys*, vol. 13, no. 2, pp. 112–113, Feb. 2017, doi: 10.1038/nphys4030.

[106] A. A. Thiele, "Steady-State Motion of Magnetic Domains," *Phys Rev Lett*, vol. 30, no. 6, pp. 230–233, Feb. 1973, doi: 10.1103/PhysRevLett.30.230.

[107] S.-Z. Lin, C. Reichhardt, C. D. Batista, and A. Saxena, "Particle model for skyrmions in metallic chiral magnets: Dynamics, pinning, and creep," *Phys Rev B*, vol. 87, no. 21, p. 214419, Jun. 2013, doi: 10.1103/PhysRevB.87.214419.

[108] N. Nagaosa and Y. Tokura, "Topological properties and dynamics of magnetic skyrmions," *Nat Nanotechnol*, vol. 8, no. 12, pp. 899–911, Dec. 2013, doi: 10.1038/nnano.2013.243.

[109] B. L. Brown, U. C. Täuber, and M. Pleimling, "Effect of the Magnus force on skyrmion relaxation dynamics," *Phys Rev B*, vol. 97, no. 2, p. 020405, Jan. 2018, doi: 10.1103/PhysRevB.97.020405.

[110] J. C. Martinez and M. B. A. Jalil, "Topological dynamics and current-induced motion in a skyrmion lattice," *New J Phys*, vol. 18, no. 3, p. 033008, Mar. 2016, doi: 10.1088/1367-2630/18/3/033008.

[111] K. Everschor, M. Garst, R. A. Duine, and A. Rosch, "Current-induced rotational torques in the skyrmion lattice phase of chiral magnets," *Phys Rev B*, vol. 84, no. 6, p. 064401, Aug. 2011, doi: 10.1103/PhysRevB.84.064401.

[112] K. Everschor *et al.*, "Rotating skyrmion lattices by spin torques and field or temperature gradients," *Phys Rev B*, vol. 86, no. 5, p. 054432, Aug. 2012, doi: 10.1103/PhysRevB.86.054432.

[113] F. Jonietz *et al.*, "Spin Transfer Torques in MnSi at Ultralow Current Densities," *Science (1979)*, vol. 330, no. 6011, pp. 1648–1651, Dec. 2010, doi: 10.1126/science.1195709.

[114] J. C. Bellizotti Souza, N. P. Vizarim, C. J. O. Reichhardt, C. Reichhardt, and P. A. Venegas, "Spontaneous skyrmion conformal lattice and transverse motion during dc and ac compression," *New J Phys*, vol. 25, no. 5, p. 053020, May 2023, doi: 10.1088/1367-2630/acd46f.

[115] J. Iwasaki, M. Mochizuki, and N. Nagaosa, "Universal current-velocity relation of skyrmion motion in chiral magnets," *Nat Commun*, vol. 4, no. 1, p. 1463, Feb. 2013, doi: 10.1038/ncomms2442.

[116] K. Litzius *et al.*, "Skyrmion Hall effect revealed by direct time-resolved X-ray microscopy," *Nat Phys*, vol. 13, no. 2, pp. 170–175, Feb. 2017, doi: 10.1038/nphys4000.

[117] S.-Z. Lin, C. Reichhardt, C. D. Batista, and A. Saxena, "Driven Skyrmions and Dynamical Transitions in Chiral Magnets," *Phys Rev Lett*, vol. 110, no. 20, p. 207202, May 2013, doi: 10.1103/PhysRevLett.110.207202.

[118] K. Zeissler *et al.*, "Diameter-independent skyrmion Hall angle observed in chiral magnetic multilayers," *Nat Commun*, vol. 11, no. 1, p. 428, Jan. 2020, doi: 10.1038/s41467-019-14232-9.

[119] Y. Ge *et al.*, "Constructing coarse-grained skyrmion potentials from experimental data with Iterative Boltzmann Inversion," Oct. 2021.

[120] D. Rosenberger, M. Hanke, and N. F. A. van der Vegt, "Comparison of iterative inverse coarse-graining methods," *Eur Phys J Spec Top*, vol. 225, no. 8–9, pp. 1323–1345, Oct. 2016, doi: 10.1140/epjst/e2016-60120-1.

[121] M. Hanke, "Well-Posedness of the Iterative Boltzmann Inversion," *J Stat Phys*, vol. 170, no. 3, pp. 536–553, Feb. 2018, doi: 10.1007/s10955-017-1944-2.

[122] P. Dillmann, G. Maret, and P. Keim, "Comparison of 2D melting criteria in a colloidal system," *Journal of Physics: Condensed Matter*, vol. 24, no. 46, p. 464118, Nov. 2012, doi: 10.1088/0953-8984/24/46/464118.

[123] R. Gruber *et al.*, "300-Times-Increased Diffusive Skyrmion Dynamics and Effective Pinning Reduction by Periodic Field Excitation," *Advanced Materials*, vol. 35, no. 17, Apr. 2023, doi: 10.1002/adma.202208922.

[124] M. A. Brems, M. Kläui, and P. Virnau, "Circuits and excitations to enable Brownian token-based computing with skyrmions," *Appl Phys Lett*, vol. 119, no. 13, Sep. 2021, doi: 10.1063/5.0063584.

[125] O. Lee, R. Msiska, M. A. Brems, M. Kläui, H. Kurebayashi, and K. Everschor-Sitte, "Perspective on unconventional computing using magnetic skyrmions," *Appl Phys Lett*, vol. 122, no. 26, Jun. 2023, doi: 10.1063/5.0148469.

[126] K. Raab *et al.*, "Brownian reservoir computing realized using geometrically confined skyrmions," Mar. 2022.

Curriculum Vitae

Florian Dittrich

Personal Details

Address	Zum Staudchen 13, 56237 Nauort
Born	17.12.1988, Neuwied, Germany
Citizenship	German
Email	mail@florian-dittrich.de

Education

Since 04/2017	PhD studies *Johannes Gutenberg-Universität Mainz*
04/2007 - 03/2017	Diploma in Physics *Johannes Gutenberg-Universität Mainz*

Thesis title:	„Modellierung von aktiven Teilchen in einem Gitter-Gas-Modell und Bestimmung des kritischen Punktes im kanonischen Ensemble"
Grade:	„sehr gut" (1.0)
Minors:	Computer simulations, Nuclear chemistry

08/1999 - 03/2007	Abitur *Wilhelm-Remy-Gymnasium Bendorf*

Adv. courses:	English, Mathematics, Physics
Grade:	1.0

Career

Since 05/2023	Consultant & Data Scientist *Freelancer*
04/2022 - 04/2023	Consultant *Bain & Company Germany, Inc.*
10/2017 - 03/2022	Research Fellow *Johannes Gutenberg-Universität Mainz*
09/2007 - 06/2014	Accelerator operator of MAMI (Mainzer Mikrotron) *Johannes Gutenberg-Universität Mainz*

Languages

German (native), English (fluent), French (basic)